

Aus dem

Institut für Kardiovaskuläre Physiologie und Pathophysiologie im Walter-Brendel-Zentrum für Experimentelle Medizin

Institut der Ludwig-Maximilians-Universität München



Role of hemostasis for neutrophil trafficking into malignant tumors

Dissertation

zum Erwerb des Doctor of Philosophy (Ph.D.)

an der Medizinischen Fakultät

der Ludwig-Maximilians-Universität München

vorgelegt von

Bojan Smiljanov

aus

Shtip / Nordmazedonien

Jahr

2025

Mit Genehmigung der Medizinischen Fakultät der
Ludwig-Maximilians-Universität München

Erstes Gutachten: Prof. Dr. Christoph Reichel
Zweites Gutachten: Prof. Dr. Christian Schulz
Drittes Gutachten: Priv. Doz. Dr. Leo Nicolai
Viertes Gutachten: Priv. Doz. Dr. Philipp Freiherr von Hundelshausen

Dekan: Prof. Dr. med. Thomas Gudermann

Tag der mündlichen Prüfung: 03.04.2025



LUDWIG-
MAXIMILIANS-
UNIVERSITÄT
MÜNCHEN

Dekanat Medizinische Fakultät
Promotionsbüro



Affidavit

Smiljanov, Bojan

Surname, first name

I hereby declare, that the submitted thesis entitled

Role of hemostasis for neutrophil trafficking into malignant tumors

is my own work. I have only used the sources indicated and have not made unauthorised use of services of a third party. Where the work of others has been quoted or reproduced, the source is always given.

I further declare that the dissertation presented here has not been submitted in the same or similar form to any other institution for the purpose of obtaining an academic degree.

Munich, 08.04.2025

Place, Date

Bojan Smiljanov

Signature doctoral candidate

Confirmation of congruency



Confirmation of congruency between printed and electronic version of the doctoral thesis

Smiljanov, Bojan

Surname, first name

Marchioninistraße 68

Street

81377, Munich, Germany

Zip code, town, country

I hereby declare, that the submitted thesis entitled:

"Role of hemostasis for neutrophil trafficking into malignant tumors"

is congruent with the printed version both in content and format.

Munich, 17.10.2024
place, date

Bojan Smiljanov
Signature doctoral candidate

Table of content

Affidavit	1
Confirmation of congruency	2
Table of content	3
List of abbreviations	4
List of publications	6
Your contribution to the publications	8
1.1 Contribution to publication I.....	8
1.2 Contribution to publication II.....	9
1.3 Contribution to Publication III	9
2. Introductory summary	11
2.1 Cancer	11
2.1.1 Cancer Immunotherapy.....	13
2.1.2 Neutrophils and platelets.....	15
2.1.3 Fibrinolysis	19
2.1.4 Objective	20
2.1.5 Visual abstract	21
3. Publication I	22
4. Publication II	77
References	107
Acknowledgements	112
Curriculum vitae	113

List of abbreviations

TNBC	Triple-negative breast cancer
IC	Immune checkpoint
ER	Estrogen receptor
HER2	Human epidermal growth factor receptor 2
CTLs	Cytotoxic T lymphocytes
ICI	Immune checkpoint inhibitors
PD-L1	Programmed death-ligand 1
PD-L2	Programmed death-ligand 2
PD-1	Programmed death receptor 1
CTLA-4	Cytotoxic T lymphocyte-associated protein-4
EMT	Epithelial-mesenchymal transition
ADP	Adenosine diphosphate
PS	Phosphatidylserine
eTLR	Endosomal toll-like receptor
DAMPs	Damage-associated molecular patterns
cMOs	Classical monocytes
ncMOs	Non-classical monocytes
TNF	Tumor necrosis factor
CypD	Cyclophilin D
TMEM	Transmembrane protein
IFN-γ	Interferon-gamma
TGF	Transforming growth factor
WT	Wild-type
PSGL-1	P-Selectin glycoprotein ligand 1
vWF	von Willebrand Factor
uPA	Urokinase-type plasminogen activator
PAI-1	Plasminogen activator inhibitor-1
PAI-2	Plasminogen activator inhibitor-2
PCI	Protein C inhibitor
TAFI	Thrombin-activatable fibrinolysis inhibitor
PN-1	Protease nexin 1
tPA	Tissue-plasminogen activator

NE	Neutrophil elastase
MMP-9	Matrix-metalloproteinase-9
VEGF	Vascular endothelial growth factor
NETs	Neutrophil extracellular traps
LFA-1	Lymphocyte function-associated antigen 1
FRP1	Formyl peptide receptor 1
MAPK	Mitogen-activated protein kinase
VLDLr	Very low-density lipoprotein receptor
LRP-1	Low-density lipoprotein receptor-related protein-1
PS	Phosphatidylserine

List of publications

Publication I

Johanna Schaubaecher*, **Bojan Smiljanov***, Florian Haring*, Katja Steiger, Zhengquan Wu, Joshua Luft, Simone Ballke, Shaan Mahameed, Vera Schneewind, Jonas Hildinger, Martin Canis, Laura Mittmann, Constanze Braun, Gabriele Zuchtriegel, Rainer Kaiser, Leo Nicolai, Matthias Mack, Wilko Weichert, Kirsten Lauber, Bernd Uhl, and Christoph A Reichel. (2024) Procoagulant platelets promote immune evasion in triple negative breast cancer. Blood. blood.2023022928

*shared first authorship

Publication II

Bernd Uhl, Laura A Mittmann, Julian Dominik, Roman Hennel, **Bojan Smiljanov**, Florian Haring, Johanna B Schaubächer, Constanze Braun, Lena Padovan, Robert Pick, Martin Canis, Christian Schulz, Matthias Mack, Ewgenija Gutjahr, Peter Sinn, Jörg Heil, Katja Steiger, Sandip M Kanse, Wilko Weichert, Markus Sperandio, Kirsten Lauber, Fritz Krombach, and Christoph A Reichel. (2021) uPA-PAI-1 heteromerization promotes breast cancer progression by attracting tumorigenic neutrophils. EMBO Mol Med. 13(6): e13110

The above cited publications were taken for the cumulative dissertation.

Publication III (submitted)

Bojan Smiljanov, Zhengquan Wu, Hellen Ishikawa-Ankerhold, Bastian Popper, Anna Titova, Huan Liu, Dominic van den Heuvel, Jonas Pieterssteiner, Anais Ugurluoglu, Jonas Hildinger, Martin Bender, Martin Canis, Matthias Mack, Katharina Simone Goetze, Carolin Mogler, Olivier Gires, David Stegner, Christian Schulz, Sven Brandau, Bernd Uhl, Steffen Massberg, Felix Meissner, Markus Moser, and Christoph A Reichel. (2024) Granulopoiesis and thrombopoiesis aberrantly synergize in cancer to promote tumor progression.

Further publications

Laura A Mittmann, Florian Haring, Johanna B Schaubächer, Roman Hennel, **Bojan Smiljanov**, Gabriele Zuchtriegel, Martin Canis, Olivier Gires, Fritz Krombach, Lesca Holdt, Sven Brandau, Thomas Vogl, Kirsten Lauber, Bernd Uhl, and Christoph A Reichel. (2021) Uncoupled biological and chronological aging of neutrophils in cancer promotes tumor progression. J Immunother Cancer. 9:e00349

Bernd Uhl, Florian Haring, Julia Slotta-Huspenina, Joshua Luft, Vera Schneewind, Jonas Hildinger, Zhengquan Wu, Katja Steiger, **Bojan Smiljanov**, Aarif M N Batcha, Oliver T Keppler, Johannes C Hellmuth, Tobias Lahmer, Konrad Stock, Bernhard G Weiss, Martin Canis, Konstantin Stark, Thomas Bromberger, Markus Moser, Christian Schulz, Wilko Weichert, Gabriele Zuchtriegel, and Christoph A Reichel (2023). Vitronectin promotes immunothrombotic dysregulation in the venular microvasculature. Front Immunol. 8;14:1078005

Your contribution to the publications

1.1 Contribution to publication I

Due to the large amount of data produced, contribution in design, planning, and performing of *in vivo* and *in vitro* experiments, analyzing data, as well as writing parts of the manuscript, I contribute as one of the first authors in the publication "Procoagulant platelets promote immune evasion in triple negative breast cancer", published in April 2024.

From the beginning of my time as a PhD student in March 2020, I worked with Florian Haring on important experiments for this manuscript. After he left the laboratory, in February 2022 until its publication in April 2024, most of the work was done by myself, which I will describe below:

In the first set of experiments, from February 2021, I repeated experiments to increase the number of replicates, resulting in figure **3b**, **3c**, **4e**, **S7a**, and **S7b**. Once we had a clear vision for the project, I started to conduct further experiments, performing confocal microscopy of blood smears from 4T1-bearing mice and resulting in figure **S16d**.

In addition, I performed confocal microscopy imaging, resulting in figures **S4e**, **S11a**, **S15c**, flow cytometry analysis, resulting in figures **S1b**, **S2d**, **S10b**, **S11b**, **S11c**, **S11d**, **S11e**, **S12**, **S14a**, **S14b**, **S14d**, **S15a**, **S15b**, **S15d**, **S16d**, **S16e**, **S18b**, **S19a**, and **S19b** and *in vitro* assays, resulting in figure **S13**. Moreover, for all *in vivo* experiments I collected data for tumor weight and volume, resulting in figure **S2c**, **S6**, **S11f**, **S18a**.

On this project, I worked continuously for almost three years. For the last two years, I was the main person working on this project under the supervision of Prof. Dr. Reichel and brought it to its publication. The effort I put and the critical role I had for this manuscript explains my shared first authorship.

1.2 Contribution to publication II

For the manuscript published in EMBO Molecular Medicine, "uPA-PAI-1 heteromerization promotes breast cancer progression by attracting tumorigenic neutrophils", I was involved in the extensive revision by planning and performing experiments as well as by analyzing data for the resubmission.

I performed *in vivo* experiments and used different methods such as flow cytometry to produce data, resulting in figure **1a** and confocal microscopy imaging resulting in figures **2b**, **S1b**, and **S1c**.

I also performed *in vitro* assays with different cell lines under different conditions and treatments, resulting in figure **S2b**.

1.3 Contribution to Publication III

For the recently submitted manuscript "Granulopoiesis and thrombopoiesis aberrantly synergize in cancer to promote tumor progression", I worked on from June 2021. With respect to the previous findings in our laboratory, especially to the findings of publication I*, me and Prof. Dr. Christoph Reichel decided to further investigate the mechanisms underlying misguidance of immune cells in TNBC, focusing on processes in the bone marrow. Completing this project took almost four years and almost the entire experimental work was done by myself:

As first PhD Student in AG Reichel, who worked on megakaryopoiesis, I established three different methods for its analysis in mice (isolation, imaging, and cell culturing of megakaryocytes). To this end, I performed *in vivo* and *in vitro* experiments and I did flow cytometry analyses resulting in figures: **1a**, **1b**, **1d**, **1e**, **2a**, **2e**, **3c**, **3d**, **4b**, **4c**, **4e**, **4f**, **4i**, **5a**, **5b**, **5c**, **5e**, **5f**, **5g**, **5h**, **6b**, **6d**, **6f**, **S1a**, **S1b**, **S1c**, **S1e**, **S1f**, **S2**, **S3a**, **S4b**, **S6a**, **S6b**, **S6c**, **S6c**, **S7**, **S8a**, **S8b**, **S8c**, **S8d**, **S8f**, **S8g**, **S8i** and **S9**. Moreover, I performed confocal microscopy imaging and analysis resulting in figures: **1b**, **2a**, **2b**, **2c**, **3b**, **4d**, **5d**, **6c**

and **S8e**, as well as intravital microscopy and analysis resulting in figure: **S1d**. Furthermore, I have collected data for tumor weight after different treatments and conditions resulting in figures: **1c**, **4g**, **5j**, **5e**, **6e**, **6g** and **S8h**. To analyze the protein level of TPO in tumors, different organs, and blood, I performed ELISA resulting in figure: **4a**. For this project we had three important collaborations. PD Dr. Bastian Popper performed electron microscopy imaging and analysis resulting in figure **2d**. These samples were collected and prepared by my person. In collaboration with Prof. Dr. Felix Meissner, we performed proteomic analysis of megakaryocytes resulting in figure **7**. For this set of experiments, I have sorted and collected the cells. Together with PD Dr. Hellen Ishikawa-Ankerhold, we performed two photon *in vivo* imaging of the bone marrow, and I did the analysis resulting in figure **3a** and supplemental videos **S1-S4**.

2. Introductory summary

2.1 Cancer

With 20 million deaths in 2023, cancer is a leading cause of death worldwide and its incidence is still rising. Cancer describes unregulated and uncontrolled proliferation of cells, whose origin can be any organ or cell type and can spread to each part of the human body [1].

The most common types of cancer in the last decade are lung cancer, prostate and bladder cancer, colorectal cancer, and melanoma in males, as well as breast cancer, ovarian and cervical cancer, colorectal cancer, and lung cancer in women (**Fig. 1**) [2]. In many tumor entities, therapeutic concepts include surgical tumor removal, chemotherapy, and radiotherapy [3]. Combination of these treatments is a common therapeutic strategy ('multimodality therapy'), unfortunately with limitations in many cancer entities. The major challenging issues in these treatment modalities remain dosage selection, lack of specificity and drug resistance, as well as damaging of healthy cells, organs, and tissues [4]. Besides these conventional therapies, novel 'targeted' therapeutic approaches brought significant progress into cancer therapy, which are based on the specific molecular properties of the tumors. Prominent examples for such specific therapeutic approaches include hormone therapy (e.g., Her2 blockade or androgen receptor blockade to inhibit hormone-triggered tumor cell proliferation in breast cancer), immunotherapy (e.g., blockade of the PD-L1-PD-1 axis or the CD80/CD86-CTLA4 axis to (re)activate anti-tumoral immune cell responses in skin tumors), as well as cell-based therapies in non-solid cancers (e.g., stem-cell therapy and CAR T cell therapy) such as leukemia and multiple myeloma. Thereof, stem cell therapy involves transplantation of stem cells, typically derived from the bone marrow of healthy donors, to restore functionality of the immune system after receiving high-dose chemotherapy [5] [6]. Chimeric antigen receptor (CAR) T cell therapy is a novel approach in cancer immunotherapy using specifically

engineered T cells based on antigen reaction against the tumor. [7] Moreover, (experimental) therapies under development include oncolytic virus therapy that uses genetically modified viruses to target and eliminate cancer cells while sparing immune cells. Further, tumor vaccination is another approach to activate the body's immune defense mechanisms against tumor antigens [8, 9].

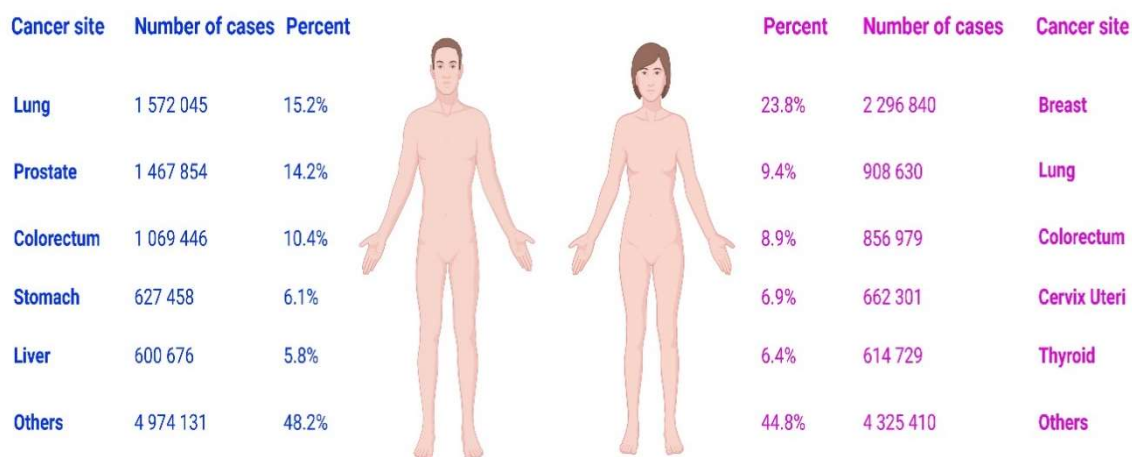


Figure 1. Estimated new cancer cases worldwide in 2022. A schematic illustration based on Ferlay J et al. (2024) is shown, non-melanoma skin cancers are included in 'Others'.

TNBC (Triple negative breast cancer)

Breast cancer is the most diagnosed cancer type in women worldwide. Different factors, such as patient age and genetic predisposition, tumor stage, as well as its molecular profile including hormone receptor status play an important role in response to therapy, and survival prognosis [10].

TNBC is a distinct and aggressive subtype of breast cancer characterized by the absence of three key receptors: estrogen receptor (ER), progesterone receptor (PR), and human epidermal growth factor receptor 2 (HER2). This lack of receptor expression means that TNBC does not respond to anti-hormonal therapies or HER2-targeted treatments, which are effective in other types of breast cancer. 20% of TNBC cases present

in woman aged in their 20s, with a further 20% presenting within women in their 50s. TNBC is mostly driven genetically, for example in women bearing *BRCA1/2* gene mutation that results in a higher risk of developing this tumor entity or other cancer types [11]. Due to molecular, genomic, and transcriptomic differences in these cancer cells, TNBC belongs to the most heterogeneous breast cancer entities. As a consequence, the efficacy of conventional and 'targeted' treatment strategies in this cancer type remain very restricted [12, 13].

2.1.1 Cancer Immunotherapy

From the late 1990s and early 2000s, immunotherapy evolved as a further treatment modality in malignant disorders [14]. Cancer Immunotherapy is a treatment focused on (re)-activation of the anti-tumorigenic properties of immune cells. So far, different pathways were clinically harnessed to counteract the immunosuppressive action of malignant tumors (**Fig. 2**):

PD-1/PD-L1 axis is a critical immune checkpoint pathway involved in the regulation of immune responses, especially in cancer. PD-1 is a receptor found on the surface of T cells, which are playing an important role in host defense. This receptor acts as a break and regulates T cell activity in order to prevent excessive immune activation against healthy cells. Different cell populations, including tumor cells, express PD-L1 as inhibitory signal and helps them to manipulate the immune system and prevent their killing by cytotoxic T cells. [15] Therefore, inhibition of this axis and less PD-L1 expression drives higher accumulation of cytotoxic T-cells in the tumor microenvironment, which has a better prognostic outcome for the patients. The most effective response rates of this therapeutic approach are observed in tumors with high mutational burden, which include Hodgkin's lymphoma and skin tumors such as Merkel cell carcinoma, cutaneous squamous cell carcinoma, and melanoma [16].

CTLA-4 is another immune checkpoint molecule expressed by T cells, with a function similar to PD-1 that downregulates immune responses. This molecule binds to its ligands CD80/CD86 and suppresses the activation of T cells. Tumors can exploit the CTLA-4 pathway to evade attack by T cells [17]. For that reason, therapeutically blocking the cytotoxic T lymphocyte-associated protein-4 (CTLA-4) receptor can also improve intratumoral infiltration of cytotoxic T cells [18].

Chimeric Antigen Receptor (CAR) T-cell therapy involves the genetic modification of a patient's autologous T-cells to enhance their ability to recognize and eliminate neoplastic cells. These engineered T-cells are specifically designed to target and bind to specific antigens expressed on the surface of cancer cells, thereby facilitating targeted cytotoxic T cell responses. The first CAR T cell therapy engineered for TNBC is c-Met-CAR-T cells that target a cell surface molecule highly expressed in TNBC tumors [19, 20].

Numerous further immunotherapeutic approaches are currently under development, which include tumor vaccines and oncolytic viruses (see above) [21].

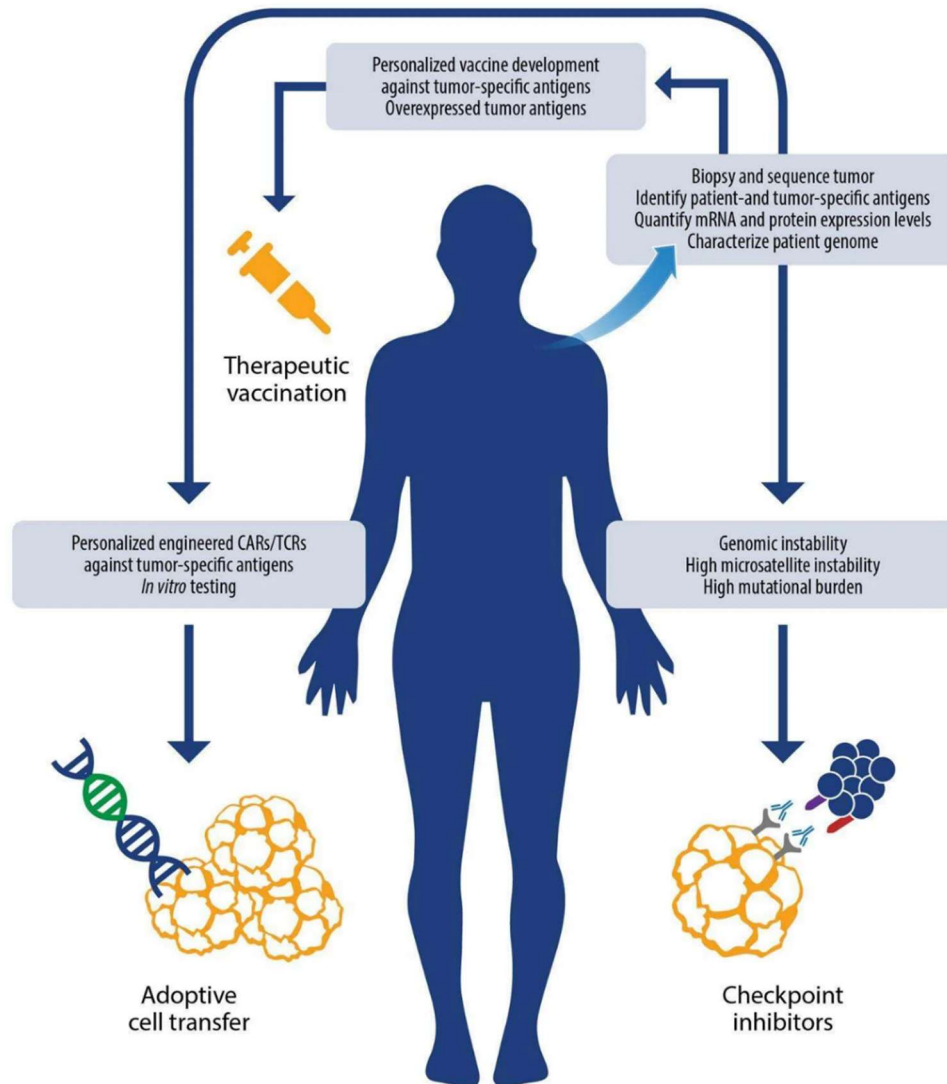


Figure 2. Immunotherapeutic strategies. A schematic illustration adopted from Bourré, L., (2018) [modified] is shown.

2.1.2 Neutrophils and platelets

Neutrophilic granulocytes (=neutrophils) represent the most frequent immune cell subset in the peripheral blood of human beings [22, 23], which usually exhibit a lifespan of only 6 – 8 hours – notwithstanding that this lifetime can be extended under certain (inflammatory) conditions [24]. Under pathological conditions (e.g., bacterial or fungal infection), neutrophils are recruited to the site of inflammation or tissue injury to combat pathogens by phagocytosis and reactive oxygen species release [25]. However, neutrophils not only eliminate pathogens in blood or tissue [26], they also take part in unfavorable processes

such as the propagation of tissue remodeling and injury [27, 28] or of vascular thrombosis [29, 30].

Neutrophils were initially thought to represent a homogeneous cell population, but related to their functional and phenotypic properties, recent studies pointed to different ‘subsets’ of this immune cells (**Fig. 3**). In cancer, at least two phenotypes of neutrophils can be distinguished (termed N1, anti-tumorogenic, and N2, pro-tumorogenic) [31]. Cancer cells release different cyto- and chemokines and attract neutrophils into tumor microenvironment. In addition, mediators such as TGF- β or ligands of the chemokine receptor CXCR2 are able to re-program neutrophils towards a tumor-supporting ‘N2’ phenotype [32, 33]. Specifically, N2 neutrophils express high levels of MMP-9, VEGF, NE, or arginase-1, and release neutrophils extracellular traps (NETs), which stimulates aberrant tumor angiogenesis, fuels tumor cell proliferation, and suppresses anti-tumoral immune cell responses [34]. Accordingly, clinical observations documented that high numbers of neutrophils in the circulation and/or in tumor tissue relates to poor survival of cancer patients [35, 36].

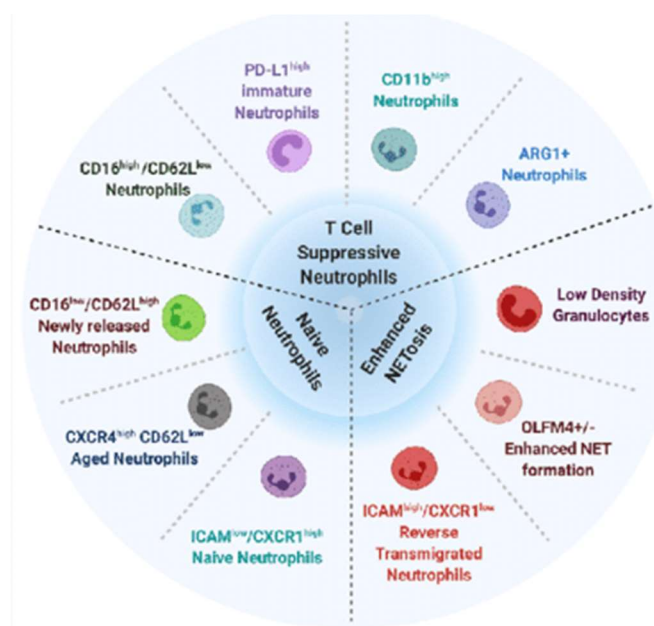


Figure 3. Heterogeneity of blood neutrophils. A schematic illustration adopted from [37] [modified] is shown.

Platelets play an essential role in hemostasis by preventing bleeding upon vascular injury. Once they are activated, platelets can display (at least) two different phenotypes, exhibiting aggregatory and procoagulant functional properties. The differential calcium signaling is key to the functional divergence. Aggregatory platelets, with their moderate calcium rise, focus on forming the platelet plug. Procoagulant platelets, in contrast, through their high and sustained calcium rise, expose PS on their surface, bind coagulation factors, and trigger integrin inactivation, ultimately leading to a procoagulant response that supports the coagulation cascade and clot stabilization [38, 39]. In addition, these cellular blood particles are critically involved in the regulation of immune responses as well as in tissue repair and regeneration [40] [41].

In cancer [42], platelets release growth factors [43] and angiogenic mediators to promote tumor progression [44]. Moreover, they support tumor cells to escape the immunological surveillance, fuel tumor metastasis [45-47], and humiliate tumor cell apoptosis and anoikis [48]. Tumor cells release different microparticles and cytokines (VEGF), thereby activating the endothelium within the tumor and attracting platelets onto its surface [42]. Moreover, activated platelets release different proteins, such as IL-1 β , which activates the endothelium, increases its permeability and supports the recruitment of leukocytes [49] [50]. Whether platelets play an immunomodulatory role in cancer remains largely unclear.

Granulopoiesis and thrombopoiesis

During embryonic development, various organs such as spleen, thymus, liver, and bone marrow represent the sites of hematopoiesis. After the 8th month of gestation, only the bone marrow maintains this role [51]. Under physiological conditions, all immune cells produced in the bone marrow originate from pluripotent hematopoietic stem cells [52] [53]. In chronic diseases and cancer, however, hematopoiesis can occur in other organs too – mostly in liver and spleen – a process termed extramedullary hematopoiesis (EMH)

[54]. The differentiation process of neutrophils follows a defined sequence of stages beginning with the common myeloid progenitor (CMP) cells, that, in turn, give rise to the granulocyte-monocyte progenitor (GMP) cells. This process is controlled by colony-stimulating factor 3 (CSF3), which is managing their development to mature neutrophils *via* promyelocyte, myelocyte, metamyelocyte, and banded neutrophil stages, in concert with other cytokines such as ligands of the chemokine receptors CXCR2 and CXCR4 (**Fig. 4**).

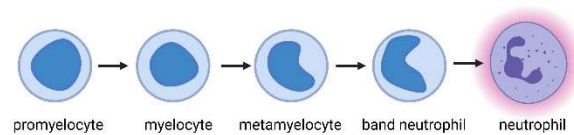


Figure 4. Neutrophil developmental stages in the bone marrow. A schematic illustration is shown.

Platelets are cellular particles produced by megakaryocytes in a process driven by the hepatic hormone TPO [55]. Pro-platelets are elongated extensions from the megakaryocytes that are directly released into the bone marrow's vascular system. Here, they undergo fragmentation and are released as single platelets into the blood stream [56]. Megakaryocytes themselves develop from common myeloid progenitors (CMP) and further differentiate into megakaryocyte-erythroid progenitors (MEPs). Their maturation and the process of platelet release are regulated by various cytokines (such as IL-6 and IL-3), chemokines (*e.g.*, SDF-1) or inflammatory mediators (*e.g.*, P-Selectin, L-Selectin), and interactions with immune cells under homeostatic conditions [57]. Interestingly, neutrophils also affect the process of platelet release through direct interactions (plucking) with megakaryocytes under homeostatic conditions as well as in cardiovascular diseases [58, 59].

2.1.3 Fibrinolysis

Fibrinolysis is the main process mediating the degradation of blood clots by cleaving fibrin monomers, thus restoring blood perfusion [60]. Plasmin is the principal effector protease in the fibrinolytic system, whose zymogen plasminogen is proteolytically activated by the plasminogen activators tPA and uPA. This process is tightly controlled by their inhibitors PAI-1, PAI-2, α_2 -Antiplasmin, or TAFI. PAI-1 is a protein secreted by endothelial cells and inhibits the activation of both, tPA and uPA. Similar to PAI-1, PAI-2 regulates the activation of tPA and uPA, but is mostly secreted by monocytes and macrophages, as well as produced in the placenta. In contrast, α_2 -Antiplasmin directly inhibits plasmin activity. Furthermore, TAFI plays an important role in breakdown of clots. This proenzyme is activated by thrombin and inhibits fibrinolysis by removing lysine residues from fibrin clots, which prevents the binding of plasminogen and other fibrinolytic enzymes to the clot (**Fig. 5**). Clinical observations documented that high concentrations of these inhibitors in the peripheral blood of patients associate with thrombotic events [61].

In addition to resolving vascular thrombosis, the fibrinolytic system plays a regulatory role in women's menstrual cycle and ovulation through interactions with gonadotropin hormones secreted by the hypophysis [62]. Moreover, the synthesis of fibrinolytic factors is altered in cardiovascular and neurological diseases [63, 64], as well as in stress situations [65] and cancer. Importantly, tumor cells themselves also secrete factors of the fibrinolytic system, thus directly deregulating the fibrinolytic system and influencing its activities in the tumor microenvironment. Besides their conventional properties in the fibrinolytic system, particularly uPA and PAI-1 have been identified to be involved in tumor growth, progression, and metastasis through direct and indirect effects on tumor cells [66, 67] [68]. [69-74].

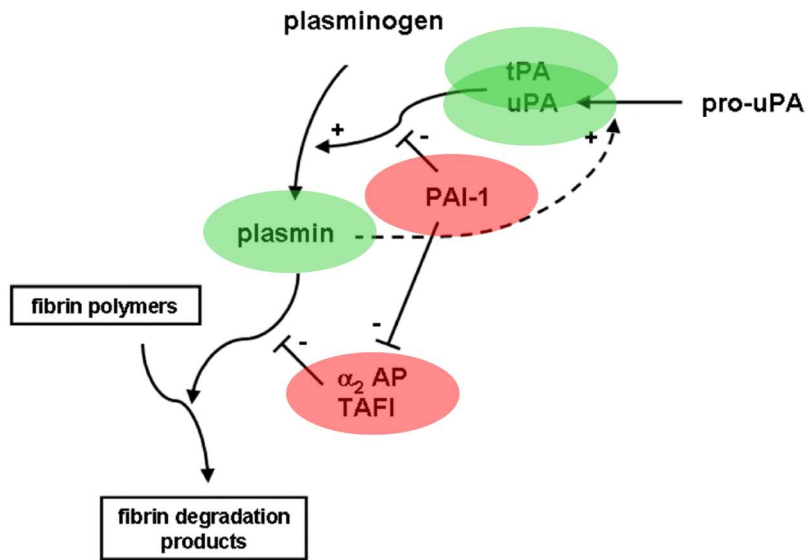
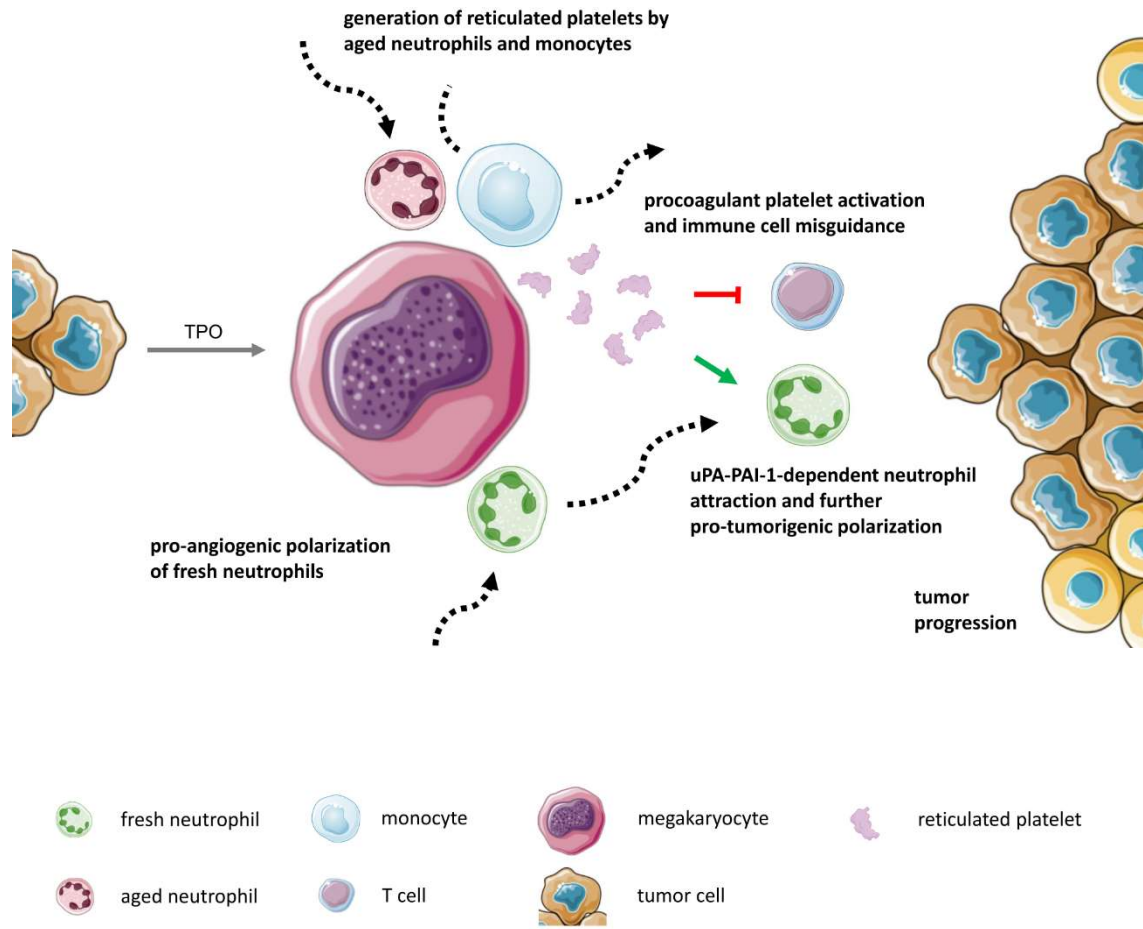


Figure 5. Schematic overview of the components of the fibrinolytic system. A schematic illustration adopted from [74] [modified] is shown.

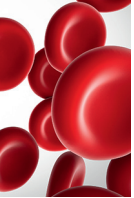
2.1.4 Objective

The objective of this PhD thesis was to characterize processes in the pathogenesis of cancer that rely on an aberrant interplay of the immune system and hemostasis/fibrinolysis.

2.1.5 Visual abstract



3. Publication I



PLATELETS AND THROMBOPOIESIS

Procoagulant platelets promote immune evasion in triple-negative breast cancer

Johanna B. Schaubaecher,^{1,2,*} Bojan Smiljanov,^{1,2,*} Florian Haring,^{1,2,*} Katja Steiger,³ Zhengquan Wu,^{1,2} Anais Ugurluoglu,^{1,2} Joshua Luft,^{1,2} Simone Ballke,³ Shaan Mahameed,^{1,2} Vera Schneewind,^{1,2} Jonas Hildinger,^{1,2} Martin Canis,^{2,4} Laura A. Mittmann,^{1,2} Constanze Braun,^{1,2} Gabriele Zuchtriegel,^{1,2} Rainer Kaiser,^{1,5,6} Leo Nicolai,^{1,5,6} Matthias Mack,⁷ Wilko Weichert,³ Kirsten Lauber,⁸ Bernd Uhl,^{1,2,†} and Christoph A. Reichel^{1,2,4,†}

¹Walter Brendel Centre of Experimental Medicine and ²Department of Otorhinolaryngology, Ludwig-Maximilians-Universität University Hospital, Munich, Germany; ³Department of Pathology, Technical University Munich, Munich, Germany; ⁴Comprehensive Cancer Center, Munich Ludwig-Maximilians-Universität and ⁵Department of Medicine I, Ludwig-Maximilians-Universität University Hospital, Munich, Germany; ⁶German Centre for Cardiovascular Research, Partner Site Munich Heart Alliance, Berlin, Germany; ⁷Department of Nephrology, University of Regensburg, Regensburg, Germany; and ⁸Department of Radiation Oncology, Ludwig-Maximilians-Universität University Hospital, Munich, Germany

KEY POINTS

- Procoagulant platelets deliver large amounts of IC molecules to malignant tumors.
- Procoagulant platelets use these IC molecules to misguide immune cell responses, thus promoting tumor progression.

Triple-negative breast cancer (TNBC) is an aggressive tumor entity in which immune checkpoint (IC) molecules are primarily synthesized in the tumor environment. Here, we report that procoagulant platelets bear large amounts of such immunomodulatory factors and that the presence of these cellular blood components in TNBC relates to protumorigenic immune-cell activity and impaired survival. Mechanistically, tumor-released nucleic acids attract platelets to the aberrant tumor microvasculature, where they undergo procoagulant activation, thus delivering specific stimulatory and inhibitory IC molecules. This concomitantly promotes protumorigenic myeloid leukocyte responses and compromises antitumorigenic lymphocyte activity, ultimately supporting tumor growth. Interference with platelet-leukocyte interactions prevented immune cell misguidance and suppressed tumor progression, nearly as effective as systemic IC inhibition. Hence, our data uncover a self-sustaining mechanism of TNBC by using platelets to misdirect immune-cell responses. Targeting this irregular multicellular interplay may represent a novel immunotherapeutic strategy for TNBC without the adverse effects of systemic IC inhibition.

Introduction

Breast cancer is the most prevalent oncological disorder in women worldwide and is one of the most common solid cancers overall. Thereof, triple-negative breast cancer (TNBC) accounts for up to 20% of the cases. These tumors do not express the therapeutically targetable receptors for estrogen (ER), progesterone, or human epidermal growth factor receptor 2 (HER2) and belong to the most aggressive breast cancer entities.¹

The immune system protects the organism against the development of malignant tumors. In particular, cytotoxic T lymphocytes (CTLs) recognize neoplastic cells and eliminate them through the release of perforins and granzymes. Furthermore, Th1-polarized CD4⁺ T lymphocytes collaborate with CTLs in cytotoxic killing, increase antigen presentation in neoplastic cells, and induce antitumor activity in peritumoral macrophages. Strategies to enhance the responses of these antitumorigenic immune cells (eg, immune checkpoint inhibitors [ICI]) have already proven effective in clinical trials for different

cancer entities.² Here, primary interference with the interactions of tumor-released programmed death-ligand 1 (PD-L1) with programmed death receptor 1 (PD-1) expressed on the surface of CTLs and/or CD80 and CD86 with their receptor cytotoxic T-lymphocyte-associated protein-4 (CTLA-4) increased the anti-tumor activity of CTLs, ultimately compromising malignant growth.² However, in TNBC, PD-L1 expression is largely restricted to the tumor environment, while tumor cells produce only low amounts of this IC molecule.³ Importantly, >10% of anti-PD-L1/PD-1 ICI-treated patients experience severe or life-threatening autoimmune-related side effects due to compromised homeostatic PD-L1 activity in healthy tissues, causing excessive local CTL activity. The prevalence of these side effects is further enhanced upon the addition of other ICI (eg, anti-CTLA-4 antibodies) to a single ICI treatment.⁴ Consequently, the benefits of ICI in TNBC are subject to controversial discussions.⁵ Moreover, distinct leukocyte subsets can interfere with CTL activity or even increase B-cell-mediated protumorigenic humoral responses (eg, T helper cell type 2 [Th2] T cells; regulatory T cells and T_{reg}). Specifically, myeloid leukocytes (eg, neutrophils, and monocytes) exhibit potent protumorigenic

properties by producing pro-proliferative, proangiogenic, and immunosuppressive factors, notwithstanding that these immune cells are also able to exhibit antitumorigenic properties.^{6,7} Although tremendous insights have been gained into the individual anti- and protumorigenic functions of different immune cell populations, it remains poorly understood how specific leukocyte subsets reach malignant lesions.

In addition to their essential role in hemostasis, platelets are increasingly being recognized to participate in tumorigenesis.⁸⁻¹¹ To this end, platelets release growth factors and angiogenic mediators,¹²⁻¹⁴ reduce tumor cell apoptosis and anoikis,¹⁵ induce gene expression¹⁶ and epithelial-mesenchymal transition in malignant cells,¹⁷⁻¹⁹ and protect tumor cells from immune responses,²⁰⁻²³ thus promoting tumor progression and metastasis.²⁴ Accordingly, cyclooxygenase inhibitors (eg, acetylsalicylic acid)²⁵⁻²⁷ and adenosine diphosphate (ADP) receptor antagonists (eg, clopidogrel, ticagrelor, or prasugrel) have been reported to exhibit beneficial effects in the prevention of different malignancies, including breast cancer.²⁸ Importantly, activated platelets acquire distinct phenotypes in thrombosis: although “aggregatory” platelets tighten the platelet plug, “procoagulant” platelets expose negatively charged phospholipids (particularly phosphatidylserine), on their surface upon contact to subendothelial collagen to promote plasmatic coagulation.²⁹⁻³¹ However, the role of activated platelet phenotypes in cancer remains unclear.

Reciprocal interactions with platelets are well-known to support the extravasation of immune cells to the perivascular tissue under inflammatory conditions.³²⁻³⁸ However, the functional relevance of platelets in the regulation of immune cell responses in malignant tumors is still elusive. Interestingly, platelets have recently been reported to express IC molecules, including PD-L1.³⁹⁻⁴¹ With respect to the already known protumorigenic effects of platelets and their established role in immune cell trafficking in inflammation, we hypothesized that these anucleate cell particles use their specific immunomodulatory properties to promote tumor progression in TNBC.

Methods

Systemic trafficking dynamics of platelets including their interplay with immune cells in the intra-/peritumoral microvasculature were analyzed in female BALB/c mice using orthotopic (mammary fat pad: flow cytometry and confocal microscopy) and heterotopic (auricle: *in vivo* microscopy) syngeneic TNBC models (4T1 tumor cells) at early tumor stages. To characterize the underlying mechanisms, flow cytometry in a mouse peritoneal assay, *in vivo* microscopy in a mouse cremaster muscle assay, and different *in vitro* assays were used. Toward translational perspectives, immunohistochemical analyses of human breast cancer samples, flow cytometry in primary human platelets, and bioinformatic analyses of published transcriptomic data were performed.

Additional details on methods are provided in supplemental Data, available on the *Blood* website.

All animal experiments were performed according to the German law for animal protection and were approved by the local government authorities (Regierung von Oberbayern).

Results

Procoagulant platelets accumulate in the tumor microvasculature

In this study, we hypothesized that platelets use their immunomodulatory properties to regulate tumor growth in TNBC. To prove this, we first sought to follow the tracks of platelets in an orthotopic syngeneic mouse model of TNBC at the early stages. Flow cytometry revealed that the total number of circulating platelets initially declined in tumor-bearing animals compared with that in healthy controls before increasing (supplemental Table 1A). A pulse-labeling approach further documented that the proportion of aged platelets of the total circulating platelets was significantly diminished in diseased animals (Figure 1A), pointing to a reduced circulatory time of these anucleate cell particles in the peripheral blood. In this context, confocal microscopy of tissue sections demonstrated that platelets primarily accumulated in tumors, but barely in the major peripheral organs of the diseased animals (Figure 1B; supplemental Table 1B). These events were associated with a (compensatory) increase in bone marrow megakaryocyte and platelet content (supplemental Table 1B-C), as well as slight splenic organ enlargement (supplemental Table 1D), and enhanced splenic accumulation of platelets (supplemental Table 1E), collectively unveiling an accelerated platelet turnover in diseased animals. In particular, *in vivo* microscopy in a heterotopic 4T1 breast cancer model (mouse auricle) documented that platelets (together with neutrophils, lymphocytes, and, to a lesser degree, classical monocytes (cMOs), but not non-cMOs (supplemental Figure 1A) increasingly roll and adhere to the endothelial surface of peritumoral and, later on, of the developing intratumoral aberrant microvessels with the progression of the tumors (Figure 1C). Importantly, the accumulating immune cells were preferentially bound to adherent platelets (Figure 1C; supplemental Video 1). As a result of these events, fewer aggregates of platelets and immune cells were formed in the peripheral blood of diseased animals than in healthy controls (Figure 1D). Interestingly, immunostaining and flow cytometry of tumor tissue homogenates revealed an almost 100-fold higher content of platelets exhibiting high surface levels of phosphatidylserine (supplemental Table 1F) than in the peripheral blood, which is indicative of the interactive “procoagulant” phenotype of these anucleate cell particles (exhibiting a larger cell size, more nucleic acid content, as well as higher surface levels of P-selectin, GPIIb/IIIa, and coagulation factor Xa as opposed to nonprocoagulant platelets including platelets with “aggregatory” or resting phenotypes; supplemental Figure 1B).²⁹⁻³¹ Hence, circulating platelets “settle down” in malignant lesions, in which they interact with immune cells upon procoagulant activation (Figure 1E).

DAMPs promote platelet trafficking into the tumor microvasculature

Cell death occurs frequently in malignant tumors, leading to the release of damage-associated molecular patterns (DAMPs) (eg, nucleic acids, and ADP) into the extracellular space.^{42,43} Accordingly, *in vivo* propidium iodide staining in our heterotopic 4T1 breast cancer model demonstrated a broad deposition of extracellular nucleic acids in the tumor environment, as assessed by *in vivo* microscopy (Figure 2A). With respect to these observations, we hypothesized that nucleic acid-recognizing endosomal toll-like receptors (eTLR)-7, -8, and -9

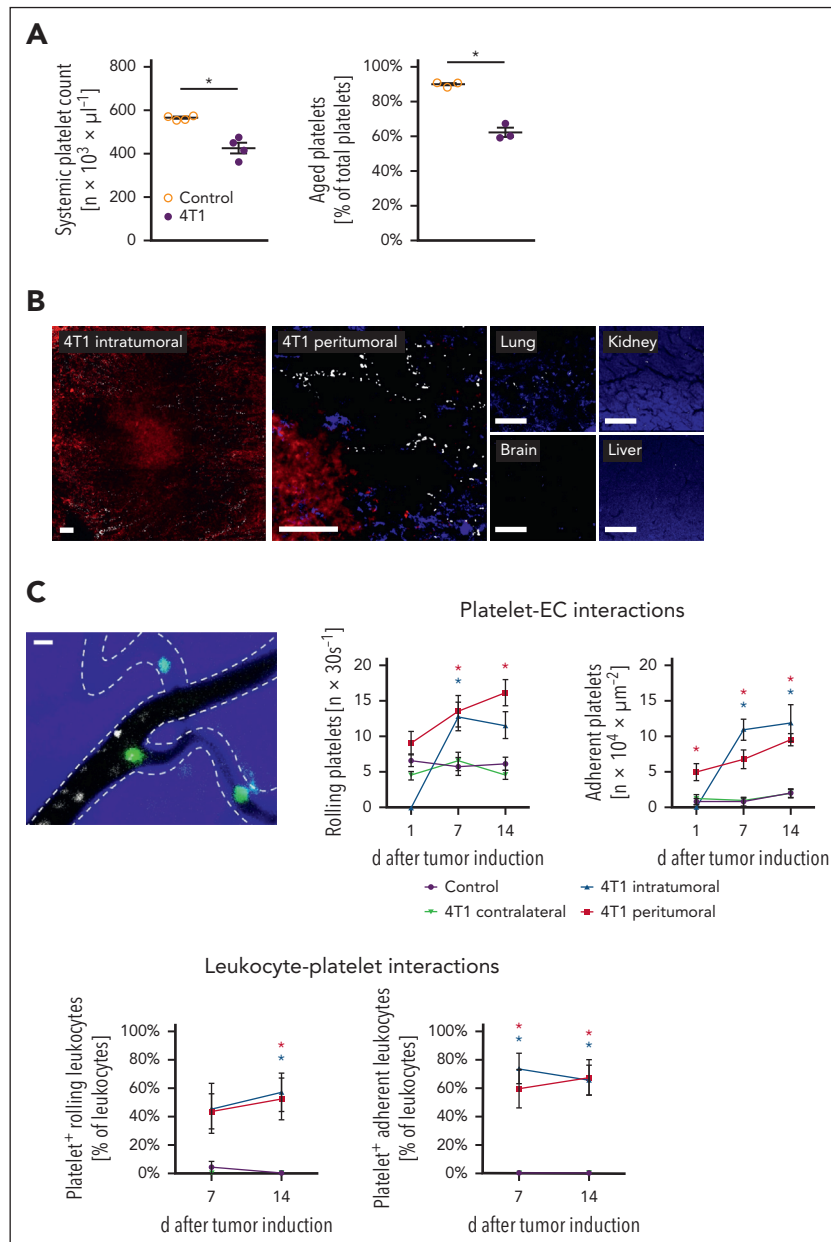


Figure 1. Platelet trafficking in experimental breast cancer. (A) Systemic platelet count as well as a proportion of aged platelets of total platelets in the peripheral blood of tumor-free control or orthotopic 4T1 tumor-bearing mice as assessed by flow cytometry; quantitative data are shown (mean \pm standard error of the mean [SEM] for $n = 3$ -4 mice per group; $*P < .05$ vs control). (B) Representative confocal microscopy images of GPIIb/IIIa⁺ platelets (white) in the intra- and peritumoral microvasculature of 4T1 tumors (tdTomato-transduced fluorescent tumor cells; red) and lungs, brain, kidneys, and liver (parenchymal structure in blue; scale bars: 100 μm) harvested from 4T1 tumor-bearing mice. (C) Interactions of platelets (white), endothelial cells (EC; broken lines), and leukocytes (green) in the peri- and intratumoral microvasculature of 4T1 tumors (blue) implanted into the auricle as assessed by *in vivo* microscopy, a representative image (scale bar: 10 μm) and quantitative data for the tumor microvasculature and the tumor-free auricular microvasculature are shown (mean \pm SEM for $n = 6$ mice per group; $*P < .05$ vs control). (D) Proportion of neutrophils, monocytes, and lymphocytes bound to platelets of total neutrophils/monocytes/lymphocytes in the peripheral blood of mice 10 days after 4T1 tumor induction; quantitative data are shown (mean \pm SEM for $n = 10$ mice per group; $*P < .05$ vs control). (E) Proportion of leukocytes bound to procoagulant platelets (phosphatidylserine⁺ GPIIb/IIIa⁺ cells) of leukocytes (CD45⁺ cells) bound to platelets (GPIIb/IIIa⁺ cells) accumulating in the intra- and peritumoral microvasculature, quantitative data and a representative *in vivo* microscopy image is shown (mean \pm SEM for $n = 3$ mice per group).

initiate the trafficking of platelets and immune cells into malignant lesions. In line with this assumption, inhibition of these eTLRs by blocking oligonucleotides significantly decreased the recruitment of platelets (Figure 2B), neutrophils, cMOs, and CD4⁺ T cells (but not CTLs or B cells) into the tumor microvasculature as compared with control oligonucleotide-treated animals (Figure 2C-D). These immunomodulatory effects of the blocking oligonucleotides were associated with

significantly reduced tumor size and weight (Figure 2E). Notably, exposure of TLR7, -8, or -9 agonists to 4T1 cancer cells did not alter 4T1 tumor cell proliferation *in vitro* (Figure 2F), collectively implying that tumor-released nucleic acids recruit platelets and immune cells into malignant lesions through eTLRs and subsequently support tumor progression. Importantly, ADP receptor blockade did not significantly alter procoagulant platelet (supplemental Figure 2A) or immune cell

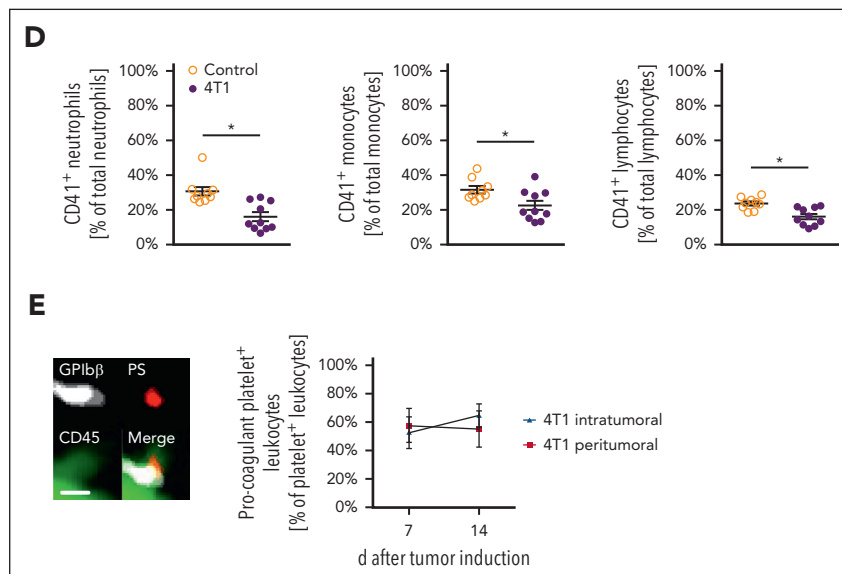


Figure 1 (continued)

(supplemental Figure 2B) accumulation in the orthotopic TNBC model but decreased nonprocoagulant platelet accumulation (supplemental Figure 2A) and, partially, tumor growth (supplemental Figure 2C). Furthermore, the surface levels of sialic acid on platelets (which decrease with chronological platelet aging and modulate systemic immune responses)⁴⁴ were not significantly altered upon ADP receptor blockade (supplemental Figure 2D), collectively pointing to non-immunomodulatory protumorigenic effects of nonprocoagulant platelets.

Toward a more comprehensive mechanistic understanding of these eTLR-dependent processes, we used flow cytometry analyses in a mouse peritoneal assay and in vivo microscopy in the mouse cremaster muscle. Here, agonists of TLR7, -8, or -9 (but not TLR3) induced the trafficking of neutrophils, cMOs, and lymphocytes (supplemental Figure 3A) and platelets (supplemental Figure 3B) to the site of application compared with the controls. In vitro analyses further revealed that agonism of these eTLRs directly activates neutrophils and cMOs (indicated by increased surface expression of Mac-1; supplemental Figure 4A) and lymphocytes (indicated by L-selectin shedding; supplemental Figure 5) but did not directly activate platelets (indicated by unchanged surface expression of activated GPIIb/IIIa) or microvascular endothelial cells (indicated by unaltered ICAM-1, VCAM-1, E-selectin, and P-selectin surface expression). Instead, agonism of TLR7, -8, or -9 profoundly induced the production of the cytokine tumor necrosis factor in macrophages (supplemental Figure 4B), which, in turn, activated endothelial cells to induce the expression of adhesion molecules on their surface (supplemental Figure 4C-D). Accordingly, endothelial expression of these molecules in the microvasculature was more pronounced in the vicinity of perivascular macrophages (supplemental Figure 4E), collectively initiating endothelial interactions with platelets and immune cells. Thus, nucleic acids mediate platelet and immune cell responses via direct and indirect eTLR-dependent effects.

Platelets differentially regulate responses of distinct immune cell subsets

In our TNBC model, antibody-mediated depletion of neutrophils or cMOs attenuated tumor growth, whereas depletion of CTLs supported tumor progression (supplemental Figure 6). To characterize the functional relevance of platelets for responses of these immune cells in TNBC, we performed experiments in thrombocytopenic animals (supplemental Table 2A). Here, antibody-mediated depletion of platelets almost completely abolished the migration of protumorigenic neutrophils and cMOs into orthotopically grown 4T1 tumors, whereas the infiltration of antitumorigenic CTLs was significantly enhanced compared with isotype control antibody-treated tumor-bearing mice (Figure 3A). To a lesser extent, tumor infiltration by Th17 and Th22 cells, antitumorigenic Th9 cells, and protumorigenic T_{reg} and Th2 cells, but not of B cells or antitumorigenic Th1 cells (Figure 3A-B), was intensified in thrombocytopenic animals. The resulting overall immunomodulatory effect of platelet depletion was associated with a significant reduction in tumor size and weight compared with isotype control antibody-treated controls (Figure 3C). Our findings were confirmed in the more reductionist peritoneal assay, as eTLR-dependent extravasation of neutrophils and cMOs to the peritoneal cavity was significantly attenuated upon platelet depletion, whereas responses of lymphocytes were significantly elevated (supplemental Figure 7A). Importantly, antibody-mediated depletion of neutrophils (supplemental Table 2B) significantly diminished the recruitment of cMOs into the peritoneal cavity but did not alter lymphocyte responses (supplemental Figure 7B). Thus, platelets differentially regulate innate and adaptive immune cell responses in the tumor microenvironment and (subsequent) tumor progression. Most interestingly, immunohistochemical analyses of human TNBC samples documented that intravascular accumulation of platelets positively correlated with high neutrophil-CTL ratios in the perivascular tumor immune cell infiltrate (Figure 3D), confirming our experimental data and translating them into human disease. Accordingly, the gene expression data from the METABRIC (Molecular Taxonomy of Breast Cancer International

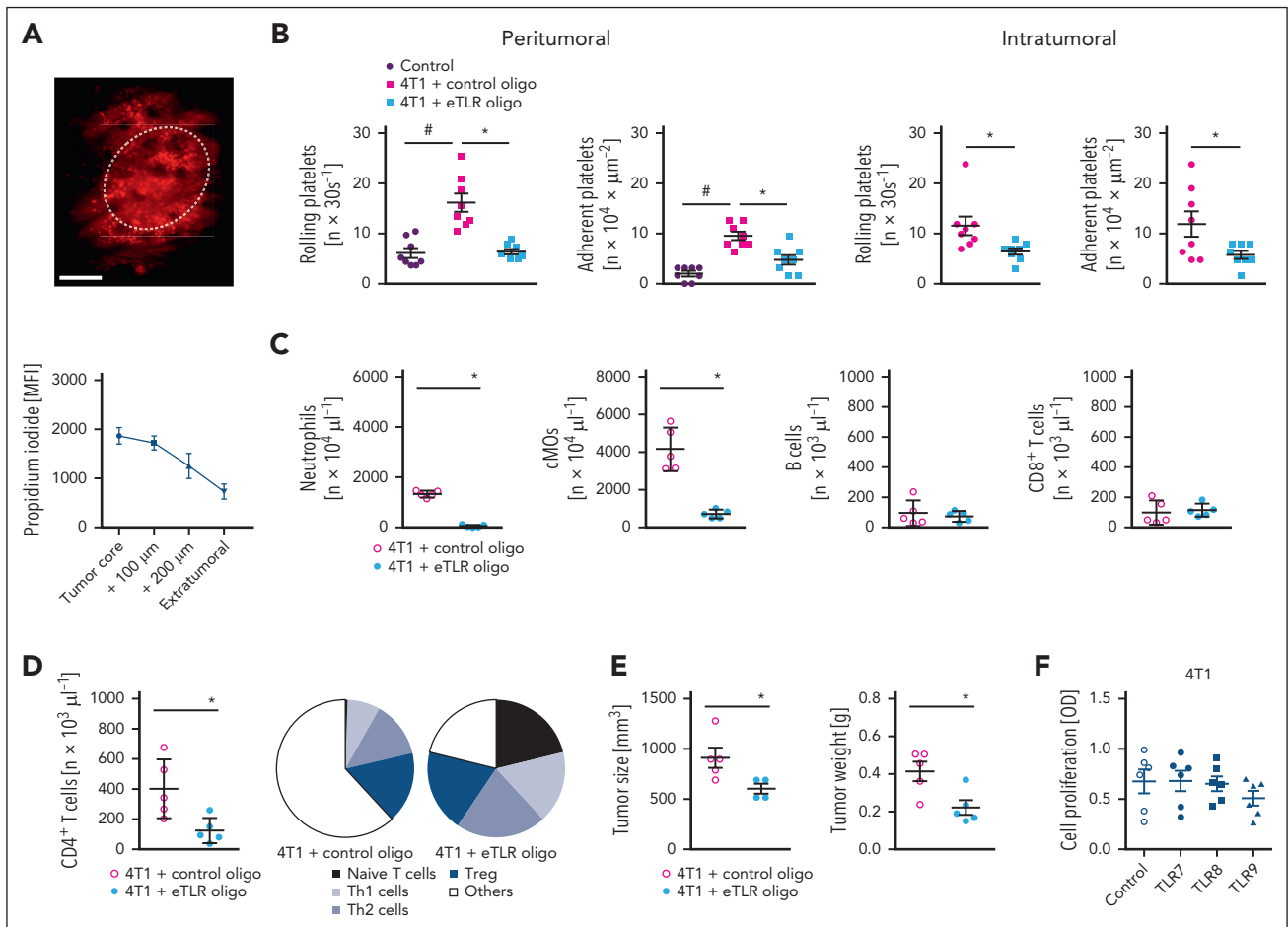


Figure 2. Effects of tumor-released extracellular nucleic acids on platelet and immune cell trafficking in experimental breast cancer. (A) Extracellular nucleic acids (red) released into the environment of 4T1 tumors as assessed by propidium iodide staining and in vivo microscopy on day 10 after tumor induction, a representative image (scale bar: 100 μm) and quantitative data for the fluorescence intensity relative to the distance from the tumor core (dotted line) are shown (mean \pm SEM). (B) EC interactions of platelets in the peri- and intratumoral microvasculature of 4T1 tumors implanted into the left auricle in mice treated with blocking eTLR oligonucleotides or control oligonucleotides and of the left auricle of tumor-free mice; quantitative data are shown (mean \pm SEM for $n = 7$ mice per group; # $P < .05$ vs control oligo). Infiltration by (C) neutrophils, cMOs, B cells, CD8⁺ T cells, and (D) CD4⁺ T-cell subsets as assessed by flow cytometry as well as (E) size and weight of orthotopic 4T1 tumors, quantitative data are shown (mean \pm SEM for $n = 5$ mice per group; * $P < .05$ vs control oligo). (F) Proliferation of 4T1 tumor cells exposed to agonists of TLR-7, -8, or -9 as assessed by 3-(4,5-dimethylthiazol-2-yl)-2,5 diphenyl tetrazolium bromide assay and quantitative data are shown (mean \pm SEM for $n = 6$ mice per group).

Consortium) breast cancer cohort (supplemental Figure 8A) indicated that recurrence free (Figure 3E) and overall (supplemental Figure 8B) survival of patients with breast cancer with high RNA expression of the platelet surrogate marker integrin α_{IIb} (ITGA2B/CD41) in their tumors was significantly impaired compared to patients with low ITGA2B RNA levels. Interestingly, ITGA2B^{high}-expressing METABRIC cases were enriched with the ER⁺/HER2^{high}-proliferating subtype and histological grade 3 (supplemental Figure 8A,C). At the molecular level, ITGA2B expression was positively correlated with the expression of gene sets involved in proliferation, DNA synthesis, and repair, and negatively correlated with gene sets associated with immune mechanisms and inflammation (supplemental Figure 8D). Notably, tumoral ITGA2B RNA expression did not positively correlate with the expression of the endothelial cell marker PECAM-1, whereas tumor RNA expression of PECAM-1 positively correlated with the expression of PD-L1, CD80, CD86, CD40, and CD40L (supplemental Figure 8E), collectively suggesting that higher expression levels of ITGA2B do not simply reflect higher tumor vascularization.

Procoagulant platelets deliver IC molecules into tumors

Recently, IC molecules were detected on the surface of platelets.³⁹⁻⁴¹ Here, we show that particularly procoagulant platelets bear large amounts of the inhibitory IC molecules PD-L1, CD80, and CD86 (but not of PD-L2) as well as of the stimulatory IC molecules CD40 and CD40L on their surface as compared with nonprocoagulant platelets or immune cells isolated from the peripheral blood of tumor-bearing mice (Figure 4A; supplemental Figure 9). Similar results were obtained in primary human platelets (supplemental Figure 10). Confocal microscopy further documented that platelets in the aberrant microvasculature of orthotopically raised 4T1 tumors colocalized with exposed collagen (supplemental Figure 11A). Interestingly, collagen-stimulated procoagulant activation of platelets was associated in vitro, particularly with high surface expression of PD-L1, which was mediated by the platelet receptors GPVI and GPIIb/IIIa as well as through cyclophilin D- and scramblase transmembrane protein 16F-dependent pathways (supplemental Figure 11B-C). Accordingly, the

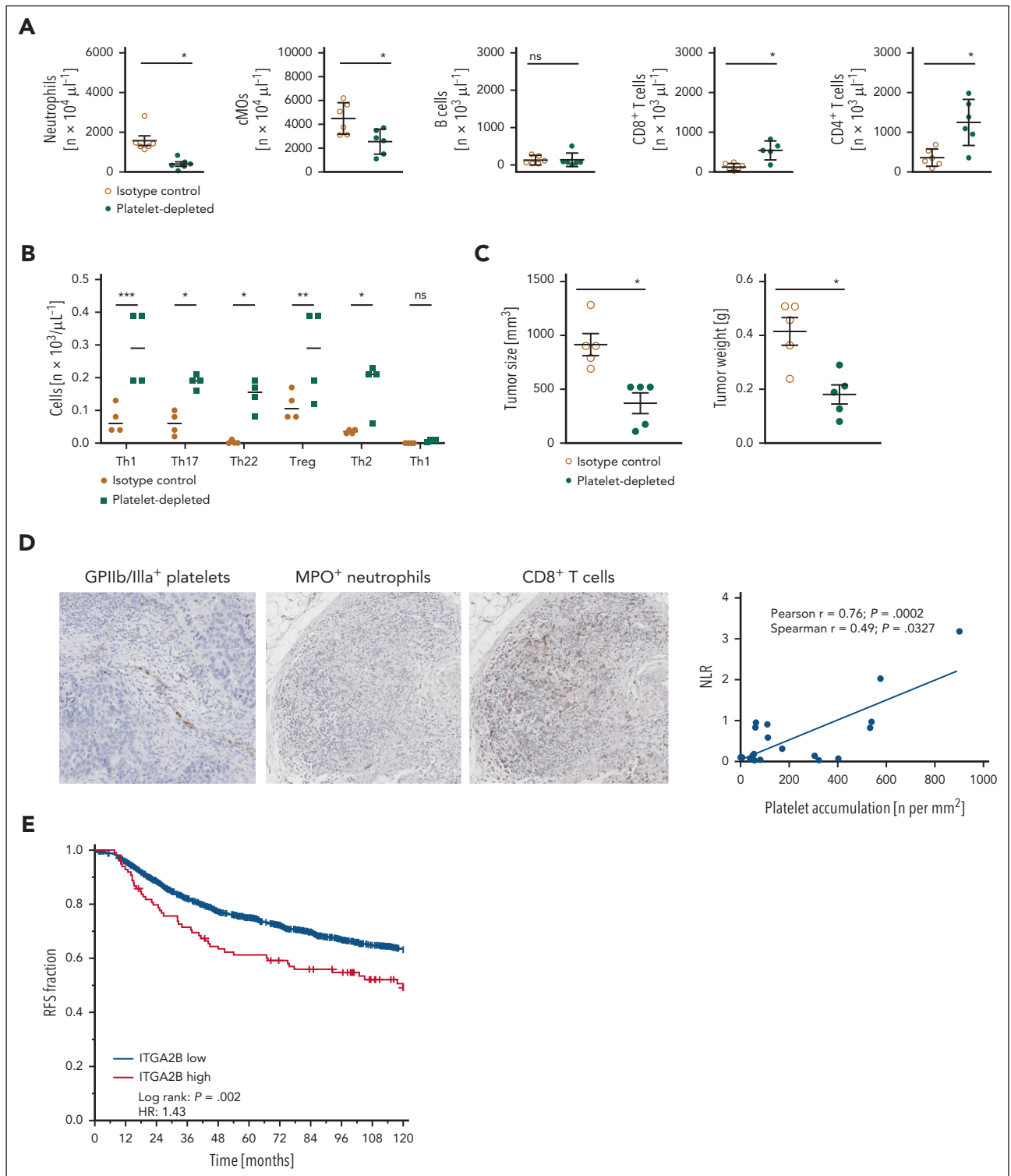


Figure 3. Effects of platelets on immune cell trafficking in breast cancer. (A) Infiltration by neutrophils, cMOS, B cells, CD8⁺ T cells, CD4⁺ T cells, and (B) CD4⁺ T-cell subsets as assessed by flow cytometry, as well as (C) size and weight of orthotopic 4T1 tumors in mice receiving platelet depleting or isotype control antibodies; quantitative data are shown (mean \pm SEM for $n = 4$ -6 mice per group; * $P < .05$ /** $P < .01$ /*** $P < .001$ vs isotype control; ns, not significant). (D) Correlation between the ratio of extravascular MPO⁺ neutrophils and CD8⁺ T cells (NLR, neutrophil/lymphocyte ratio) and intravascularly accumulated integrin β^3 platelets, as assessed by immunohistochemical analyses of human TNBC samples; representative images and quantitative data are shown. (E) Recurrence-free survival of patients with breast cancer from the METABRIC breast cancer cohort exhibiting ITGA2B^{low} and ITGA2B^{high} expression levels (z -value ≥ 1.5 served as the cutoff).

blockade of GPVI and, to a lesser extent, GPIIb/IIIa significantly attenuated the accumulation of procoagulant platelets in 4T1 tumors (supplemental Figure 11D). In addition, blockade of GPVI

or GPIIb/IIIa diminished intratumoral numbers of non-procoagulant platelets and myeloid leukocytes while increasing intratumoral lymphocyte responses (supplemental Figure 11D-E).

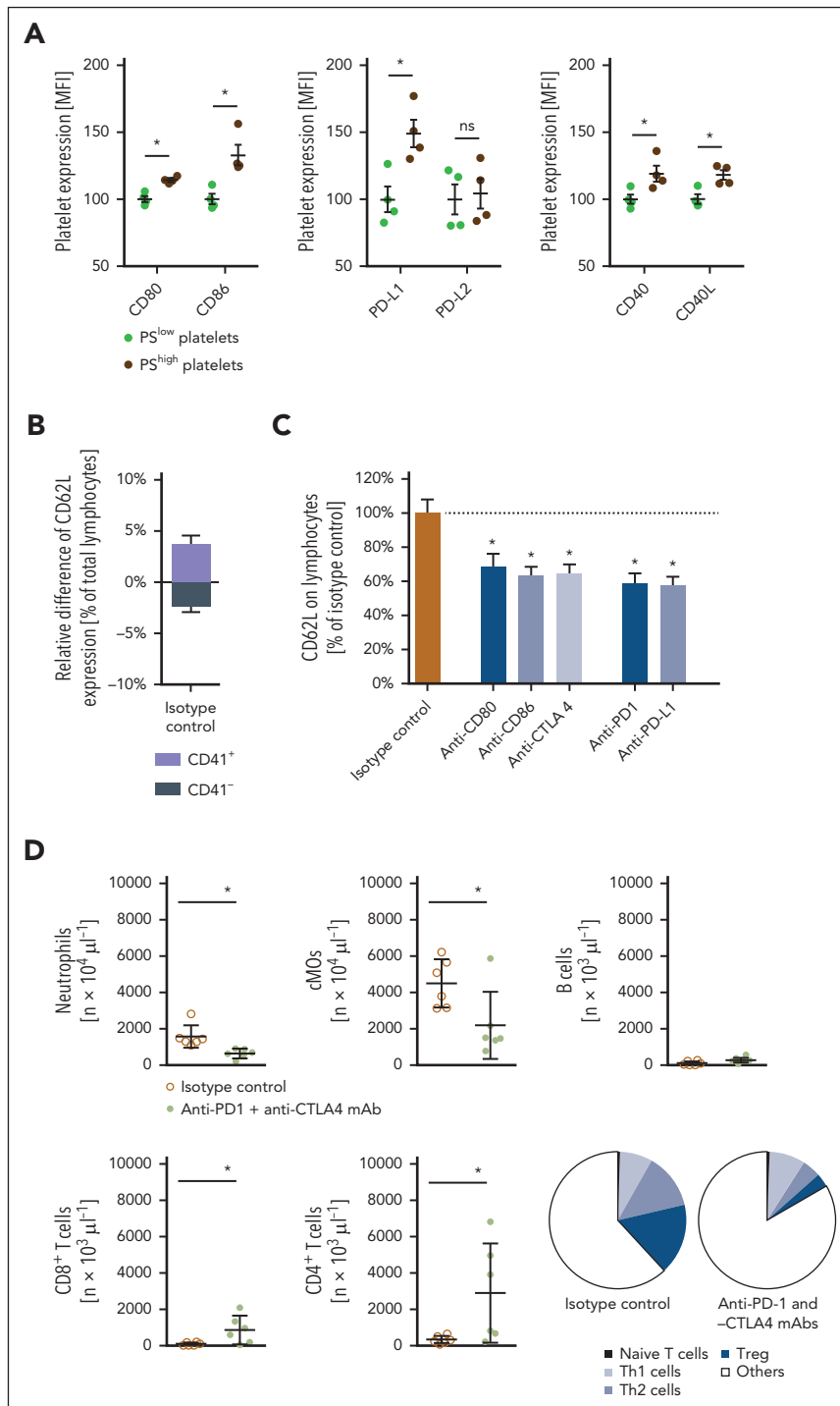


Figure 4. Synergistic effects of antiplatelet therapy and IC inhibition in experimental breast cancer. (A) Surface expression of CD80, CD86, PD-L1, PD-L2, CD40, and CD40L on phosphatidylerine^{low} or phosphatidylerine^{high} platelets from the peripheral blood of mice; quantitative data are shown (mean ± SEM for n = 3 mice per group; *P < .05 vs phosphatidylerine^{low}). (B) Activation status of platelet-bound (CD41⁺) or -unbound (CD41⁻) lymphocytes isolated from orthotopically raised 4T1 tumors as assessed by L-selectin/CD62L surface expression by flow cytometry, and quantitative data are shown (mean ± SEM for n = 3 mice per group). (C) Activation status of platelet-bound (CD41⁺) lymphocytes, as assessed by L-selectin/CD62L surface expression in flow cytometry upon antibody blockade of CD80, CD86, CTLA4, PD-L1, or PD-1, quantitative data are shown (mean ± SEM for n = 3 mice per group). (D) Infiltration by neutrophils, cMOs, B cells, CD8⁺ T cells, and CD4⁺ T-cell subsets of orthotopic 4T1 tumors in mice receiving anti-PD-1 and -CTLA4 monoclonal antibodies (mAbs) or isotype control antibodies as assessed by flow cytometry; quantitative data are shown (mean ± SEM for n = 5 mice per group; *P < .05 vs isotype control). (E) Relative volume and weight of tumors as well as (F) relative infiltration by lymphocytes and myeloid leukocytes of orthotopically grown 4T1 tumors in mice receiving anti-GPIIb/IIIa mAbs, and/or anti-PD-1 and -CTLA4 mAbs, or isotype control antibodies; quantitative data are shown (mean ± SEM for n = 5 mice per group; *P < .05 vs isotype control).

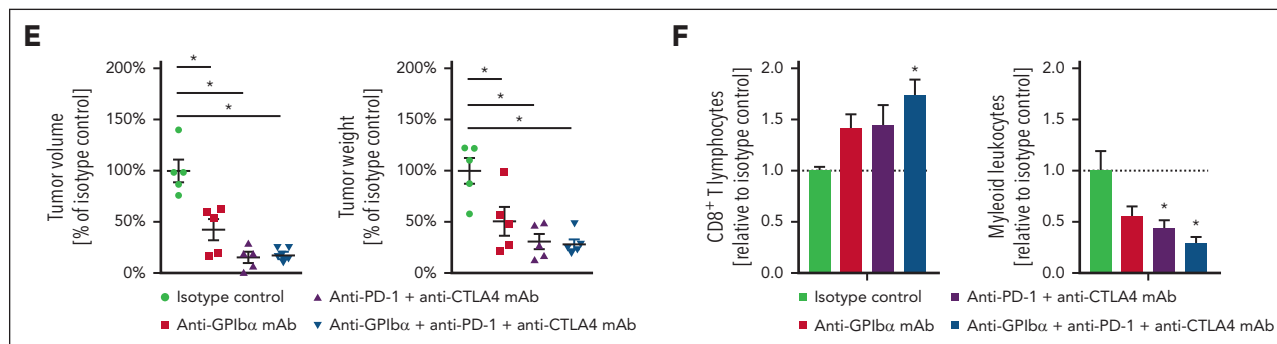


Figure 4 (continued)

As a consequence, tumor growth was strongly impaired (supplemental Figure 11F).

Furthermore, procoagulant platelets exhibited higher expression levels of the immunomodulatory cytokines CCL5 and transforming growth factor- β than nonprocoagulant platelets (supplemental Figure 12). The binding of platelets to T lymphocytes significantly decreased the activation status of these immune cells (indicated by elevated surface expression of the activation marker L-selectin (Figure 4B), as well as by reduced surface expression of the activation markers CD25 and CD69, cytokine interferon-gamma, promigratory integrin CD49d, and proliferation marker Ki-67 (supplemental Figure 13). Antibody blockade of the inhibitory IC molecule receptors PD-1 and CTLA-4 consequently attenuated these inhibitory effects on platelets (Figure 4C; supplemental Figure 13), suggesting that platelet-dependent, PD-1/CTLA-4 ligand-mediated inhibition of T lymphocyte activation compromises diverse T lymphocyte functions. Concomitant interference with the PD-L1 receptor PD-1 and the CD80/CD86 receptor CTLA-4 accordingly increased eTLR-dependent trafficking of CTLs to the level of platelet-depleted animals in the peritoneal assay, whereas blockade of the CD40L receptor CD40 expectedly attenuated the responses of myeloid leukocytes and lymphocytes (supplemental Figure 14). Moreover, concomitant inhibition of PD-1 and CTLA-4 significantly enhanced tumor infiltration by antitumorigenic CTLs and Th1 cells and reduced (protumorigenic) myeloid leukocyte responses as well as tumor growth in the orthotopic 4T1 breast cancer model compared with isotype control antibody-treated tumor-bearing animals (Figure 4D-E). In line with the low IC molecule expression in poorly immunogenic 4T1 tumor cells, combined PD-1 and CTLA-4 inhibition achieved comparable immunomodulatory and tumor-suppressing effects as antibody-mediated platelet depletion (Figures 4E-F and 3A-B). Importantly, upon platelet depletion, the remaining viable tumor cells exhibited a slightly enhanced proliferation status (indicated by the average Ki-67 expression; supplemental Figure 15A) as compared with control animals (which might be due to the survival of the “fittest,” most proliferative cells), but unaltered epithelial-mesenchymal transition status (measured by epithelial cellular adhesion molecule expression; supplemental Figure 15A) or, in line with the lack of IC molecule expression in human TNBC cells, tumor cell expression of IC molecules supplemental Figure 15B), as well as the vascularization of the tumors (supplemental Figure 15C), as identified in orthotopic and heterotopic 4T1 tumor models. Thus, our experimental data suggest that procoagulant

platelets primarily modulate immune cell responses by delivering IC molecules to the tumor microvasculature. As a consequence, numbers of viable tumor cells were significantly decreased in platelet-depleted animals (Figure 4E; supplemental Figure 15).

GPIIb/alpha blockade and PD-1/CTLA-4 inhibition exhibit similar effects in experimental TNBC

Interestingly, because of intratumoral procoagulant platelet activation (supplemental Figure 11), the proportion of procoagulant platelets among the total platelets bound to lymphocytes was significantly higher in 4T1 tumors than in peripheral blood (supplemental Figure 16A). Toward a translational perspective, we therefore tested different platelet molecules for their ability to interfere with the formation of platelet-lymphocyte complexes in the systemic circulation before procoagulant platelet activation in the tumor. Using blocking antibodies and inhibitors, we showed that the platelet receptor GPIIb/alpha, but not GPVI, GPIX, GPIIb/IIIa, ICAM-2, P-selectin, PSGL-1, P2Y12, or the enzyme cyclooxygenase, facilitates the binding of platelets to circulating lymphocytes (supplemental Figure 16B). Confocal microscopy analyses further indicate that platelet GPIIb/alpha interacts with von Willebrand factor-decorated CD3⁺ T cells (supplemental Figure 16C-D). Accordingly, a priori blockade of GPIIb/alpha showed similar immunomodulatory and tumor-suppressing effects as combined PD-1- and CTLA-4 inhibition in the orthotopic TNBC model (Figure 4E-F). Importantly, blocking or platelet-depleting antibodies efficiently bound to platelets but not to 4T1 tumor cells (supplemental Figure 16E). Most interestingly, triple blockade of GPIIb/alpha, PD-1, and CTLA-4 did not significantly enhance tumor infiltration by antitumorigenic CTLs or further attenuate (protumorigenic) myeloid leukocyte responses and suppression of tumor growth as compared with isolated ICI treatment. This lack of synergistic effects of ICI and GPIIb/alpha blockade in the 4T1 tumor model, in which ligands of PD-1 and CTLA-4 are predominantly expressed by platelets, suggests that platelets may promote tumor progression in this experimental model mainly via their immunomodulatory properties. From a therapeutic perspective, the treatment of existing tumors with anti-GPIIb/alpha or anti-PD-1/CTLA-4 antibodies significantly reduced tumor progression (supplemental Figure 17A) and enhanced tumoral CTL accumulation without affecting the presence of myeloid leukocytes in the tumors (supplemental Figure 17B), which might be due to the dominance of intravascular lymphocyte responses in established tumors (supplemental Figure 1A). Similar results were obtained in an orthotopic mouse model of poorly

immunogenic head and neck squamous cell carcinoma (supplemental Figure 18), suggesting platelet-mediated IC molecule delivery to malignant tumors as a more general pathological mechanism. Moreover, despite the low number of platelets in the peripheral organs of orthotopically 4T1 tumor-bearing mice (Figure 1B; supplemental Table 1B), procoagulant platelet activation was also detected at sites of tumor metastases in bone marrow ($7.9\% \pm 0.2\%$ of total platelets), liver ($11.8\% \pm 0.8\%$ of total platelets), and lungs ($12.5\% \pm 0.6\%$ of total platelets). Platelet depletion critically modulated neutrophil (but not cMO, CD4⁺ T cell, CTL, and B cell) accumulation (supplemental Figure 19A) and (subsequently) compromised metastatic seeding of breast cancer cells (supplemental Figure 19B), further indicating that platelets exhibit common and distinct immunoregulatory effects in primary tumors and at sites of tumor metastasis. This might be explained by the contribution of tissue-specific properties to the control of immune cell responses (eg, the presence of DAMPs and inflammatory cytokines in tumors, as opposed to homeostatic cytokines in peripheral tissues during initial metastatic stages).

Discussion

Platelets substantially contribute to the pathogenesis of malignant tumors. Their systemic trafficking dynamics in cancer, however, remain obscure. In this study, we showed that the circulatory time of platelets in peripheral blood decreased in the early stages of experimental TNBC, despite (reactively) enhanced bone marrow megakaryocytopoiesis and stable splenic platelet clearance, because these cellular blood components massively accumulate in the aberrant tumor microvasculature. Here, platelets heavily interacted with neutrophils, cMOs, lymphocytes, and endothelial cells, resembling platelet-immune cell interactions in inflamed tissue.³²⁻³⁴ Most interestingly, the majority of these interactive platelets in the tumor environment exhibited a highly reactive “procoagulant” phenotype, which shares distinct phenotypic properties with the hyperreactive young, reticulated subset of platelets⁴⁵ and is triggered by exposure to subendothelial collagen in defective vessels.²⁹⁻³¹ Hence, platelets instantly traffick to neoplastic lesions in early TNBC in which they undergo procoagulant activation. At later stages of the disease, reactive thrombocytopoiesis might further intensify tumoral platelet responses and even overcompensate for the initial decline of circulating platelets, ultimately leading to clinically reported thrombocytosis and thrombotic events in advanced stages of breast cancer.⁴⁶⁻⁴⁸

DAMPs are host biomolecules released in a variety of pathologies,⁴⁹ including cancer, as a consequence of inflammation, cell death, and tissue destruction.^{42,43} Upon recognition of these specific molecular signals by eTLRs, distinct inflammatory programs are initiated, mediating the activation of cells.³⁵ In our experiments, we expectedly detected an enormous accumulation of extracellular nucleic acids in the tumor environment. These tumor-released DAMPs (but not ADP, which is also known to be liberated by necrotic cells) attract platelets and immune cells into the tumor environment by instructing perivascular macrophages through eTLRs to induce the expression of distinct adhesion molecules on microvascular endothelial cells capable of recruiting and activating circulating platelets and immune cells.⁵⁰ Notably, previous experimental studies

have suggested that the activation of endosomal TLR7 and/or TLR8 primarily stimulates antitumor immune responses.⁵¹ In clinical trials, however, eTLR agonists showed beneficial effects only in precancerous skin lesions but did not improve the survival of patients with (head and neck) cancer.⁵¹ This lack of antitumor effects of eTLR agonism might be due to the concomitant induction of eTLR-dependent protumor immune platelet responses in invasive tumors.

Under inflammatory conditions, platelets are well-known to promote the migration of immune cells to their target destinations via diverse molecular interactions.³²⁻³⁸ The role of these anucleate cell particles in the recruitment of immune cells to malignant tumors is still unclear. Here, we unveil a previously unrecognized immunomodulatory function of platelets that concurrently promotes the trafficking of innate immune cells into neoplastic lesions while inhibiting the responses of adaptive immune cells, independent of their effects on tumor cell proliferation, epithelial-mesenchymal transition, and angiogenesis. Most importantly, analyses of human TNBC samples clearly confirmed our experimental results, as the presence of platelets in tumors was associated with a protumor immune cell milieu. Accordingly, transcriptomic data from the METABRIC cohort document particularly impaired survival of individuals with high tumoral expression levels of the platelet surrogate marker ITGA2B, presumably originating from a more aggressive subtype as indicated by enrichment of histological grade 3, the ER⁺/HER2^{high}-proliferating subtype, and gene sets associated with proliferation, DNA synthesis, and repair. Furthermore, the enrichment of ITGA2B across all tumor stages and different breast cancer subtypes point to a more general role of platelets in this tumor entity.

IC molecules control immune cell responses under homeostatic and pathological conditions.⁵² Whereas stimulatory ICs enhance immune reactions,³⁴ inhibitory ICs dampen the immune cell activity. In cancer, particularly interactions of inhibitory PD-1 and PD-L1, as well as of CTLA-4 and its ligands CD80 and CD86, drive adaptive immune cell evasion.⁵² Extending previous observations,³⁹⁻⁴¹ we here demonstrate that primarily procoagulant platelets expose large amounts of these IC molecules on their surface as compared with non-procoagulant platelets or other blood cells, which is mediated via GPVI, GPIIb/IIIa, cyclophilin D, and transmembrane protein 16F. Accordingly, platelets attenuate the activity of antitumor T cells and promote neutrophil responses (which are protumor in experimental TNBC)^{53,54} in malignant lesions by using these immunomodulatory factors, ultimately fueling tumor growth. Opposite lymphocyte-supporting effects of platelets observed in viral infection³⁶⁻³⁸ might be explained by context-specific differences in the models used.

Most interestingly, we here demonstrate that platelet depletion achieved similar immunomodulatory and tumor-suppressing effects as compared with combined PD-1 and CTLA-4 inhibition in our model of TNBC. Consequently, targeting interactions between platelets and immune cells might represent a promising treatment strategy for TNBC without the side effects of systemic ICI. In line with this assumption, we showed that blockade of the platelet receptor GPIIb/IIIa nearly reached the immunomodulatory effects of platelet depletion or combined PD-1 and CTLA-4 inhibition in experimental TNBC. This

approach might be particularly beneficial in individual tumors lacking tumor cell expression of IC molecules,⁴⁰ in which platelets primarily deliver these molecular factors to malignant lesions, and in paraneoplastic thrombocytosis⁵⁵ as GPIIb additionally supports thrombopoietin-dependent platelet production.⁵⁶ Of note, antiplatelet strategies might enhance the risk of hemorrhage, albeit they do not exhibit the severe or life-threatening autoimmune-related adverse effects observed in ICI-treated patients.⁴ Although hereditary GPIIb or von Willebrand factor defects associate with severe bleeding episodes,^{57,58} pharmacological GPIIb blockade might be safe as it does not increase the risk of intracranial hemorrhage in experimental cerebral ischemia,^{52,59} in contrast to conventional antiplatelet drugs and besides targeting procoagulant platelet activation via GPVI, cyclophilin D, or transmembrane protein 16F.

In conclusion, our findings uncover a previously unrecognized immunomodulatory activity of procoagulant platelets in the tumor microvasculature that concurrently promotes protumorigenic myeloid immune cell responses and impedes anti-tumorigenic T-cell activity, thus supporting TNBC progression. Targeting this self-sustaining mechanism of such malignant neoplasms effectively interferes with their expansion, hence providing a novel strategy to counteract immune evasion in TNBC without the side effects of systemic ICI.

Acknowledgments

The authors thank Claudia Fahney for excellent technical assistance.

This study was supported by Deutsche Forschungsgemeinschaft, Sonderforschungsbereich 914, projects B03 (C.A.R.) and B06 (K.L.), and Fritz-Bender-Stiftung (C.A.R.; B.U.).

Data presented in this article are part of the doctoral thesis of J.B.S. and B.S.

Authorship

Contribution: J.B.S., F.H., B.S., Z.W., A.U., K.S., S.B., S.M., J.L., V.S., J.H., M.C., L.A.M., C.B., G.Z., and M.M. performed the experiments and contributed to data analysis and interpretation; R.K., L.N., W.W., K.L., B.U., and C.A.R. wrote the manuscript; C.A.R. conceived and supervised the study; and all authors read and approved the manuscript.

Conflict-of-interest disclosure: The authors declare no competing financial interests.

ORCID profiles: K.S., 0000-0002-7269-5433; S.M., 0009-0002-8372-6562; R.K., 0000-0003-1750-3395; L.N., 0000-0003-0776-5885; M.M., 0000-0002-3157-7262; C.A.R., 0000-0003-2145-0388.

Correspondence: Christoph A. Reichel, Walter Brendel Centre of Experimental Medicine, Department of Otorhinolaryngology, and Comprehensive Cancer Center, Munich Ludwig-Maximilians-Universität Hospital, Marchioninistr 15, D-81377 Munich, Germany; email: christoph.reichel@med.uni-muenchen.de.

Footnotes

Submitted 16 October 2023; accepted 8 April 2024; prepublished online on *Blood* First Edition 22 April 2024. <https://doi.org/10.1182/blood.2023022928>.

*J.B.S., B.S., and F.H. are joint first authors.

†B.U. and C.A.R. are joint senior authors.

Original data are available upon reasonable request from the corresponding author, Christoph A. Reichel (christoph.reichel@med.uni-muenchen.de).

The online version of this article contains a data supplement.

There is a [Blood Commentary](#) on this article in this issue.

The publication costs of this article were defrayed in part by page charge payment. Therefore, and solely to indicate this fact, this article is hereby marked "advertisement" in accordance with 18 USC section 1734.

REFERENCES

- Loibl S, Poortmans P, Morrow M, Denkert C, Curigliano G. Breast cancer. *Lancet*. 2021; 397(10286):1750-1769.
- Waldman AD, Fritz JM, Lenardo MJ. A guide to cancer immunotherapy: from T cell basic science to clinical practice. *Nat Rev Immunol*. 2020;20(11):651-668.
- Emens LA, Molinero L, Loi S, et al. Atezolizumab and nab-paclitaxel in advanced triple-negative breast cancer: biomarker evaluation of the IMpassion130 Study. *J Natl Cancer Inst*. 2021;113(8):1005-1016.
- Martins F, Sofiya L, Sykiotis GP, et al. Adverse effects of immune-checkpoint inhibitors: epidemiology, management and surveillance. *Nat Rev Clin Oncol*. 2019;16(9):563-580.
- Dixon-Douglas J, Loibl S, Denkert C, Telli M, Loi S. Integrating immunotherapy into the treatment landscape for patients with triple-negative breast cancer. *Am Soc Clin Oncol Educ Book*. 2022;42:1-13.
- Coffelt SB, Wellenstein MD, de Visser KE. Neutrophils in cancer: neutral no more. *Nat Rev Cancer*. 2016;16(7):431-446.
- Hedrick CC, Malanchi I. Neutrophils in cancer: heterogeneous and multifaceted. *Nat Rev Immunol*. 2022;22(3):173-187.
- Ho-Tin-Noe B, Goerge T, Wagner DD. Platelets: guardians of tumor vasculature. *Cancer Res*. 2009;69(14):5623-5626.
- Haemmerle M, Stone RL, Menter DG, Afshar-Kharghan V, Sood AK. The platelet lifeline to cancer: challenges and opportunities. *Cancer Cell*. 2018;33(6):965-983.
- Gaertner F, Massberg S. Patrolling the vascular borders: platelets in immunity to infection and cancer. *Nat Rev Immunol*. 2019; 19(12):747-760.
- Xu XR, Yousef GM, Ni H. Cancer and platelet crosstalk: opportunities and challenges for aspirin and other antiplatelet agents. *Blood*. 2018;131(16):1777-1789.
- Li R, Ren M, Chen N, et al. Presence of intratumoral platelets is associated with tumor vessel structure and metastasis. *BMC Cancer*. 2014;14:167.
- Haemmerle M, Bottsford-Miller J, Pradeep S, et al. FAK regulates platelet extravasation and tumor growth after antiangiogenic therapy withdrawal. *J Clin Invest*. 2016; 126(5):1885-1896.
- Zamora C, Canto E, Nieto JC, et al. Binding of platelets to lymphocytes: a potential anti-inflammatory therapy in rheumatoid arthritis. *J Immunol*. 2017;198(8):3099-3108.
- Haemmerle M, Taylor ML, Gutschner T, et al. Platelets reduce anoikis and promote metastasis by activating YAP1 signaling. *Nat Commun*. 2017;8(1):310.
- Michael JV, Wurtzel JGT, Mao GF, et al. Platelet microparticles infiltrating solid tumors transfer miRNAs that suppress tumor growth. *Blood*. 2017;130(5):567-580.
- Varon D, Shai E. Role of platelet-derived microparticles in angiogenesis and tumor progression. *Discov Med*. 2009;8(43): 237-241.

18. Labelle M, Begum S, Hynes RO. Direct signaling between platelets and cancer cells induces an epithelial-mesenchymal-like transition and promotes metastasis. *Cancer Cell*. 2011;20(5):576-590.
19. Boucharaba A, Serre CM, Gres S, et al. Platelet-derived lysophosphatidic acid supports the progression of osteolytic bone metastases in breast cancer. *J Clin Invest*. 2004;114(12):1714-1725.
20. Nieswandt B, Hafner M, Echtenacher B, Mannel DN. Lysis of tumor cells by natural killer cells in mice is impeded by platelets. *Cancer Res*. 1999;59(6):1295-1300.
21. Placke T, Orgel M, Schaller M, et al. Platelet-derived MHC class I confers a pseudonormal phenotype to cancer cells that subverts the antitumor reactivity of natural killer immune cells. *Cancer Res*. 2012;72(2):440-448.
22. Rachidi S, Metelli A, Riesenberger B, et al. Platelets subvert T cell immunity against cancer via GARP-TGFbeta axis. *Sci Immunol*. 2017;2(11):eaai7911.
23. Joseph R, Soundararajan R, Vasaikar S, et al. CD8(+) T cells inhibit metastasis and CXCL4 regulates its function. *Br J Cancer*. 2021;125(2):176-189.
24. Ho-Tin-Noe B, Goerge T, Cifuni SM, Duerschmied D, Wagner DD. Platelet granule secretion continuously prevents intratumor hemorrhage. *Cancer Res*. 2008;68(16):6851-6858.
25. Algra AM, Rothwell PM. Effects of regular aspirin on long-term cancer incidence and metastasis: a systematic comparison of evidence from observational studies versus randomised trials. *Lancet Oncol*. 2012;13(5):518-527.
26. Rothwell PM, Fowkes FG, Belch JF, Ogawa H, Warlow CP, Meade TW. Effect of daily aspirin on long-term risk of death due to cancer: analysis of individual patient data from randomised trials. *Lancet*. 2011;377(9759):31-41.
27. Patrignani P, Patrono C. Aspirin and cancer. *J Am Coll Cardiol*. 2016;68(9):967-976.
28. Cho MS, Noh K, Haemmerle M, et al. Role of ADP receptors on platelets in the growth of ovarian cancer. *Blood*. 2017;130(10):1235-1242.
29. Agbani EO, Poole AW. Procoagulant platelets: generation, function, and therapeutic targeting in thrombosis. *Blood*. 2017;130(20):2171-2179.
30. Josefsson EC, Ramstrom S, Thaler J, Lordkipanidze M; COAGAPO study group. Consensus report on markers to distinguish procoagulant platelets from apoptotic platelets: communication from the Scientific and Standardization Committee of the ISTH. *J Thromb Haemost*. 2023;21(8):2291-2299.
31. Kaiser R, Escaig R, Kranich J, et al. Procoagulant platelet sentinels prevent inflammatory bleeding through GPIIb/IIIa and GPVI. *Blood*. 2022;140(2):121-139.
32. Sreeramakumar V, Adrover JM, Ballesteros I, et al. Neutrophils scan for activated platelets to initiate inflammation. *Science*. 2014;346(6214):1234-1238.
33. Rossaint J, Kuhne K, Skupski J, et al. Directed transport of neutrophil-derived extracellular vesicles enables platelet-mediated innate immune response. *Nat Commun*. 2016;7:13464.
34. Zuchtriegel G, Uhl B, Puh-Westerheide D, et al. Platelets guide leukocytes to their sites of extravasation. *PLoS Biol*. 2016;14(5):e1002459.
35. Pelka K, Shibata T, Miyake K, Latz E. Nucleic acid-sensing TLRs and autoimmunity: novel insights from structural and cell biology. *Immunol Rev*. 2016;269(1):60-75.
36. Diacovo TG, Puri KD, Warnock RA, Springer TA, von Andrian UH. Platelet-mediated lymphocyte delivery to high endothelial venules. *Science*. 1996;273(5272):252-255.
37. Iannacone M, Sitia G, Isogawa M, et al. Platelets mediate cytotoxic T lymphocyte-induced liver damage. *Nat Med*. 2005;11(11):1167-1169.
38. Guidotti LG, Inverso D, Sironi L, et al. Immunosurveillance of the liver by intravascular effector CD8(+) T cells. *Cell*. 2015;161(3):486-500.
39. Rolfes V, Idel C, Pries R, et al. PD-L1 is expressed on human platelets and is affected by immune checkpoint therapy. *Oncotarget*. 2018;9(44):27460-27470.
40. Zaslavsky AB, Adams MP, Cao X, et al. Platelet PD-L1 suppresses anti-cancer immune cell activity in PD-L1 negative tumors. *Sci Rep*. 2020;10(1):19296.
41. Hinterleitner C, Strahle J, Malenke E, et al. Platelet PD-L1 reflects collective intratumoral PD-L1 expression and predicts immunotherapy response in non-small cell lung cancer. *Nat Commun*. 2021;12(1):7005.
42. Srikrishna G, Freeze HH. Endogenous damage-associated molecular pattern molecules at the crossroads of inflammation and cancer. *Neoplasia*. 2009;11(7):615-628.
43. Pradere JP, Dapito DH, Schwabe RF. The Yin and Yang of Toll-like receptors in cancer. *Oncogene*. 2014;33(27):3485-3495.
44. Li J, Karakas D, Xue F, et al. Desialylated platelet clearance in the liver is a novel mechanism of systemic immunosuppression. *Research (Wash D C)*. 2023;6:0236.
45. Roweth HG, Malloy MW, Goreczny GJ, et al. Pro-inflammatory megakaryocyte gene expression in murine models of breast cancer. *Sci Adv*. 2022;8(41):eabo5224.
46. Long Y, Wang T, Gao Q, Zhou C. Prognostic significance of pretreatment elevated platelet count in patients with colorectal cancer: a meta-analysis. *Oncotarget*. 2016;7(49):81849-81861.
47. Gao L, Zhang H, Zhang B, Zhang L, Wang C. Prognostic value of combination of preoperative platelet count and mean platelet volume in patients with resectable non-small cell lung cancer. *Oncotarget*. 2017;8(9):15632-15641.
48. Zhang M, Huang XZ, Song YX, Gao P, Sun JX, Wang ZN. High platelet-to-lymphocyte ratio predicts poor prognosis and clinicopathological characteristics in patients with breast cancer: a meta-analysis. *BioMed Res Int*. 2017;2017:9503025.
49. Sims GP, Rowe DC, Rietdijk ST, Herbst R, Coyle AJ. HMGB1 and RAGE in inflammation and cancer. *Annu Rev Immunol*. 2010;28:367-388.
50. Theoret JF, Yacoub D, Hachem A, Gillis MA, Merhi Y. P-selectin ligation induces platelet activation and enhances microaggregate and thrombus formation. *Thromb Res*. 2011;128(3):243-250.
51. Frega G, Wu Q, Le Naour J, et al. Trial Watch: experimental TLR7/TLR8 agonists for oncological indications. *Oncoimmunology*. 2020;9(1):1796002.
52. Wykes MN, Lewin SR. Immune checkpoint blockade in infectious diseases. *Nat Rev Immunol*. 2018;18(2):91-104.
53. Mittmann LA, Haring F, Schaubacher JB, et al. Uncoupled biological and chronological aging of neutrophils in cancer promotes tumor progression. *J Immunother Cancer*. 2021;9(12):e003495.
54. Uhl B, A Mittmann L, Dominik J, et al. uPA-PAI-1 heteromerization promotes breast cancer progression by attracting tumorigenic neutrophils. *EMBO Mol Med*. 2021;13(6):e13110.
55. Stone RL, Nick AM, McNeish IA, et al. Paraneoplastic thrombocytosis in ovarian cancer. *N Engl J Med*. 2012;366(7):610-618.
56. Xu M, Li J, Neves MAD, et al. GPIIb/alpha is required for platelet-mediated hepatic thrombopoietin generation. *Blood*. 2018;132(6):622-634.
57. McEwan PA, Yang W, Carr KH, et al. Quaternary organization of GPIb-IX complex and insights into Bernard-Soulier syndrome revealed by the structures of GPIIb/IIIa and GPIIb/IIIa chimera. *Blood*. 2011;118(19):5292-5301.
58. Sharma R, Flood VH. Advances in the diagnosis and treatment of von Willebrand disease. *Hematology Am Soc Hematol Educ Program*. 2017;2017(1):379-384.
59. Kleinschnitz C, Pozgajova M, Pham M, Bendszus M, Nieswandt B, Stoll G. Targeting platelets in acute experimental stroke: impact of glycoprotein Ib, VI, and IIb/IIIa blockade on infarct size, functional outcome, and intracranial bleeding. *Circulation*. 2007;115(17):2323-2330.

© 2024 American Society of Hematology. Published by Elsevier Inc. All rights are reserved, including those for text and data mining, AI training, and similar technologies.

SUPPLEMENTAL DATA

Supplemental Methods

Ethics

All animal experiments were performed according to German law for animal protection and approved by the local government authorities ('Regierung von Oberbayern').

Animals

Female BALB/c mice, male C57BL/6NCrl mice, and male C3H/HeN mice (age 6-8 weeks, body weight 15-18 g) were purchased from Charles River (Sulzfeld, Germany). C57BL/6J and PF4cre mice were purchased from The Jackson Laboratory and maintained at our animal facility. The TMEM16F^{fl/fl} line was provided by the RIKEN BioResource Center (BRC) through the National BioResource Project of the Ministry of Education, Culture, Sports, Science, and Technology (MEXT)/Agency for Medical Research and Development (Japan). The platelet- and megakaryocyte-specific TMEM16F-deficient (Pf4cre-TMEM16F^{fl/fl}) line has been phenotyped by the authors previously.¹ Animals were kept under conventional conditions (22±2°C, 30-60% humidity, 12h light/dark cycle, lights on at 7am) with free access to water and food.

Anesthesia

For all experimental procedures, mice were anaesthetized intra-peritoneally (i.p.) with a ketamine/xylazine mixture (100mg/kg ketamine and 10mg/kg xylazine) and kept on a heating plate at 37°C.

M. cremaster assay

For the surgical preparation of the mouse cremaster muscle, anesthetized mice were kept on a heating plate at 37°C and the cremaster muscle was superfused with warm buffered saline. Animals received a catheter (Smiths Medical International Ltd, Hythe, Kent, UK) for the application of antibodies and microspheres in the left femoral artery. Afterwards, the right cremaster muscle was opened by a ventral incision of the scrotum and bleeding was stopped by careful electrocautery as described previously with minor modifications.² The epididymis and testicles were placed back into the abdominal cavity after detaching them from the cremaster muscle. The cremaster muscle was then spread over the pedestal of a custom-made microscopy stage. During surgical preparation and the entire course of the experiment, the muscle was superfused with warm buffered saline.

Inflammation in the mouse cremaster muscle was induced by superfusion of the endosomal TLR agonists poly(I:C) (TLR3), CL264 (TLR7), TL8-506 (TLR8), or ODN2395 (TLR9) (100µg in 900µl saline; InvivoGen, San Diego, CA, USA). Videos were recorded at baseline conditions directly prior to stimulation as well as 30, 60, 90, 120, 150, and 180min after induction of inflammation.

In vivo microscopy

For *in vivo* microscopy, an AxioTech-Vario 100 Microscope (Zeiss MicroImaging GmbH, Goettingen, Germany) with a Colibri LED light source (Zeiss) for fluorescence epi-illumination microscopy was employed. Videos were acquired by an AxioCam Hsm digital camera and a 20x or 40x water immersion lens (0.5 NA, Zeiss). For processing the videos, the software AxioVision 4.6 (Zeiss) was used. Video analysis was performed by the software ImageJ (National Institutes of Health, Bethesda, MD, USA).

For the analysis of intravascular blood cell interactions, animals received an intravenous injection of fluorescence-labeled anti-CD115 mAb (clone AFS98; eBioscience, San Diego, CA, USA), anti-Ly6G/Ly6C mAb (clone RB6-8C5; Biolegend, San Diego, CA, USA), anti-GPIIbβ mAb (emfret, Eibelstadt, Germany), anti-CD4 mAb (CD4⁺ lymphocytes; clone RM4-5,

Biolegend), anti-CD8 mAb (CD8⁺ lymphocytes; clone 53-6.7, Biolegend), or anti-CD19 mAb (B lymphocytes; clone 6D5, Biolegend). Neutrophils were identified as Gr-1⁺ CD115⁻ cells, classical monocytes (cMOs) as Gr-1⁺ CD115⁺ cells, and non-classical monocytes (ncMOs) as Gr-1⁻ CD115⁺ cells. Rolling cells were defined as cells moving slower than the associated blood flow and quantified for 60s per venule. Firmly adherent cells were defined as cells resting in the associated blood flow for >30s and quantified per 100µm vessel length.

Confocal microscopy

Male C57BL/6NCrl mice received an intrascrotal injection of 5µg of CL264 (TLR7 agonist), TL8-506 (TLR8 agonist), and ODN2395 (TLR9 agonist) in 50µl saline (InvivoGen). After 6 hours, the cremaster muscles were excised. Subsequently, tissues were immunostained with fluorescence-labeled monoclonal antibodies directed against ICAM-1/CD54 (clone YN1/1.7.4; Biolegend), PECAM-1/CD31 (clone MEC13.3; Biolegend), F4/80 (clone BM8; Biolegend), CD106/VCAM-1 (clone 429 (MVCAN.A); Biolegend), CD62P/P-Selectin (clone Wug.E9; Emfret), and CD62E/E-Selectin (clone, 10-E9.6; BD Bioscience). Digital images were acquired by a Zeiss LSM 880 confocal microscope. Using Fiji ImageJ, mean fluorescence intensity for ICAM-1/CD54, VCAM-1/CD106, P-selectin/CD62P, and E-selectin/CD62E in PECAM-1/CD31⁺ endothelial cells was determined with respect to the distance (<25 µm vs. >25µm) of analyzed endothelial cells to F4/80⁺ perivascular macrophages in the digital images.

Experimental groups

In a first set of experiments, animals received intravenous injections of 50µg of platelet-depleting anti-GPIIbα mAb (CD42d; clone R300; emfret) or isotype control antibodies 48 h, 24 h, and 5 min prior to induction of inflammation for the induction of thrombocytopenia, according to previously published protocols ³. For the induction of neutropenia, 50µg of neutrophil-depleting anti-Ly6G mAb (clone 1A8; BioXcell, Lebanon, NH, USA) was injected intravenously

into mice 24 h and 6 h prior to induction of inflammation according to previously published protocols³. In further experiments, animals received intravenous injections of 50 µg of blocking antibodies directed against PD-1 (clone 29F.1A12; Biolegend) and CTLA-4 (clone 9H10; Biolegend), CD40 (clone 1C10; Biolegend) and CD40L (clone MR1; Biolegend), or isotype control antibodies 5min prior to induction of inflammation (n=5 per group).

Peritonitis assay

Inflammation of the peritoneal cavity was induced by an intraperitoneal injection of the endosomal TLR agonists poly(I:C) (TLR3), CL264 (TLR7), TL8-506 (TLR8), or ODN2395 (TLR9; 100µg in 200µl saline; InvivoGen). After 6h, the peritoneal cavity was flushed with 15ml ice-cold saline before the cell count was determined in the peritoneal lavage fluid using a ProCyte Hematology analyzer (IDEXX, Westbrook, ME, USA).

The lavage fluid was incubated for 30min on ice in the dark with fluorescence-labeled anti-CD45 mAb (clone 30-F11; BD Bioscience, San Jose, CA, USA), anti-CD11b mAb (clone M1/70; eBioscience), anti-Gr-1 mAb (clone RB6-8C5; eBioscience), anti-F4/80 mAb (clone BM8; eBioscience), anti-CD115 mAb (clone AFS98; eBioscience), anti-CD19 mAb (clone eBio1D3; eBioscience), anti-CD3 mAb (clone 17A2; Biolegend), anti-CD4a mAb (clone GK1.5; eBioscience), and anti-CD8a mAb (clone 53-6.7; eBioscience). After the lysis of erythrocytes (addition of 1ml lysing solution per sample; 1:10; BD FACS lysing solution; BD Bioscience) for 10min on ice in the dark, samples were washed with 1ml saline. Finally, the cell pellet was re-suspended for flow cytometry analysis in 200µl saline (**Fig. S20**).

Flow cytometry

Flow cytometry was performed using a Gallios flow cytometer (Beckman Coulter Inc, Brea, CA, USA) and data was analyzed by the software FlowJo (Treestar, Ashland, OR, USA). Myeloid leukocytes were identified by the expression of CD45 and CD11b. Thereof, neutrophils

(Gr-1^{high} CD115⁻ F4/80⁻), cMOs (Gr-1^{high} CD115⁺ F4/80⁺), and ncMOs (Gr-1^{low} CD115⁺ F4/80⁺) were further subdivided. CD4⁺ lymphocytes were characterized as CD45⁺ CD11b⁻ CD3⁺ CD4⁺ cells and CTLs as CD45⁺ CD11b⁻ CD3⁺ CD8a⁺ cells. B cells were identified as CD45⁺ CD11b⁻ CD19⁺ cells. In selected experiments, CD4⁺ T lymphocytes were further differentiated into T-bet⁺ Th1 cells, GATA3⁺ Th2 cells, FOXP3 T_{reg} cells (**Fig. S20**).

Experimental groups

In a first set of experiments, animals received intravenous injections of 50µg of platelet-depleting anti-GPIb α mAb (CD42d; clone R300; emfret) or isotype control antibodies 48h, 24h, and 5min prior to induction of inflammation according to previously published protocols ³. For the induction of neutropenia, 50µg of neutrophil-depleting anti-Ly6G mAb (clone 1A8; BioXell, Lebanon, NH, USA) was injected intravenously into mice 24h and 6h prior to induction of inflammation according to previously published protocols ³. In further experiments, animals received an intravenous injection of 50µg blocking anti-CD40 mAb (clone 1C10; Biolegend) and anti-CD40L mAb (clone MR1; Biolegend), anti-PD-1 mAb (clone 29D.1A12; Biolegend) and anti-CTLA-4 mAb (clone UC10-4B9; Biolegend), or isotype control antibodies 5min prior to induction of inflammation (n=3-4 per group).

Cell lines

The 4T1 mammary carcinoma cell line (native or TdTomato-transduced) and the SCC VII head and neck squamous cell carcinoma (HNSCC) cell line, received from Kirsten Lauber (Department of Radiotherapy and Radiation Oncology, LMU University Hospital, Munich, Germany), were cultured at 37 °C and 5% CO₂ in RPMI media (Thermo Fisher Scientific, Waltham, MA, USA), supplemented with 10% FBS (Biochrom, Berlin, Germany) and 1% HEPES (PromoCell, Heidelberg, Germany). Mouse microvascular endothelial cells (bEnd.3)

and RAW 264.7 macrophages were purchased from ATCC (Manassas, VA, USA) and cultured at 37°C and 5% CO₂ in DMEM media (ATCC), supplemented with 10% FBS.

Orthotopic TNBC model

Immunotherapy in breast cancer patients is currently used for the treatment of TNBC. We therefore focused on analyses in a fully immunocompetent syngeneic mouse model of TNBC employing the well-established transplantable 4T1 tumor model. At baseline conditions (day 0), female BALB/c mice received an injection of 2×10^5 4T1 cells/20 μ l into the left mammary fat pad. At day 14 after tumor cell injection, tumors – and in selected experiments: organs – were explanted and their weight and size were measured by a special accuracy weighting machine (Mettler-Toledo, Columbus, OH, USA) and a caliper gauge (Mitutoyo Corporation, Kawasaki, Japan).

Flow cytometry

Harvested tumors were subsequently homogenized with a homogenizer (8ml; Schuett biotec GmbH, Göttingen, Germany) in 15ml saline. After incubation with fluorescence-labeled anti-CD45 mAb (clone 30-F11; BD Bioscience), anti-CD11b mAb (clone M1/70; eBioscience), anti-Gr-1 mAb (clone RB6-8c5; eBioscience), anti-F4/80 mAb (clone BM8; eBioscience), anti-CD115 mAb (clone AFS98; eBioscience), anti-CD19 mAb (clone eBio1D3; eBioscience), anti-CD8a mAb (clone 53-6.7; eBioscience), anti-CD3 mAb (clone 17A2; Biolegend), and anti-CD4a mAb (clone GK1.5; eBioscience) for 30 min on ice in the dark the flow cytometry analysis (Gallios, Beckman Coulter Inc) was performed.

In separate experiments, cells were incubated with anti-CD45 mAb (clone 30-F11; BD Bioscience), anti-CD3 mAb (clone 17A2; Biolegend), anti-CD4 mAb (clone GK1.5; eBioscience), anti-CD62L mAb (clone MEL14; eBioscience), anti-CD44 mAb (clone IM7; Biolegend), anti-T-bet mAb (clone O4-46; BD Pharmingen; Franklin Lakes, NJ, USA), anti-

GATA-3 mAb (clone L50-823; BD Pharmingen), anti-FOXP3 mAb (clone MF23; BD Pharmingen), anti-IL-9 mAb (clone RM9A4, BioLegend), anti-IL-17 mAb (clone TC11-18H 10.1, BioLegend), or anti-IL-22 mAb (Poly5164, BioLegend). Here, Th1 cells were identified as CD45⁺ CD3⁺ CD4⁺ T-bet⁺, Th2 cells as CD45⁺ CD3⁺ CD4⁺ GATA-3⁺, T_{reg} cells as CD45⁺ CD3⁺ CD4⁺ FOXP3⁺ cells, Th9 cells as CD45⁺ CD3⁺ CD4⁺ IL-9⁺ cells, Th17 cells as CD45⁺ CD3⁺ CD4⁺ IL-17⁺ cells, and Th22 cells as CD45⁺ CD3⁺ CD4⁺ IL-22⁺ cells (**Fig. S20**).

For the characterization of different platelet subsets, tumor homogenates were incubated with fluorescence-labeled anti-CD41 mAb (clone MWRReg30, BioLegend), Annexin V (BioLegend), and anti-P-selectin/CD62P mAb (clone RMP-1, BioLegend). Pro-coagulant platelets were identified as CD41⁺ Annexin V^{high} cells, aggregatory platelets as CD41⁺ Annexin V^{low} CD62P⁺ cells, and resting platelets as CD41⁺ Annexin V^{low} CD62P⁻ cells by flow cytometry (**Fig. S20**). In selected experiments, thiazole orange (Sigma Aldrich) staining of platelets was performed as a measure of the intracellular nucleic acid content. To analyze the sialylation of platelets, staining with Ricinus Communis Agglutinin I (RCA I), Fluorescein (VEC-FL-1081-5, Biozol) was employed.

Confocal microscopy

To evaluate the co-localization of platelets and collagen in the aberrant tumor microvasculature as well as in the peritumoral microvasculature, tumor sample sections were immunostained with anti-CD41 mAb (clone MWRReg30, BioLegend), anti-CD31/PECAM-1 mAb (clone MEC13.3, BioLegend), and anti-collagen I mAb (ITM3765-50µg-488, G-Biosciences). Digital images were acquired by a Zeiss LSM 880 confocal microscope. Using Fiji ImageJ, the proportion of CD41⁺ platelets co-localizing with collagen I of total platelets in CD31⁺ microvessels was determined.

Experimental groups

In a first set of experiments, animals received intravenous injections of ODN2088 (InvivoGen), control oligonucleotides, the ADP receptor P2Y₁₂ antagonist ticagrelor (600µg i.p., twice daily; Sigma Aldrich), the GPIIb/IIIa inhibitor tirofiban (0.5mg/kg BW i.p., every 24 hours, Sigma Aldrich), or drug vehicle 5 min prior to tumor cell implantation and further on every other day (n=5-6 per group). In additional experiments, animals received intravenous injections of 50 µg of platelet-depleting antibodies (anti-GPIb α ; clone R300, emfret), neutrophil-depleting anti-Ly-6G mAb (clone 1A8; BioXCell, Lebanon, NH, USA), classical monocyte-depleting anti-CCR2 mAb (clone MC-21, provided by Matthias Mack, University of Regensburg, Germany), CTL-depleting anti-CD8a mAb (clone 2.43; BioXCell, Lebanon, NH, USA), anti-GPVI mAb (2mg/kg BW every 72 hours i.p.; clone JAQ1, emfret), or isotype control antibodies 5 min prior to tumor cell implantation and further on every other day (n=5 per group). In further experiments, animals received intravenous injections of 50 µg of blocking monoclonal antibodies directed against PD-1 (clone 29F.1A12; Biolegend) and CTLA-4 (clone 9H10; Biolegend), GPIb α (clone Xia.B2; emfret), or isotype control antibodies 5 min prior to tumor cell implantation and further on every other day (n=5 per group). These experiments were repeated in animals receiving the treatments starting from day 7 after tumor cell injection (n=4 per group).

In separate experiments, platelets from female BALB/c mice or 4T1 tumor cells were incubated with platelet-depleting (1µg, clone R300; emfret) or blocking (1µg, clone Xia.B2; emfret) anti-GPIb α mAb for 30min at 37°C. Subsequently, cells were immunostained with a fluorescence-labeled anti-CD41 mAb (clone MWRReg30, Biolegend) and a secondary differentially fluorescence-labeled goat anti-rat antibody (Invitrogen). Antibody binding to CD41⁺ platelets or 4T1 tumor cells was analyzed by flow cytometry.

In selected experiments, blood, bone marrow, spleen, liver, lungs, kidneys, brain, and tumor were harvested for the quantification of splenic megakaryocyte content (CD42d, clone 1C2, Biolegend), of tumor cell metastasis formation, and/or related (procoagulant/non-procoagulant) platelet / immune cell content in peripheral organs, as well as of primary tumor

cell expression of Ki-67 (clone SolA, Thermo Fisher), EpCAM (clone G8.8, Biolegend), uptake of NucBlue (R37605, Invitrogen), CD80 (clone 1610A1, Biolegend), CD86 (clone GL-1, Biolegend), and PD-L1 (clone 10F.9G2) 14 days after injection of tdTomato-transduced tumor cells into the mammary fat pad (analyzed by flow cytometry) in animals receiving intravenous injections of 50 µg of platelet-depleting antibodies (anti-GPIb α ; clone R300, emfret) or isotype control antibodies (n=3-4 per group).

Heterotopic tumor model

Although our heterotopic TNBC model in the mouse auricle generates a different tissue environment than the usual tissue environment in the mammary fat pad, this experimental approach was employed for *in vivo* microscopy analyses since in the orthotopic TNBC model such real-time analyses are beyond today's technical limitations. At baseline conditions (day 0), female BALB/c mice received a subcutaneous injection of 10⁵ 4T1 cells/10 µl or saline into the left auricle. On day 1, 7, and 14 after tumor cell injection, *in vivo* microscopy analyses of blood cell interactions in the tumoral and peritumoral (within a distance of 250 µm to the tumor boundaries) microvasculature were performed.

In vivo microscopy

For *in vivo* microscopy, an AxioTech-Vario 100 Microscope (Zeiss MicroImaging GmbH, Goettingen, Germany) with a Colibri LED light source (Zeiss) for fluorescence epi-illumination microscopy was employed. Videos were acquired by an AxioCam Hsm digital camera and a 20x or 40x water immersion lens (0.5 NA, Zeiss). For processing the videos, the software AxioVision 4.6 (Zeiss) was used. Video analysis was performed by the software ImageJ (National Institutes of Health, Bethesda, MD, USA).

For the analysis of intravascular blood cell interactions, animals received an intravenous injection of fluorescence-labeled anti-CD115 mAb (clone AFS98; eBioscience, San Diego, CA,

USA), anti-Ly6G/Ly6C mAb (clone RB6-8C5; Biolegend, San Diego, CA, USA), anti-GPIIb β mAb (emfret, Eibelstadt, Germany), anti-CD4 mAb (CD4⁺ lymphocytes; clone RM4-5, Biolegend), anti-CD8 mAb (CD8⁺ lymphocytes; clone 53-6.7, Biolegend), or anti-CD19 mAb (B lymphocytes; clone 6D5, Biolegend). In selected experiments, animals received an intravenous injection of an anti-MFG-E8 mAb (Santa Cruz Biotechnology, Dallas, TX, USA) for the differentiation of procoagulant and aggregatory platelets. Neutrophils were identified as Gr-1⁺ CD115⁻ cells, classical monocytes (cMOs) as Gr-1⁺ CD115⁺ cells, and non-classical monocytes (ncMOs) as Gr-1⁻ CD115⁺ cells. Rolling cells were defined as cells moving slower than the associated blood flow and quantified for 60s per venule. Firmly adherent cells were defined as cells resting in the associated blood flow for >30s, quantified per 100 μm vessel length, and calculated per μm^2 endothelial cell surface area.

Experimental groups

In a first set of experiments, animals received intravenous injections of ODN2088 (InvivoGen) or control oligonucleotides 5 min prior to tumor cell implantation and further on every other day (n=5 per group). In separate experiments, propidium Iodide (200 μl of 1mg/ml in saline; Sigma Aldrich) was injected intravenously for the visualization of extracellular nucleic acids. The mean fluorescence intensity was measured by Fiji ImageJ software (National Institutes of Health). In additional experiments, tumor vascularization was visualized on day 14 after tumor cell injection by *in vivo* fluorescence microscopy 5 min after intravenous application of FITC dextran (molecular weight 2.000 kDa; Sigma-Aldrich; n=3 per group) in animals receiving intravenous injections of 50 μg of platelet-depleting antibodies (anti-GPIIb α , clone R300, emfret) or isotype control antibodies every other day starting from day 0 after tumor cell injection.

The architecture of the microvasculature was analyzed using the Skeleton plugin of the imaging software Fiji. Briefly, by generating skeletonized maps of the vessel network, this plugin is able to determine the number of branches and junctions as well as the average branch

length of the high-power field. The vessel density was characterized as the number of branches multiplied by the average branch length / area of the high-power field.

Confocal microscopy

For confocal microscopy analyses, tumor-bearing ears were excised on day 14 after tumor cell injection, before carefully removing the epidermis. After fixation for 10min in 4% paraformaldehyde (PFA), the tissue was washed three times with PBS and blocked/permeabilized with PBS supplemented with 2% bovine serum albumin (BSA; Sigma Aldrich) and 0.5% Triton X-100 (Sigma Aldrich) for 2h. Subsequently, the tissue was incubated at 4°C for 24h with fluorescence-labeled monoclonal antibodies directed against GP1b β (emfret) and Mac-1/CD11b (BV421; clone M1/70; Biolegend). In addition, liver, kidneys, lungs, and brain of tumor-bearing mice were harvested, embedded in TissueTek (Sakura Finetek), and frozen using dry ice. Next, the organs were cut into 50 μ m slices employing a Histology Cryostat (Eprexia CryoSta NX70; Thermo Fisher Scientific), put on glass slides and fixed in 4% PFA for 10min. The slices were then washed three times with PBS and blocked with 2% BSA in PBS for 60min at 4°C. After another washing step with PBS, the samples were immunostained as described above.

For the analysis of the surface expression of ICAM-1/CD54 on microvascular endothelial cells, mouse cremaster muscles of male BALB/c mice were excised 6h after intrascrotal injection of agonists of TLR7, -8, -9 (100 μ g in 200 μ l saline; InvivoGen), TNF (300ng in 200 μ l saline; Biolegend), or vehicle. Subsequently, tissues were immunostained using the above detailed protocol with fluorescence-labeled monoclonal antibodies directed against ICAM-1/CD54 (clone YN1/1.7.4; Biolegend), PECAM-1/CD31 (clone MEC13.3; Biolegend), and CD45 (clone 30-F11; Invitrogen). In separate experiments, the expression/deposition of GPIb α and vWF on platelets and T cells isolated from the peripheral blood of BALB/c mice was analyzed in blood smears immunostained with antibodies directed against GPIb α /CD42b (clone 1C2; Biolegend), CD3 (clone 17A2; Biolegend), and vWF (primary rabbit polyclonal antibody; Novus

Biologicals, Centennial, Colorado, USA; secondary fluorescence-labeled anti-rabbit polyclonal antibodies; Invitrogen, Waltham, MA, USA).

Immunostained samples were mounted in PermaFluor (Beckman Coulter, Fullerton, CA, USA) and covered by cover glasses. Z-stacks typically covering 30µm (z-spacing 0.2µm; objective magnification 20 x) were acquired using a confocal laser-scanning microscope (LSM 880 with Airyscan; Zeiss) and all images were analyzed with Fiji ImageJ software (National Institutes of Health, Bethesda, Maryland, USA).

Phenotypic properties of platelets

For the characterization of platelets, peripheral blood was taken from the *V. cava* of healthy control mice and of orthotopically 4T1 tumor-bearing mice 14d after tumor cell injection. Systemic platelet counts were determined using the XN-1000 Hematology Analyzer (Sysmex, Norderstedt, Germany). After immunostaining (see above), platelets were identified as CD45⁻ CD41⁺ cells by flow cytometry.

To determine the subtype of circulating platelets, whole blood samples were additionally immunostained with fluorescence-labeled mAbs directed against CD45 (clone 30-F11; BD Biosciences), or CD41 (clone MWReg30; Biolegend), Annexin V binding to PS (eBioscience). Procoagulant platelets were defined as Annexin V^{high} platelets, aggregatory platelets as Annexin V^{low} platelets.

To determine the relative age of circulating platelets, healthy control mice and orthotopically 4T1 tumor-bearing mice received an intravenous injection of an APC-labeled anti-CD41 mAb (clone MWReg30; Biolegend) 24 h prior to harvesting the whole blood of the animals. Subsequently, blood samples were immunostained using differentially fluorescence-labeled mAbs directed against CD41 (BV421-labeled; clone MWReg30; Biolegend) and CD45 (clone 30-F11; BD Biosciences). Aged platelets were defined as CD41 (APC)⁺ CD41 (BV421)⁺ double-positive CD45⁻ cells, non-aged platelets as CD41 (APC)⁻ CD41 (BV421)⁺ CD45⁻ cells.

Additionally, activation of platelets was determined upon immunostaining with fluorescence-labeled mAbs directed against active GPIIb/IIIa (clone JON/A; emfret).

Expression of immune checkpoint molecules / cytokines on platelets was evaluated by using fluorescence-labeled mAbs directed against CD45 (clone 30-F11; BD Biosciences), annexin V (eBioscience), CD41 (clone MWRReg30; Biolegend), CD80 (clone 16-10A1), CD86 (clone GL-1; Biolegend), PD-L1 (clone 10F.9G2; Biolegend), PD-L2 (clone TY25; Biolegend), CD40 (clone 3/23; Biolegend), and CD40L (clone SA047C3; Biolegend), CCL5 (clone 2E9, Biolegend), and TGF- β (clone TW7-16B4, BioLegend). Due to the capability to bind to phosphatidyl serine (PS), annexin V binding was used as a measure of PS surface expression.

Samples were analyzed using a BD FACSCanto II (Becton, Dickinson and Company, Franklin Lakes, New Jersey, USA).

Phenotypic and functional properties of myeloid leukocytes

Neutrophils and cMOs harvested from the peripheral blood of 4T1 tumor bearing BALB/c or healthy control mice were exposed to 100ng of different TLR agonists (CL264 (TLR7), TL8-506 (TLR8), ODN2395 (TLR9); InvivoGen), or vehicle for 30min at 37°C in the dark. As a measure of cell activation, surface expression of Mac-1/CD11b of neutrophils (CD45⁺ CD11b⁺ Gr-1^{high} CD115⁻) and cMOs (CD45⁺ CD11b⁺ Gr-1^{high} CD115⁺) was determined. For this purpose, samples were then incubated for 30min at 37°C in the dark with fluorescence-labeled anti-CD45 mAb (clone 30-F11; BD Bioscience), anti-Gr-1 mAb (clone RB6-8C5; Biolegend), anti-CD115 mAb (clone AFS98; Lifetechnologies, Carlsbad, California, USA), anti-F4/80 mAb (clone BM8; eBioscience), and anti-Mac-1/CD11b mAb (clone M1/70; eBioscience). To evaluate the expression of immune checkpoint molecules on these myeloid cells, samples were incubated for 30min at 37°C in the dark with fluorescence-labeled anti-CD11b mAb (clone M1/70; eBioscience), anti-Gr-1 mAb (clone RB6-8c5; eBioscience), anti-F4/80 mAb (clone BM8; eBioscience), anti-CD45 mAb (clone 30-F11; BD Bioscience), anti-CD86 mAb (clone GL-1; Biolegend), anti-PD-L1 mAb (clone 10F.9G2; Biolegend), anti-CD80 mAb (clone 16-10-

A1; Biolegend), anti-CD40 mAb (clone 3112; Biolegend), or anti-CD40L mAb (clone MR1; Biolegend). Samples were finally analyzed by a flow cytometry (Gallios, Beckman Coulter Inc).

Procoagulant activation of platelets

Blood was taken from the *V. cava* of BALB/c mice and incubated with native equine collagen I (1mg/mL collagen reagens HORM®, Takeda Austria GmbH) as well as with anti-GPVI mAb (1µg/mL, emfret), the GPIIb/IIIa inhibitor tirofiban (2µg/mL, Sigma Aldrich), the cyclophilin D inhibitor cyclosporin A (100µg/mL, MedChemExpress), or isotype control antibodies/drug vehicle for 30min at 37°C. Subsequently, cells were immunostained with fluorescence-labeled anti-CD41 mAb (clone MWReg30, BioLegend), Annexin V (BioLegend), anti-CD86 mAb (clone GL-1, BioLegend), anti-CD80 mAb (clone 16-10A1, BioLegend), and anti-CD274/PD-L1 mAb (clone 10F.9G2, BioLegend), before immune checkpoint molecule expression on platelets was analyzed by flow cytometry. These experiments were repeated using peripheral blood from PF4cre-TMEM16F^{fl/fl} cre- (TMEM16F^{pl^{+/+}}) and cre+ (TMEM16F^{pl^{-/-}}) mice.

Activation of lymphocytes

In a first set of experiments, primary lymphocytes were harvested from the peripheral blood of 4T1 BALB/c mice and exposed to 100ng of different TLR agonists (CL264 (TLR7), TL8-506 (TLR8), ODN2395 (TLR9); InvivoGen), or vehicle for 30min at 37°C in the dark. In separate experiments, lymphocytes isolated from the peripheral blood of BALB/c mice incubated with blocking mABs directed against CD80 (clone 16-10A1; Biolegend), CD86 (clone GL-1; Biolegend), CTLA4 (clone 9H10; Biolegend), anti-PD-L1 (clone 10F.9G2; Biolegend), anti-PD-1 (clone 29F.1A12; Biolegend), or isotype control antibodies for 60min at 37°C. Subsequently, the samples were immunostained with fluorescence-labeled mABs directed against CD45 (clone 30-F11; BD Biosciences), CD41 (clone MWReg30; Biolegend), CD3 (clone 17A2; Biolegend), CD4 (clone RM4-5; BD Biosciences), CD8a (clone 53-6.7; eBioscience), CD19

(clone eBio1D3; eBioscience), and L-selectin/CD62L (clone MEL 14; eBioscience). As a measure of cell activation, surface expression of L-selectin was determined.

To evaluate effects of different compounds on the binding of platelets to lymphocytes, blood was incubated for 60min at 37 °C with blocking anti-CD11b/Mac-1 mAbs (clone M1/70; Biolegend), anti-CD62P/P-selectin mAbs (clone RMP-1; Biolegend), anti-CD102/ICAM-2 mAbs (clone 3C4 (MIC2/4); Biolegend), anti-GPIX mAbs (clone Xia.B4; emfret), anti-GPVI mAbs (clone JAQ1; emfret), anti-GPIb α mAbs (clone Xia.B2; emfret), anti-GPIIb/IIIa mAbs (clone Leo.H4; emfret), or anti-PSGL-1 mAbs (clone 4RA10; BioXCell) as well as a P2Y₁₂ inhibitor (ticagrelor; Sigma Aldrich), ASS (Sigma Aldrich), or isotype control antibodies/drug vehicle. Subsequently, samples were incubated with fluorescence-labeled mAbs directed against CD45 (clone 30-F11; BD Biosciences), CD41 (clone MWReg30; Biolegend), anti-CD3 mAb (clone 17A2; Biolegend), CD4 (clone RM4-5; BD Biosciences), CD8a (clone 53-6.7; eBioscience), or isotype control antibodies. As a measure of platelet-binding to lymphocytes, the positivity of CD45⁺ CD3⁺ CD8⁺ or of CD45⁺ CD3⁺ CD4⁺ cells for CD41 were determined by flow cytometry (Gallios, Beckman Coulter Inc).

In an additional *in vitro* assay, spleen and the inguinal lymph nodes were harvested from female BALB/c mice before being placed in a sterile plastic tray containing 2mL ice-cold RPMI/FBS (RPMI 1640 with 7.5% FBS and 5% Pen Strep) and subsequently homogenized. The cells were filtered using a 70 μ m cell strainer. After centrifugation, the cells were re-suspended with 3 mL of lysing solution (BD Biosciences). 10 μ L of the Biotin-antibody Cocktail from the 'MojoSort™ Mouse CD3 T Cell Isolation Kit' (BioLegend) were added followed by 15min of incubation on ice. This step was repeated with 10 μ L of Streptavidin Nanobead. At the end, the CD3⁺ population was isolated with magnetic isolation (QuadroMACS™).

In a 6 well plate coated with fibrinogen (0.1mg/mL) 500 μ L of RPMI/FBS media (RPMI 1640 with 7.5% FBS and 5% Pen Strep) were added. For the co-culture, 25x10⁴ T cells were stimulated with 1 μ g/mL of OKT3-stimulating antibody (NovusBio, #NBP2-25186). After 30min of incubation, primary mouse platelets were added in a proportion of 1:50 (12.5x10⁶) together

with anti-CTLA-4 mAb (40µg/mL; Biolegend, #106302) and anti-PD-1 mAb (10µg/mL; Biolegend, #135246). For this purpose, platelets were isolated from whole anticoagulated blood harvested from *V. cava* of female BALB/c mice. Subsequently, the blood was diluted (ratio 1:1) by Tyrode's 6.5 pH buffer. After centrifugation, the PRP was diluted again with Thyrode's 6.5 pH buffer (ratio 2:1) and 5µg of prostaglandin was added. At the end, platelets were suspended in 200µl Thyrode's 7.2 pH buffer.

After 6h, T cells were analyzed for the expression of CD25 (clone PC61, Biolegend), Ki67 (clone SolA15, ThermoFisher), IFN-γ (clone XMG12, Biolegend), CD49d (clone R1-2, BD Bioscience), and CD69 (clone H1.2F3, Biolegend) by flow cytometry.

Activation of macrophages and endothelial cells

b.End.3 microvascular endothelial cells and RAW 264.7 macrophages were seeded on 24-well plates. On the next day, cells were incubated for 6h at 37°C with either 100ng/ml of the TLR agonists CL264 (TLR7), TL8-506 (TLR8), and ODN2395 (TLR9), 1µg/ml TNF (Biolegend), or saline. Subsequently, cells were harvested and endothelial cells were incubated with mAbs directed against ICAM-1/CD54 (clone YN1/1.7.4; Biolegend), VCAM-1/CD106 (Pacific Blue; clone 429 (MVCAM.A); Biolegend), E-selectin/CD62E (PE; clone 10E9.6; BD Biosciences) and P-selectin/CD62P (APC; clone RMP-1; Biolegend). RAW macrophages were incubated with anti-TNF (clone MP6-XT22; eBioscience) monoclonal antibodies. Expression of the target molecules was analyzed by flow cytometry (Gallios, Beckman Coulter Inc).

IC molecules on human platelets

Expression of IC molecules on human platelets was evaluated in the peripheral blood of healthy volunteers. For this purpose, blood samples were stained with fluorescence-labeled mAbs directed against CD41 (clone HIP8; Biolegend), CD274/PD-L1 (clone 29EA23;

Biolegend), CD154/CD40L (clone 24-31; Biolegend), CD80 (clone W17149D; BioLegend), CD86 (clone BU63; Biolegend), CD40 (clone 5C3; Biolegend), and/or Annexin V (Biolegend). Samples were analyzed using a BD FACSCanto II (Becton, Dickinson and Company, Franklin Lakes, New Jersey, USA). Procoagulant platelets were defined as CD41⁺ Annexin V⁺ cells, aggregatory platelets as CD41⁺ Annexin V⁻ cells.

Human breast cancer samples

20 triple negative breast cancer (TNBC) samples (from breast-conserving surgery or total mastectomy) from the Institute of Pathology of the Technical University of Munich (TUM) were collected based on the confirmation by pathologists for the lack of expression of estrogen receptor (ER), progesterone receptor (PR), and the absence of overexpression of human epidermal growth factor receptor 2 (HER2). The analyzed tumor tissue specimens of TNBC were diagnosed between 2003 and 2005 and the age of patients at the time of surgery ranged between 27 and 84 years. Primary tumor size (T), regional lymph node status (N), and distant metastasis (M) were evaluated according to the UICC (2002) TNM classification. Primary tumor sizes ranged from T1 to T4 with or without lymph node metastasis and the neoplasms were moderately (G2) or poorly (G3) differentiated. The use of human tissue was approved by the local ethic committee of the Technical University of Munich (reference number: 506/17 s).

Immunohistochemical staining

2-3 µm-thin sections were prepared with a rotary microtome HM355S (Thermo Fisher Scientific) and subjected to immunohistochemical analysis. Immunohistochemistry (IHC) with CD8 (M7103, Dako) and Myeloperoxidase (MPO, RB-373-A, Thermo Fisher Scientific) primary antibodies was performed on a BenchMark XT automated stainer (Roche, all reagents from Roche) using the ultraVIEW Universal DAB Detection Kit. Briefly, the tissue sections were deparaffinized with EZ Prep at 76°C, heat pretreated in Cell Conditioning 1 (Citrat pH 6.0) for antigen retrieval at 76°C – 100°C (CD8: 60 min; MPO: 30 min) and then incubated with the

primary antibody diluted in antibody diluent (dilution: 1:100) for 32 min at 37°C after inactivation of the endogenous peroxidase using UV-inhibitor for 4 min at 37°C. The slides were incubated with a secondary antibody polymer followed by the application of HRP Universal Multimer for 8 min. Antibody binding was detected using 3,3'-Diaminobenzidine (DAB) as chromogen and slides were counterstained with hematoxylin for 8 min with subsequent bluing in bluing reagent for 4 min.

IHC with a primary antibody against Integrin $\beta 3$ (D7X3P) XP (13166, Cell Signaling) or CD274/PD-L1 (clone 29EA23; Biolegend) was performed on a Bond RXm system (Leica, all reagents from Leica). Briefly, slides were deparaffinized using deparaffinization solution, pretreated with Epitope retrieval solution 2 (corresponding to EDTA) for 30 minutes. Antibody binding was detected with a Polymer refine detection kit without post primary reagent and visualized with DAB as a dark brown precipitate. Counterstaining was done with hematoxyline. Slides were then dehydrated manually by alcohol washes of increasing concentrations (70%, 96%, 100%) and xylene and cover-slipped using Cytoseal XYL mountant (8312-4, Thermo Fisher Scientific). Slides were scanned using a digital whole slide scanner Aperio AT2 (Leica). To evaluate the association of intravascular platelets and the extravascular neutrophil-to-CTL ratio (NLR), extravascular MPO⁺ cells, extravascular CD8⁺ cells, and intravascular integrin $\beta 3$ ⁺ cells were quantified in the entire specimen using the cell detection software package 'QuPath's'.

Analyses in the METABRIC breast cancer cohort

For analyses of RNA microarray data of the METABRIC breast cancer cohort, CBioportal was employed ⁴. The subcohort of patients with documented tumor stage and available RNA microarray data was used ($n = 1,403$), and follow-up was cut to 120 months. According to the Panglao database (<https://panglaodb.se/>), ITGA2B was chosen as platelet marker gene. Survival analyses were performed with the Cox proportional hazard model, and target gene

expression z-values of ≥ 2.0 were used as strata. Furthermore, correlation coefficients of RNA expression of ITGA2B and PECAM-1, PD-L1, CD80, CD86, CD40, or CD40L were determined.

Orthotopic HNSCC model

SCC VII tumor cells (at a concentration of 2×10^5 cells/20 μ l) were injected into the floor of the mouth of male C3H mice. Animals received intravenous injections of 50 μ g of blocking monoclonal antibodies directed against PD-1 (clone 29F.1A12; Biolegend) and CTLA-4 (clone 9H10; Biolegend), GPIIb α (clone Xia.B2; emfret), or isotype control antibodies starting from day 7 after tumor cell implantation and further on every other day (n=3-5 per group). At day 14 after tumor cell injection, blood, spleen, and tumor were explanted and their weight and size were measured by a special accuracy weighting machine (Mettler-Toledo, Columbus, OH, USA) and a caliper gauge (Mitutoyo Corporation, Kawasaki, Japan). Harvested tumors were subsequently homogenized with a homogenizer (8ml; Schuett biotec GmbH, Göttingen, Germany) in 15ml saline. Platelet and immune cell contents were quantified by flow cytometry as described above in the orthotopic 4T1 model.

Statistics

Data analysis was performed with the statistical software SigmaPlot for Windows; Jandel Scientific, Erkrath, Germany). After confirming normality and equal variance of data (using the Shapiro-Wilk and Brown-Forsythe tests), the One-way ANOVA test followed by the Dunnett test (>2 groups) or the *t* test (2 groups) was used for the estimation of stochastic probability in intergroup comparisons. If normality and/or equal variance testing failed, the Kruskal-Wallis One-way ANOVA of Ranks test followed by the Dunnett test (>2 groups) or the Mann-Whitney rank sum test (2 groups) was used. Mean values and SEM are given. *P* values <0.05 were considered significant.

Supplemental Table

a

	control	4T1 (day 7)	4T1 (day 10)	4T1 (day 14)
systemic platelet count [$10^3 \mu\text{l}^{-1}$]	606.0±24.7	487.0±10.6*	275.3±38.6*	417.8±57.3*

b

platelet count [$10^3 \mu\text{l}^{-1}$]	control	4T1 (day 7)	4T1 (day 10)	4T1 (day 14)
lung	18.7±5.5	6.0±0.6*	15.7±1.9	22.3±1.2
liver	228.7±16.1	93.3±31.2*	134.0±32.0*	64.3±12.4*
brain	19.9±2.8	18.9±6.1	16.4.3±3.3	17.0±4.1
kidney	302.3±18.0	234.4±10.6*	184.6±38.6*	78.5±8.9*
bone marrow	16.2±1.6	8.0±2.7*	15.2±2.2	33.6±4.3*
tumor	-	599.5±92.3	746.5±162.2	717.3±125.4

c

	control	4T1
MKs [% of total bone marrow cells]	2.2±0.4	5.3±0.9*

d

	control	4T1
spleen weight [g]	0.13±0.02	0.31±0.02*

e

	control	4T1
spleen platelet count [$10^3 \mu\text{l}^{-1}$]	90.0±8.8	158.4±5.0*

f

	control mice (blood)	tumor-bearing mice (blood)	tumor-bearing mice (spleen)	tumor-bearing mice (tumor)
procoagulant PS ^{high} platelets [% total platelets]	0.2±0.1	0.2±0.1	2.2±0.6*	16.1±0.9*

Table S1. Platelet dynamics in healthy and 4T1 tumor-bearing mice. (a) Platelet counts in peripheral blood and (b) organs of healthy, tumor-free control mice as well as in peripheral blood, organs, and tumors of orthotopically 4T1 tumor-bearing mice at days 7, 10, and 14 after

tumor cell injection. **(c)** Relative bone marrow megakaryocyte (MK) content, **(d)** splenic organ weight, and **(e)** splenic platelet count in healthy, tumor-free control mice as well as in orthotopically 4T1 tumor-bearing mice at day 14 after tumor cell injection. **(f)** Proportion of procoagulant activated platelets of total platelets in healthy, tumor-free control mice (peripheral blood) as well as in the peripheral blood, tumor, and different organs of orthotopically 4T1 tumor-bearing mice at day 14 after tumor cell injection. Quantitative data are shown (mean \pm SEM for n=3-5 per group; *p<0.05 vs. control).

a

model	stimulus	treatment	systemic platelet count [$10^3 \mu\text{l}^{-1}$]
4T1 TNBC (day 14)	-	isotype control	296.2±30.4
4T1 TNBC (day 7)	-	anti-GPIb α	10.5±5.6*
4T1 TNBC (day 10)	-	anti-GPIb α	6.3±2.8*
4T1 TNBC (day 14)	-	anti-GPIb α	20.0±3.6*
peritoneal assay	TLR8 agonist	isotype control	484.8±31.8
peritoneal assay	TLR8 agonist	anti-GPIb α	16.2±1.9*
peritoneal assay	TLR9 agonist	isotype control	390.5±41.4
peritoneal assay	TLR9 agonist	anti-GPIb α	14.0±2.6*

b

model	stimulus	treatment	systemic neutrophil count [$10^3 \mu\text{l}^{-1}$]
peritoneal assay	TLR7 agonist	isotype control	2.0±0.2
peritoneal assay	TLR7 agonist	anti-Ly-6G	0.1±0.1*
peritoneal assay	TLR8 agonist	isotype control	0.9±0.1
peritoneal assay	TLR8 agonist	anti-Ly-6G	0.1±0.1*
peritoneal assay	TLR9 agonist	isotype control	1.2±0.1
peritoneal assay	TLR9 agonist	anti-Ly-6G	0.1±0.1*

Table S2. Antibody-mediated platelet and neutrophil depletion. (a) Platelet counts in the peripheral blood of mice receiving platelet-depleting anti-GPIb α or isotype control antibodies in an orthotopic 4T1 TNBC model on different days after tumor cell injection or in a peritoneal assay upon stimulation with TLR agonists as analyzed by flow cytometry. (b) Neutrophil counts in the peripheral blood of mice receiving neutrophil-depleting anti-Ly-6G mAb or isotype control antibodies in a peritoneal assay upon stimulation with TLR agonists as analyzed by flow cytometry, quantitative data are shown (mean±SEM for n=4-6 per group; *p<0.05 vs. control/isotype control).

	control mice (blood)	tumor-bearing mice (blood)	tumor-bearing mice (spleen)	tumor-bearing mice (tumor)
procoagulant platelets [% total platelets]	0.2±0.1	0.2±0.1	2.6±0.7*	28.6±3.5*

Table S3. Platelet counts in experimental HNSCC. The proportion of procoagulant platelets of total platelets in healthy, tumor-free control mice (peripheral blood) as well as in orthotopically SCC VII tumor-bearing mice (peripheral blood, spleen, tumor) was analyzed by flow cytometry, quantitative data are shown (mean±SEM for n=3-5 per group; *p<0.05 vs. control).

Supplemental Figures

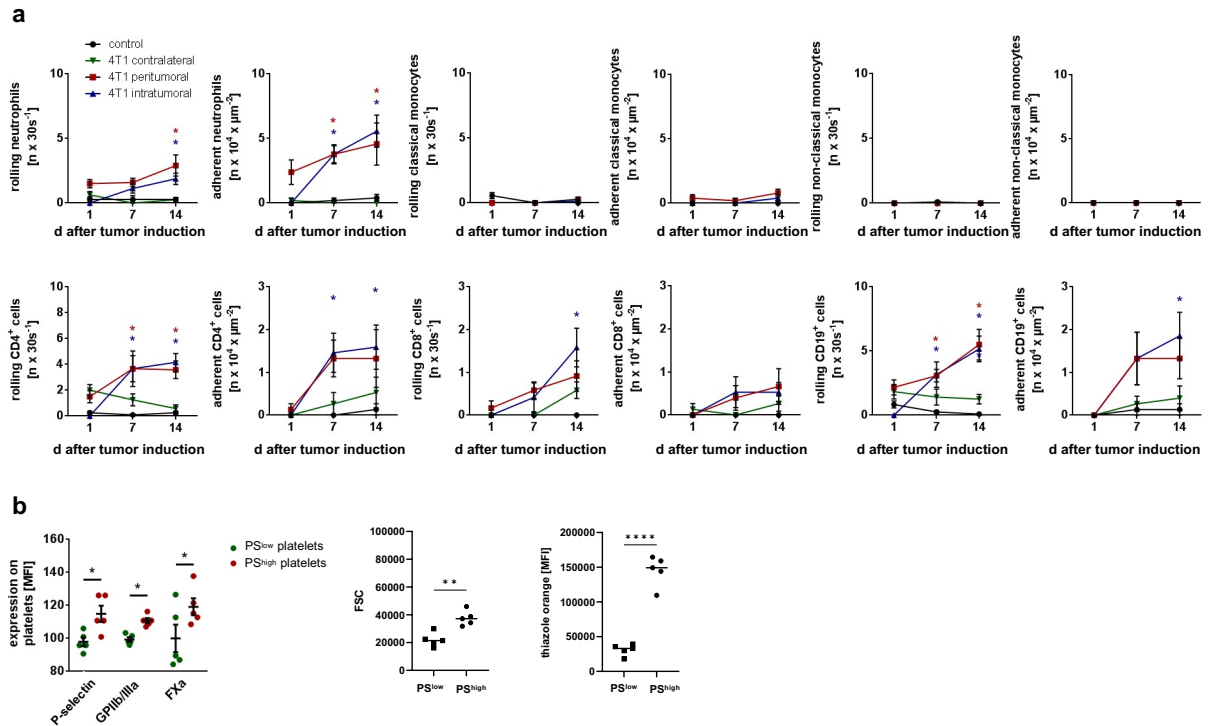


Figure S1. Peri- and intratumoral endothelial interactions of immune cells. (a) Interactions of endothelial cells and neutrophils, classical monocytes, non-classical monocytes, CD4⁺ T cells, CD8⁺ T cells, and CD19⁺ B cells in the peri- and intra-tumoral microvasculature of 4T1 tumors implanted into the left auricle, in the right tumor-free auricle, or in the left auricle of tumor-free mice as assessed by multi-channel *in vivo* microscopy, quantitative data are shown (mean±SEM for n=6 per group; *p<0.05 vs. control). **(b)** Surface expression of P-selectin/CD62P, GPIIb/IIIa, and FXa, forward scatter properties (FSC; as measure of cell size), as well as thiazole orange staining intensity (as measure of ribonucleic acid content) in PS^{low} and PS^{high} platelets isolated from the peripheral blood of mice as assessed by multi-channel flow cytometry, quantitative data are shown (mean±SEM for n=5 per group; *p<0.05/**p<0.01/****p<0.0001 vs. PS^{low}).

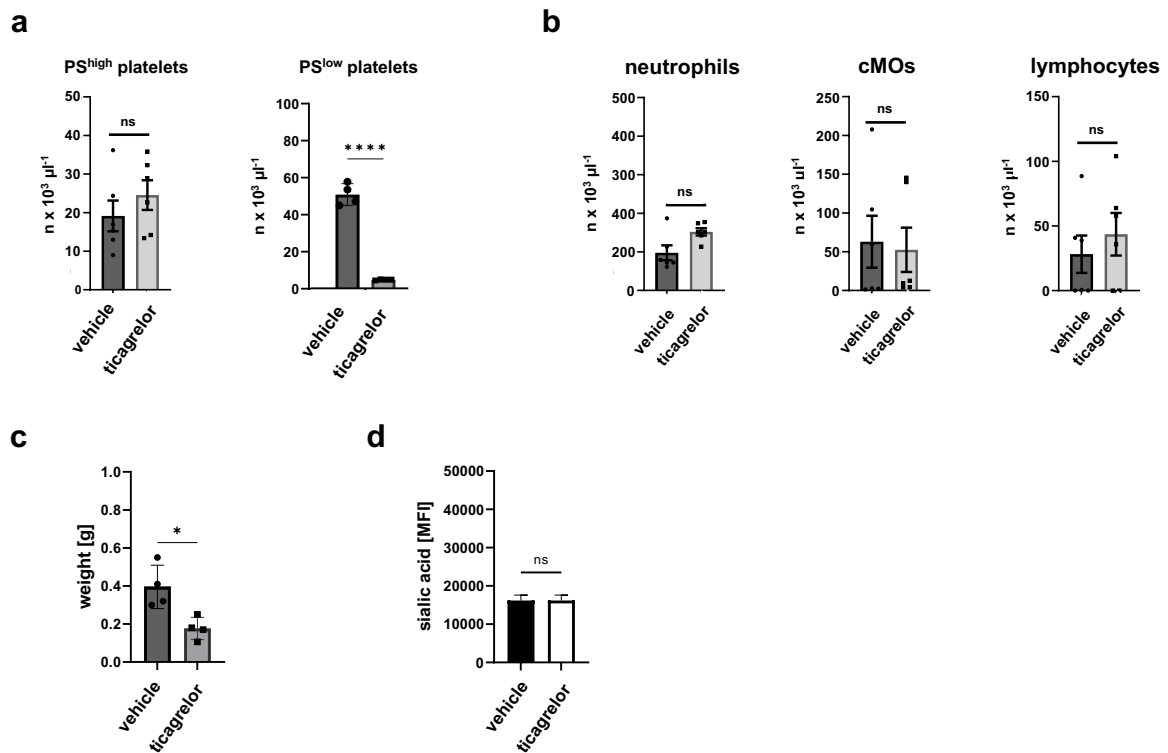


Figure S2. Effects of ADP receptor blockade on platelet and immune cell responses as well as tumor growth in experimental TNBC. (a) Intratumoral accumulation of PS^{high} and PS^{low} platelets as well as (b) of neutrophils, classical monocytes (cMOs), and lymphocytes as assessed by immunostaining and flow cytometry in tissue homogenates from orthotopically raised 4T1 tumors of mice treated with the ADP receptor antagonist ticagrelor or drug vehicle, quantitative data are shown (mean \pm SEM for n=6 mice per group; ****p<0.0001 vs. drug vehicle; ns=not significant). (c) Weight of the 4T1 tumors orthotopically raised in mice treated with the ADP receptor antagonist ticagrelor or drug vehicle and (d) surface levels of sialic acids on intratumoral platelets as assessed by immunostaining and flow cytometry, quantitative data are shown (mean \pm SEM for n=4 mice per group; ns=not significant; *p<0.05 vs. drug vehicle).

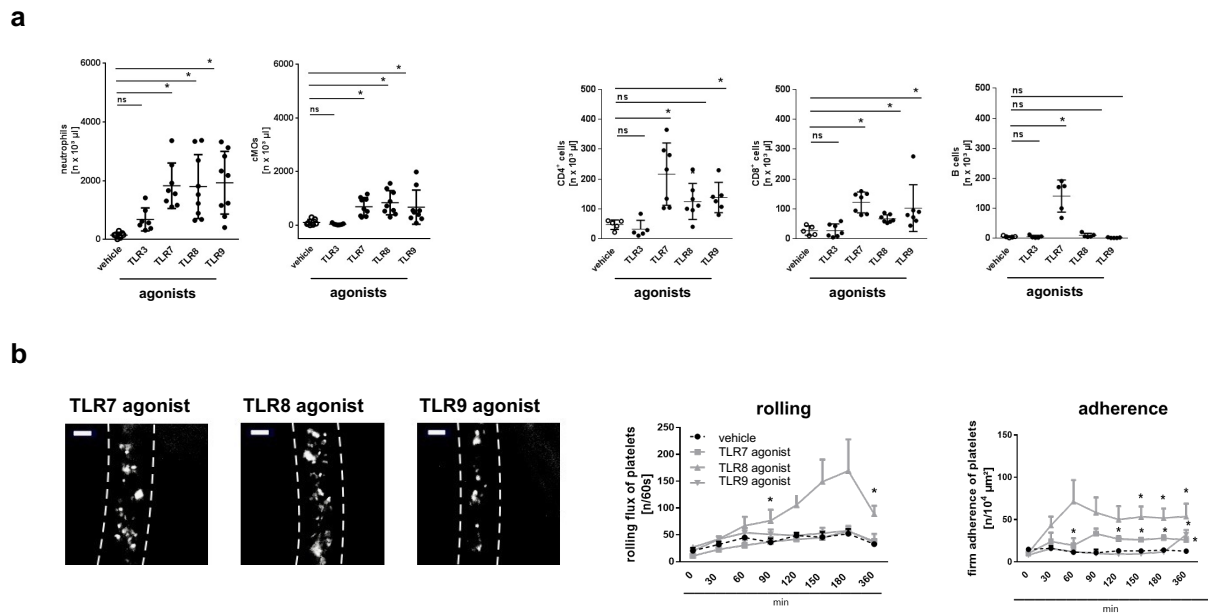


Figure S3. Effects of endosomal TLR agonists on platelet and immune cell trafficking. (a) Recruitment of neutrophils, classical monocytes (cMOs), CD4⁺ T cells, CD8⁺ T cells, and CD19⁺ B cells to the peritoneal cavity 6h after intraperitoneal injection of agonists of TLR3, -7, -8, -9, or vehicle as assessed by flow cytometry, quantitative data are shown (mean±SEM for n=6 per group; *p<0.05 vs. vehicle; ns=not significant). (b) Intravascular rolling and adherence of platelets in postcapillary venules of the mouse cremaster muscle upon superfusion of agonists of TLR7, -8, -9, or vehicle as assessed by multi-channel *in vivo* microscopy, representative images (platelets: white, vessel wall: broken line, scale bar: 5μm) and quantitative data are shown (mean±SEM for n=6 per group; *p<0.05 vs. vehicle).

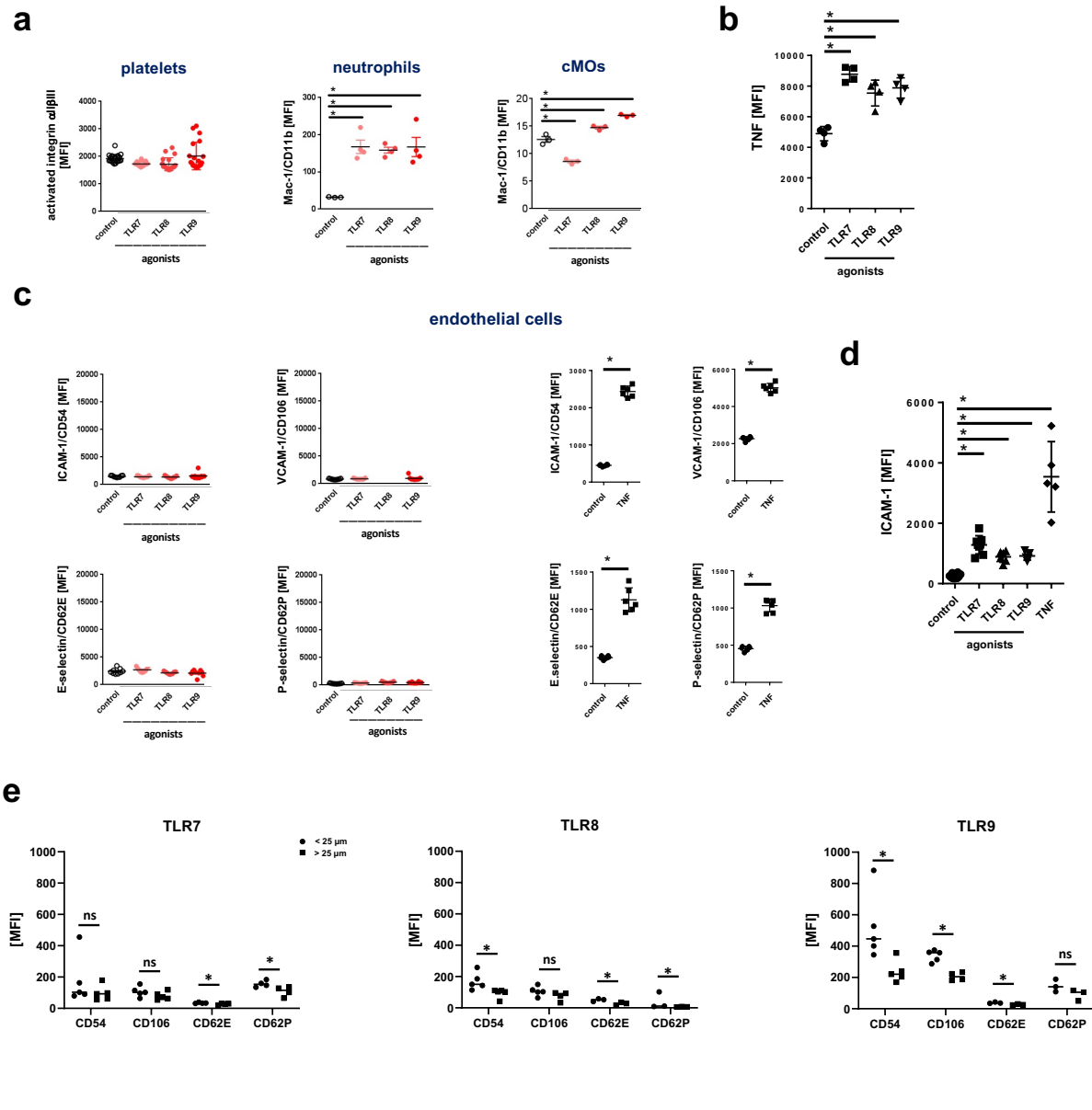


Figure S4. Effects of endosomal TLR agonists on activation of platelets, myeloid leukocytes, endothelial cells, and macrophages. (a) Surface expression of activated integrin $\alpha\text{IIb}\beta\text{3}$ on platelets, Mac-1/CD11b on neutrophils and classical monocytes (cMOs) isolated from the peripheral blood of mice, (b) TNF on mouse RAW 264.7 macrophages (c) as well as of ICAM-1/CD54, VCAM-1/CD106, E-selectin/CD62E, and P-selectin/CD62P on bEnd.3 microvascular endothelial cells as assessed *in vitro* by flow cytometry upon application of agonists of TLR7, -8, -9, TNF, or vehicle (control), quantitative data are shown (mean \pm SEM for n=3-12 per group; *p<0.05 vs. isotype control). (d) Quantitative data for surface expression of ICAM-1/CD54 on PECAM-1/CD31⁺ CD45⁻ microvascular endothelial cells in the mouse cremaster muscle 6 h after intrascrotal injection of agonists of TLR7, -8, -9, TNF, or vehicle as assessed by immunostaining and confocal microscopy, quantitative data are shown. (e) Surface expression of ICAM-1/CD54, VCAM-1/CD106, E-selectin/CD62E, and P-selectin/CD62P on CD31⁺ microvascular endothelial cells with respect to their distance to perivascular macrophages as assessed by immunostaining and confocal microscopy of cremaster muscle whole mounts undergoing stimulation with agonists of TLR7, TLR8, or TLR9, quantitative data are shown (mean \pm SEM for n=3-5 per group; *p<0.05 vs. <25 μm).

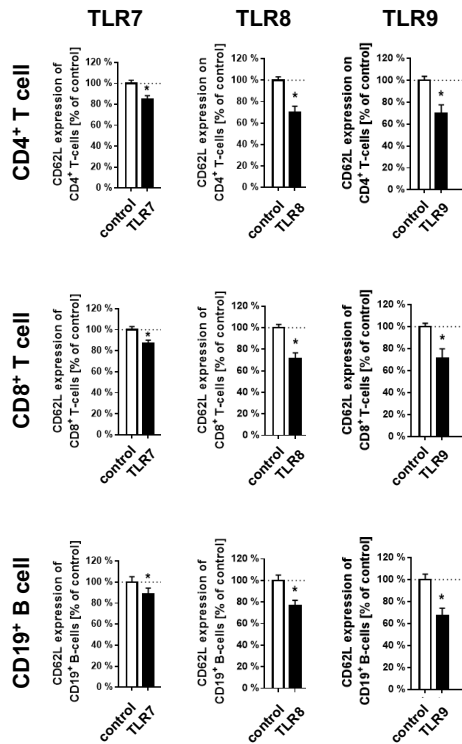


Figure S5. Effects of endosomal TLR agonists on activation of lymphocytes. Surface expression of L-selectin on CD4⁺ T cells, CD8⁺ T cells, and CD19⁺ B cells isolated from the peripheral blood of mice as assessed *in vitro* by flow cytometry upon application of agonists of TLR7, -8, -9, or vehicle (control), quantitative data are shown (mean±SEM for n=3-12 per group; *p<0.05 vs. control).

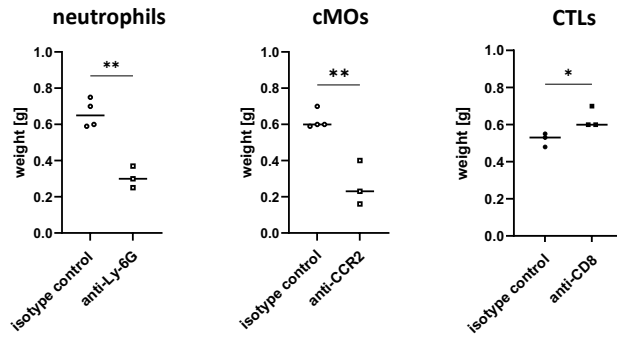
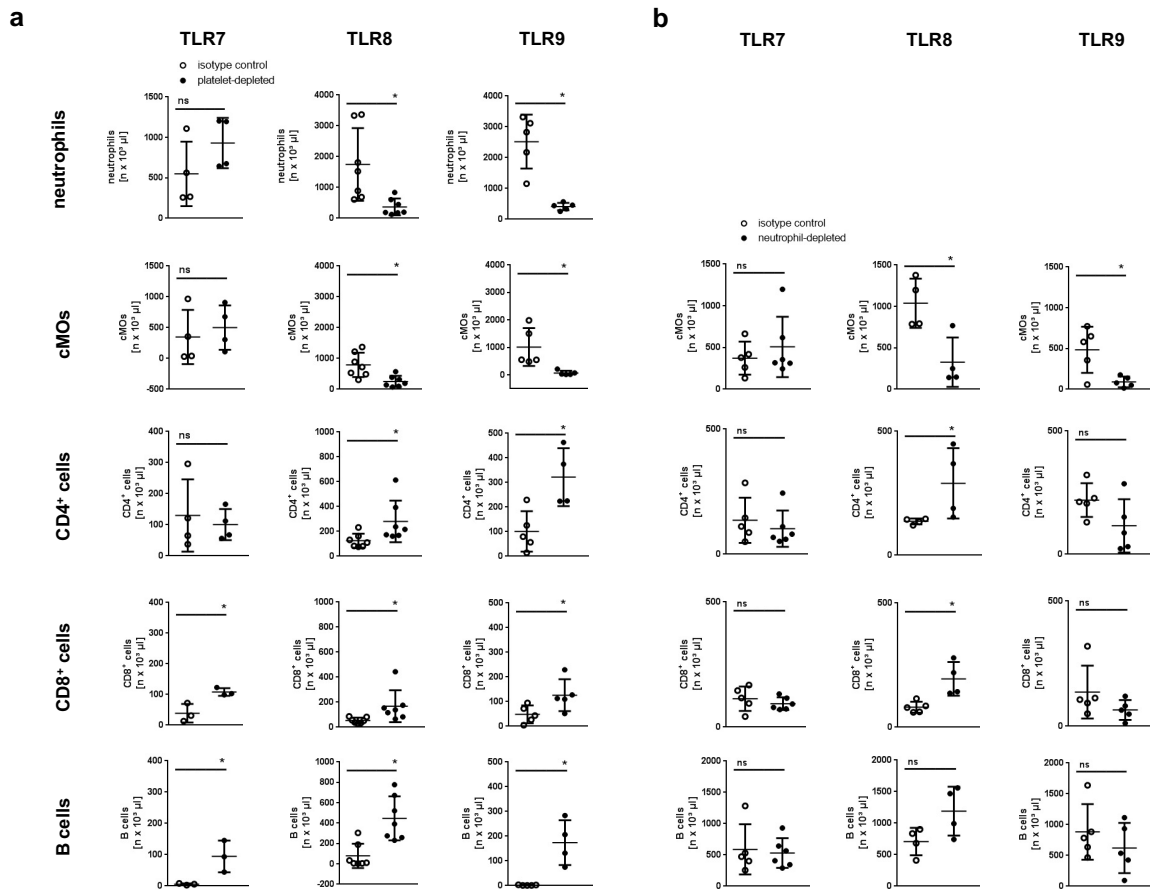


Figure S6. Role of neutrophils, classical monocytes, and CTLs for tumor growth in experimental TNBC. Weight of orthotopically grown 4T1 tumors in mice receiving neutrophil-depleting anti-Ly-6G mAb, classical monocyte (cMO)-depleting anti-CCR2 mAb, CTL-depleting anti-CD8 mAb, or isotype control antibodies, quantitative data are shown (mean±SEM for n=3-4 mice per group; *p<0.05/**p<0.01 vs. isotype control).



Figures S7. Effects of platelets and neutrophils on immune cell responses elicited by endosomal TLR agonists. Trafficking of neutrophils, classical monocytes (cMOs), CD4⁺ T cells, CD8⁺ T cells, and CD19⁺ B cells 6h after intraperitoneal injection of TLR-7, -9, or -9 agonists in mice receiving (a) platelet-depleting mAbs, (b) neutrophil-depleting mAbs, or isotype control antibodies as assessed by flow cytometry, quantitative data are shown (mean±SEM for n=5 per group; *p<0.05 vs. isotype control).

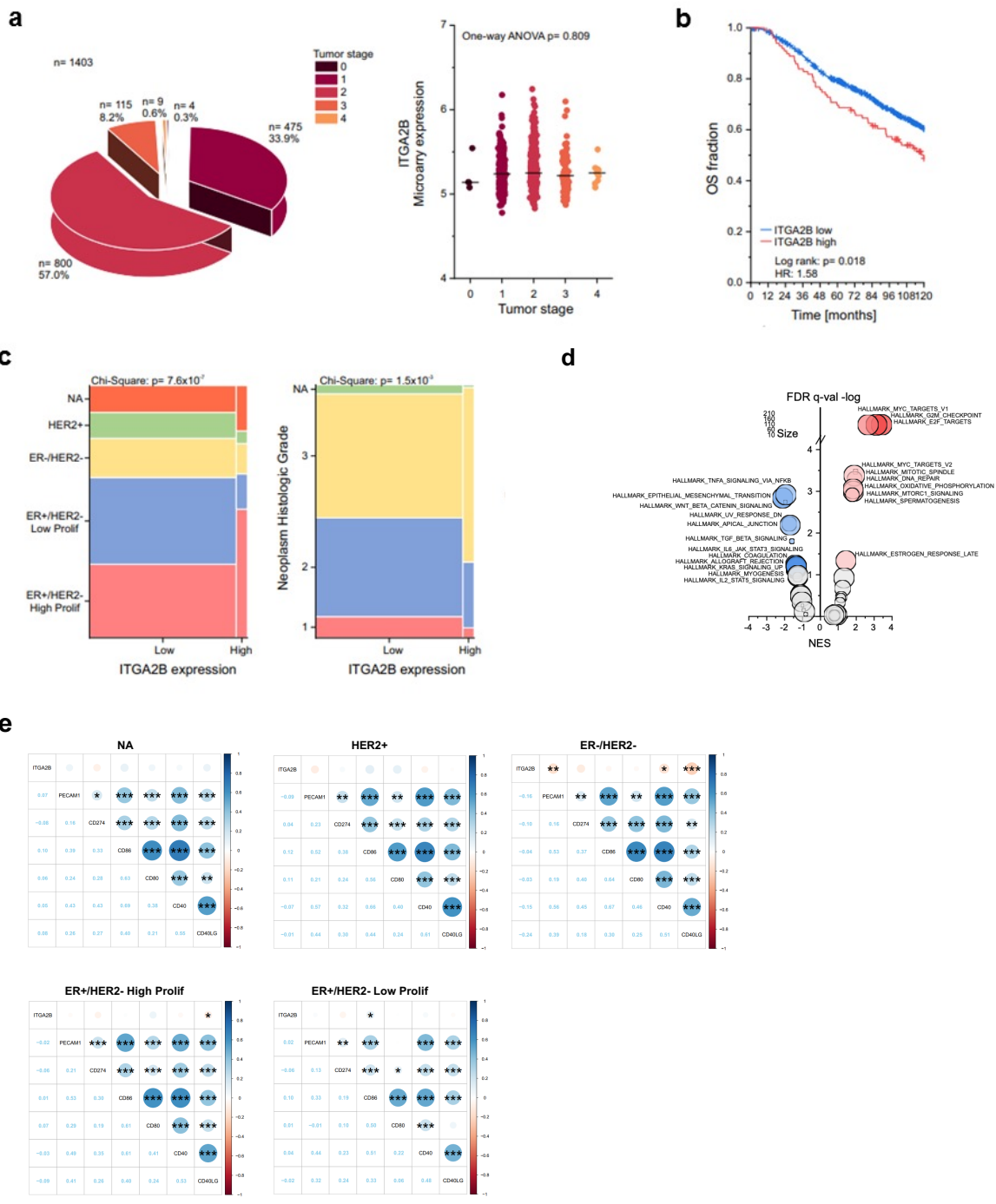


Figure S8. Overall survival of breast cancer patients of the METABRIC dependent on ITGA2B RNA expression. (a) Composition and ITGA2B RNA microarray expression of analyzed patients of the METABRIC cohort with respect to disease stage. (b) Overall survival of ITGA2B^{low} and ITGA2B^{high} breast cancer patients in all disease stages (z-value ≥ 1.5 served as cut-off). (c) Mosaic plot depicting cross-tabulation and chi-squared analysis between ITGA2B high and low expressing cases, the molecular breast cancer subtype as defined by the 3-gene-classifier (left), and the histological grade (right). (d) Gene set enrichment analysis (GSEA) of genes correlating with ITGA2B expression. (e) Positive (blue) and negative (red) correlation coefficients of RNA expression of ITGA2B and various other molecules including PECAM-1, PD-L1, CD80, CD86, CD40, and CD40L in the different breast cancer subtypes (* $p < 0.05$, ** $p < 0.01$, *** $p < 0.001$ vs. respective molecule).

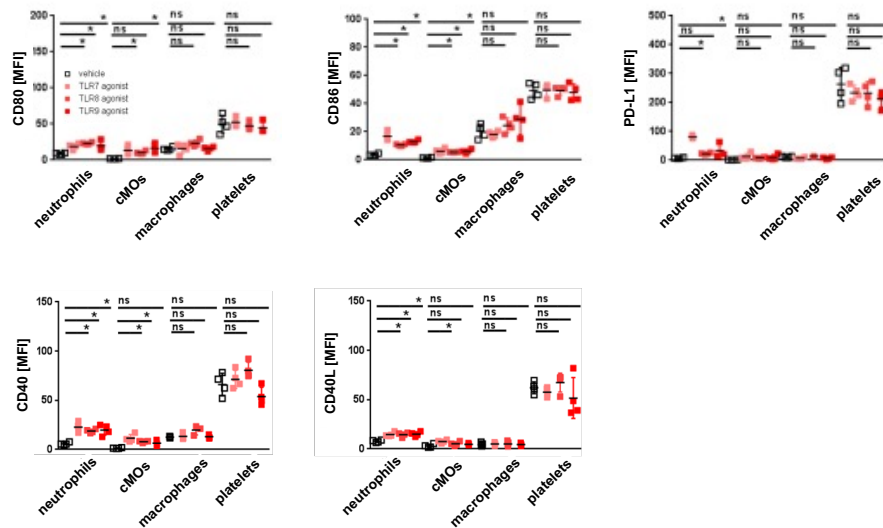
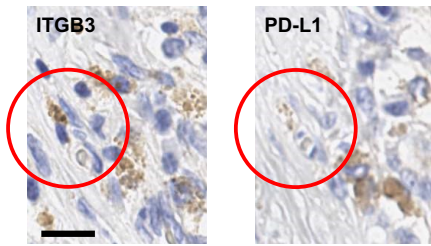


Figure S9. Immune checkpoint molecules on platelets and myeloid immune cells. Surface expression of the immune checkpoint molecules CD80, CD86, PD-L1, PD-L2, CD40, and CD40L on neutrophils, classical monocytes (cMOs), platelets isolated from the peripheral blood of mice as well as on mouse RAW macrophages as assessed by flow cytometry upon application of agonists of TLR7, -8, -9, or vehicle, quantitative data are shown (mean±SEM for n=4 per group; *p<0.05 vs. vehicle).

a



b

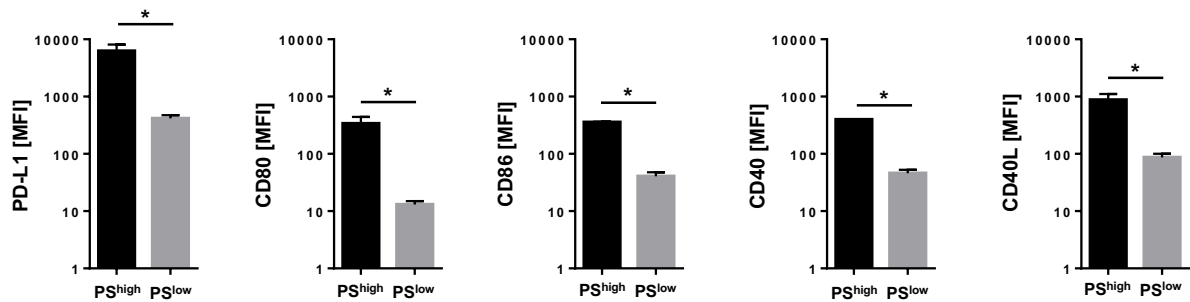


Figure S10. Immune checkpoint molecules on human platelets. (a) Representative images of PD-L1-expressing integrin $\beta 3^+$ platelets in the TNBC microvasculature as assessed by immunohistochemistry in serial tissue sections of human tumors (scale bar: 25 μ m). (b) Surface expression of PD-L1, CD80, CD86, CD40, and CD40L on non-procoagulant PS^{low} platelets and on procoagulant PS^{high} platelets isolated from the peripheral blood of human individuals as assessed by flow cytometry, quantitative data are shown (mean \pm SEM for n=3-5 per group; *p<0.05 vs. PS^{high}).

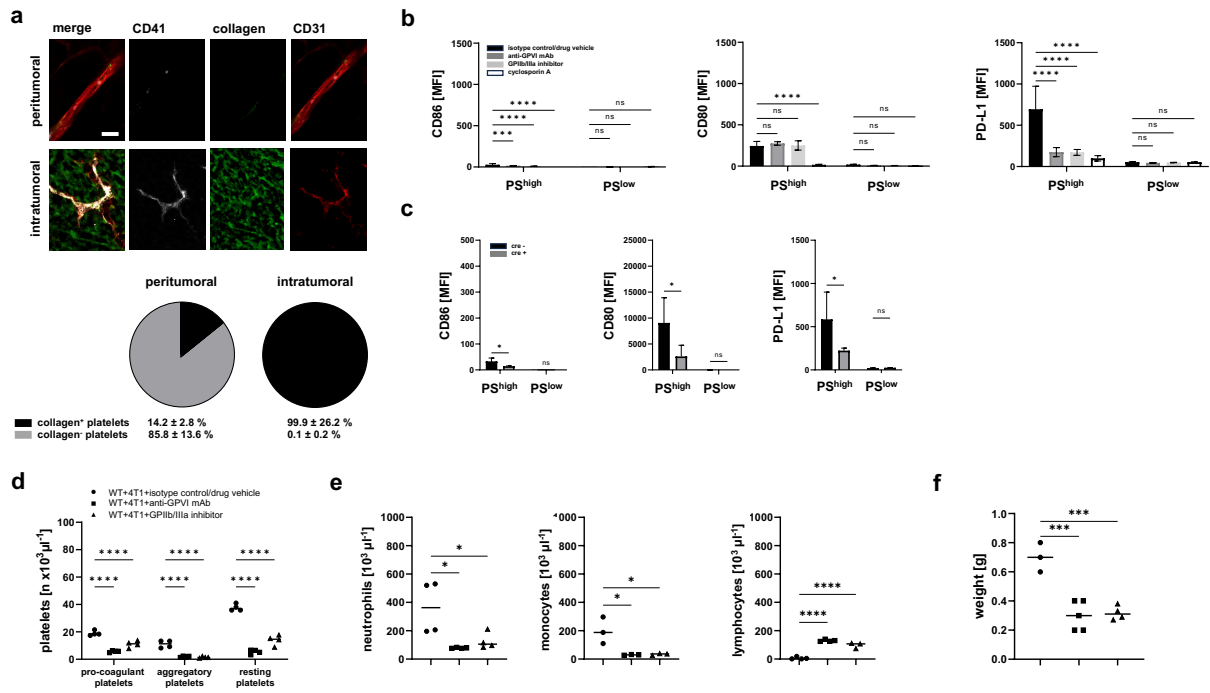


Figure S11. Procoagulant activation of platelets in the tumor microvasculature. (a) Co-localization of CD41⁺ platelets and collagen I in the CD31⁺ peritumoral or tumoral microvasculature of orthotopically raised 4T1 tumors as assessed by immunostaining and confocal microscopy, representative images (scale bar: 50 μm) and quantitative data are shown. (b) Effect of blocking anti-GPVI mAb, the GPIIb/IIIa inhibitor tirofiban, the CypD inhibitor cyclosporin A, or isotype control antibodies/drug vehicle on surface expression of PD-L1, CD80, and CD86 on platelets exposed to collagen I as assessed *in vitro* by immunostaining and flow cytometry, quantitative data are shown. (c) Surface expression of PD-L1, CD80, and CD86 on platelets exposed to collagen I isolated from PF4^{cre}-TMEM16F^{fl/fl} cre- (TMEM16F^{pl^t/+}) or cre+ (TMEM16F^{pl^t/-}) mice as assessed *in vitro* by immunostaining and flow cytometry, quantitative data are shown. (d) Intratumoral accumulation of PS^{high} and PS^{low} platelets and (e) immune cells as assessed by flow cytometry as well as (f) weight of 4T1 tumors orthotopically raised in mice treated with blocking anti-GPVI mAb, the GPIIb/IIIa inhibitor tirofiban, or isotype control antibodies/drug vehicle, quantitative data are shown.

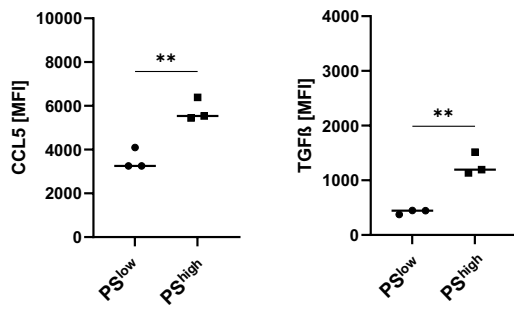


Figure S12. Cytokine expression on mouse platelets. Surface expression of CCL5 and TGFβ on non-procoagulant PS^{low} platelets and on procoagulant PS^{high} platelets isolated from the peripheral blood of female BALB/c mice as assessed by flow cytometry, quantitative data are shown (mean±SEM for n=3 per group; **p<0.01 vs. PS^{high}).

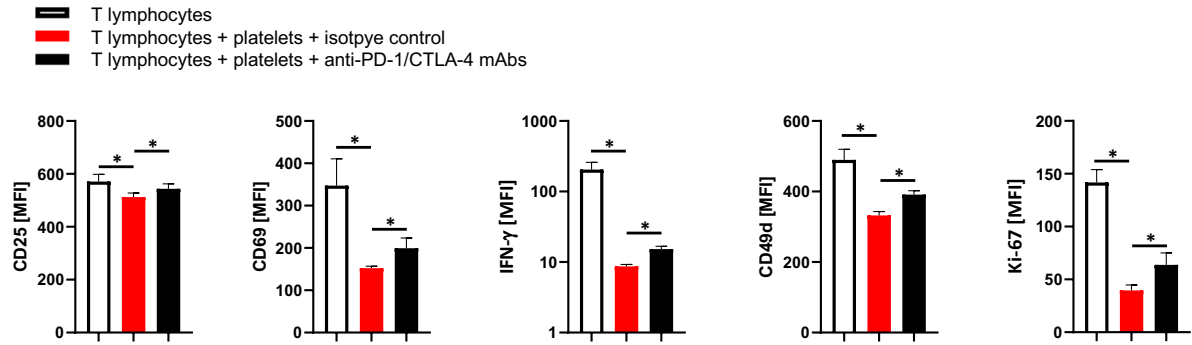


Figure S13. Effect of platelets on lymphocyte function. Activation status of primary mouse OKT3-stimulated CD3⁺ T lymphocytes exposed to platelets isolated from the peripheral blood of orthotopically 4T1 tumor-bearing mice exposed to blocking anti-PD-1/CTLA-4 mAbs or isotype control antibodies as indicated by expression of CD25, CD69, IFN- γ , CD49d, and Ki-67 assessed in flow cytometry, quantitative data are shown (mean \pm SEM for n=4 experiments per group; *p<0.05 vs indicated group).

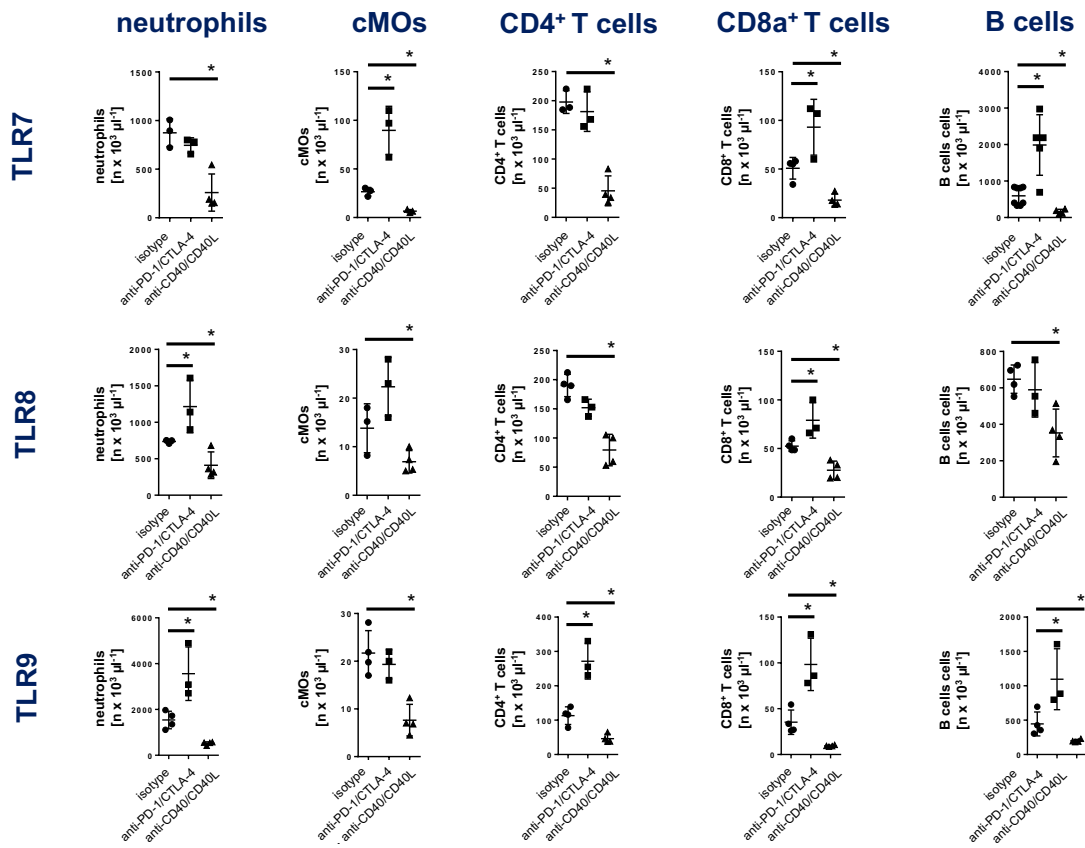


Figure S14. Effects of immune checkpoint blockades on immune cell responses elicited by endosomal TLR agonists. Recruitment of neutrophils, classical monocytes (cMOs), CD4⁺ T cells, CD8⁺ T cells, and B cells to the peritoneal cavity of mice 6h after intraperitoneal injection of agonists of TLR7, -8, or -9 receiving anti-PD-1 and -CTLA-4 mAbs, anti-CD40 and anti-CD40L mAbs, or isotype control antibodies, quantitative data are shown (mean±SEM for n=3-4 per group; *p<0.05 vs. isotype).

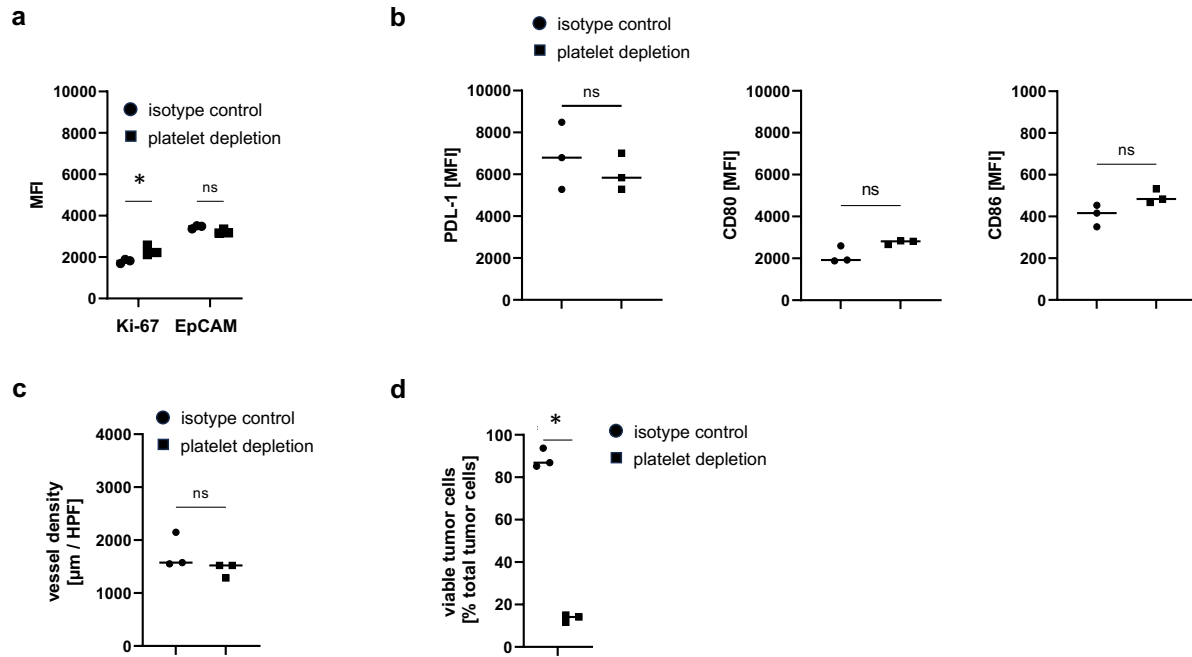


Figure S15. Effect of platelets on tumor cell properties *in vivo*. (a) 4T1 tumor cell expression of Ki-67 (as measure of cell proliferation) and EpCAM (as measure of EMT), (b) of the immune checkpoint molecules PD-L1, CD80, and CD86 as assessed by flow cytometry in homogenates of orthotopically raised 4T1 tumors in mice receiving platelet-depleting anti-GPIIb α mAb or isotype control antibodies, quantitative data are shown (mean \pm SEM for n=3 per group; *p<0.05 vs. isotype control; ns=not significant). (c) Intratumoral vessel density as assessed by *in vivo* microscopy in heterotopically raised 4T1 tumors in mice receiving platelet-depleting anti-GPIIb α mAb or isotype control antibodies, quantitative data are shown (mean \pm SEM for n=3 per group; ns=not significant). (d) Uptake of NucBlue in tumor cells (as measure of impaired cellular viability) as assessed by flow cytometry in homogenates of orthotopically raised 4T1 tumors in mice receiving platelet-depleting anti-GPIIb α or isotype control antibodies, quantitative data are shown (mean \pm SEM for n=3 per group; *p<0.05 vs. isotype control).

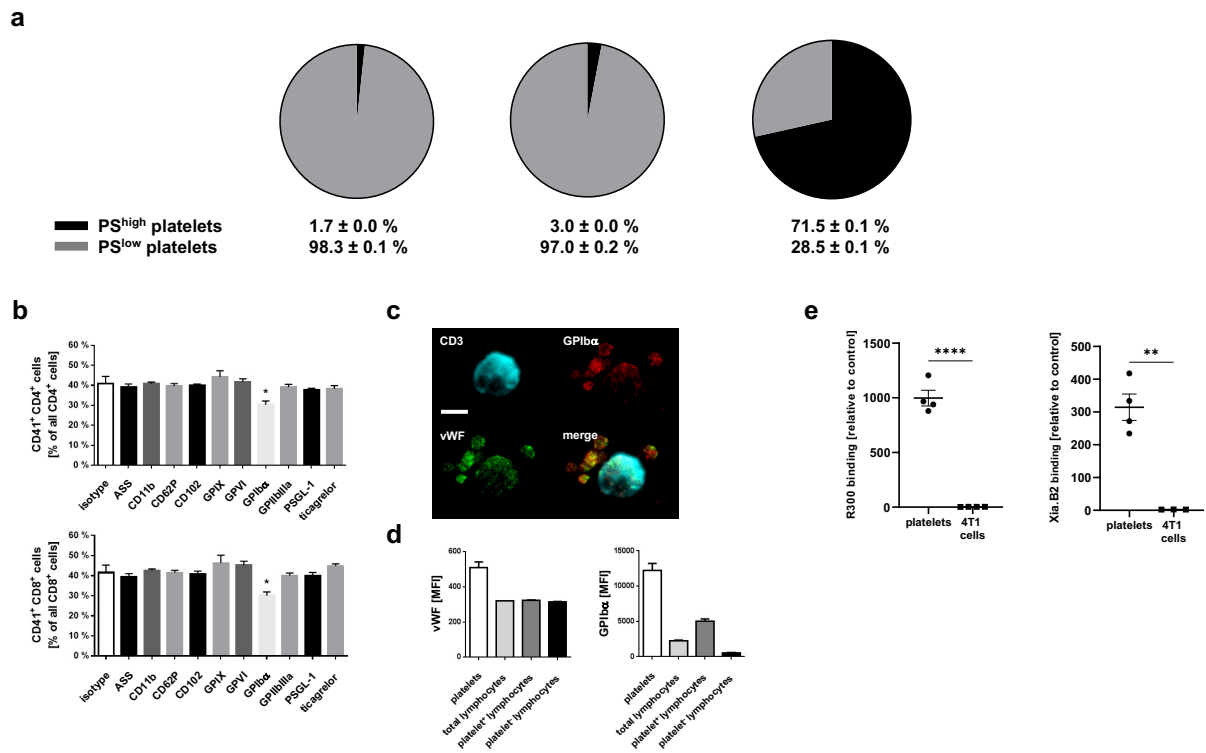


Figure S16. Effects of anti-platelet compounds on binding of platelets to lymphocytes. (a) Proportion of platelet subsets bound to CD3⁺ T lymphocytes isolated from peripheral blood of healthy mice or from peripheral blood and tumors of orthotopically 4T1 tumor-bearing mice as assessed by flow cytometry, quantitative data are shown. (b) Binding of CD41⁺ platelets to CD4⁺ or CD8⁺ T cells isolated from the peripheral blood of orthotopically 4T1 tumor-bearing mice as assessed *in vitro* by flow cytometry upon application of blocking anti-CD11b/Mac-1 mAbs, anti-CD62P/P-selectin mAbs, anti-CD102/ICAM-2 mAbs, anti-GPIX mAbs, anti-GPVI mAbs, anti-GPIIb α mAbs, anti-GPIIbIIIa mAbs, or anti-PSGL-1 mAbs as well as a P2Y₁₂ inhibitor (ticagrelor), a COX inhibitor (ASS), or isotype control antibodies/drug vehicle, quantitative data are shown (mean \pm SEM for n=5 per group; *p<0.05 vs. isotype control). (c) Confocal microscopy images and (d) quantitative flow cytometry data of GPIIb α and vWF expression on platelets and CD3⁺ T cells (mean \pm SEM for n=5 per group). (e) Binding of depleting (R300) or blocking (Xia.B2) anti-GPIIb α mAbs to platelets or 4T1 tumor cells as assessed by flow cytometry, quantitative data are shown (mean \pm SEM for n=3 per group; **p<0.01/****p<0.0001 vs. 4T1 tumor cells).

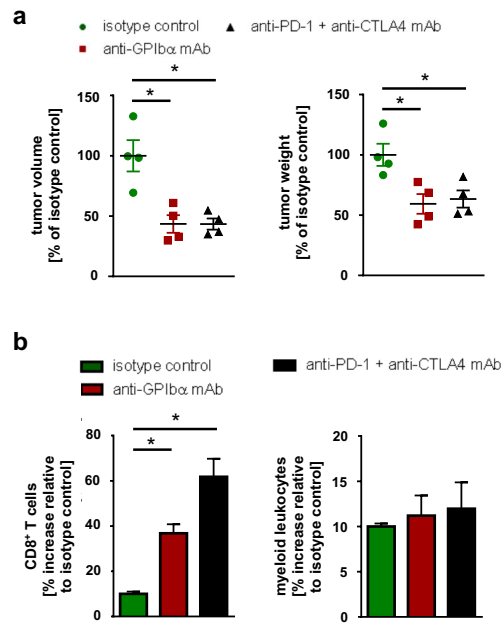


Figure S17. Effects of anti-platelet and immune checkpoint inhibitor therapy in experimental TNBC. (a) Relative volume and weight of tumors as well as (b) relative infiltration by CD8⁺ T lymphocytes and myeloid leukocytes of orthotopically grown TNBC tumors in mice receiving blocking anti-GPIIb α mAbs, anti-PD-1/-CTLA4 mAbs, or isotype control antibodies daily from day 7 – 14 after 4T1 tumor cell injection, quantitative data are shown (mean \pm SEM for n=4 mice per group; *p<0.05 vs. isotype control).

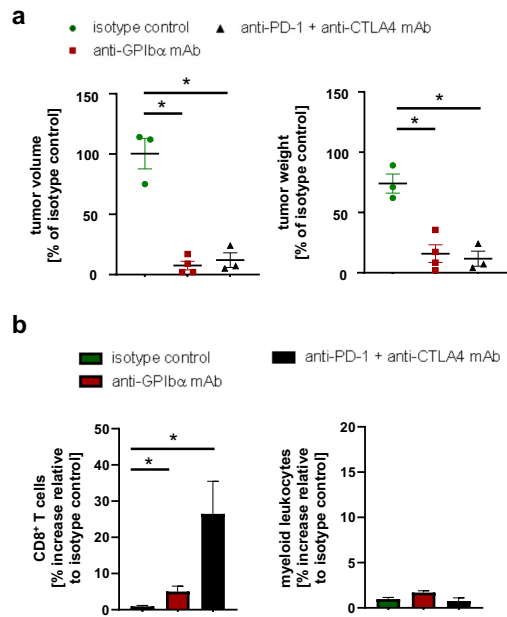
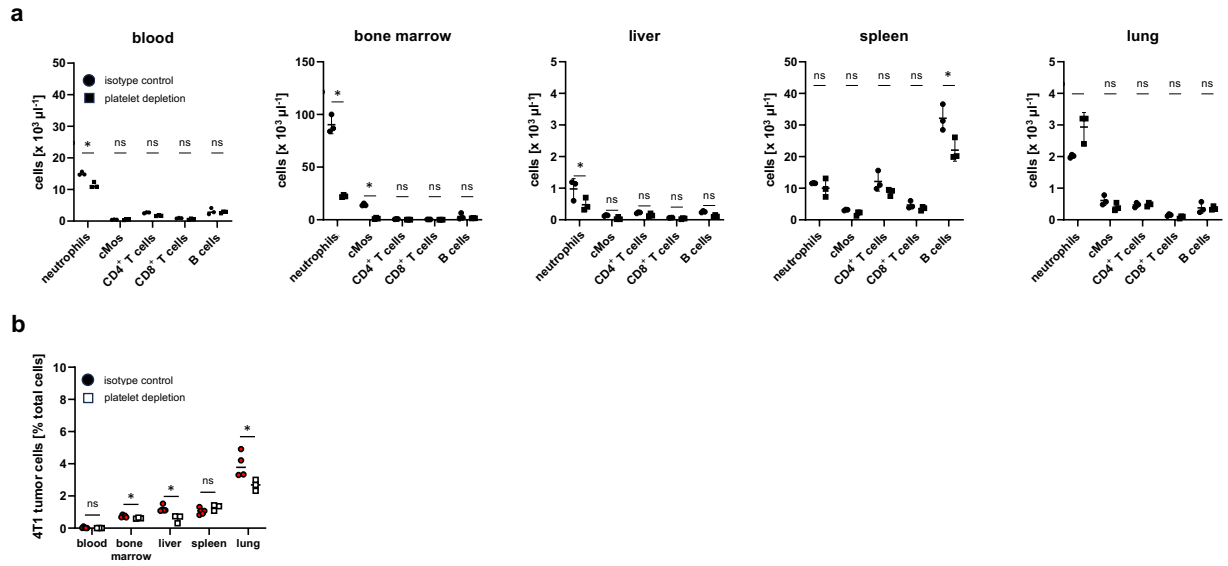
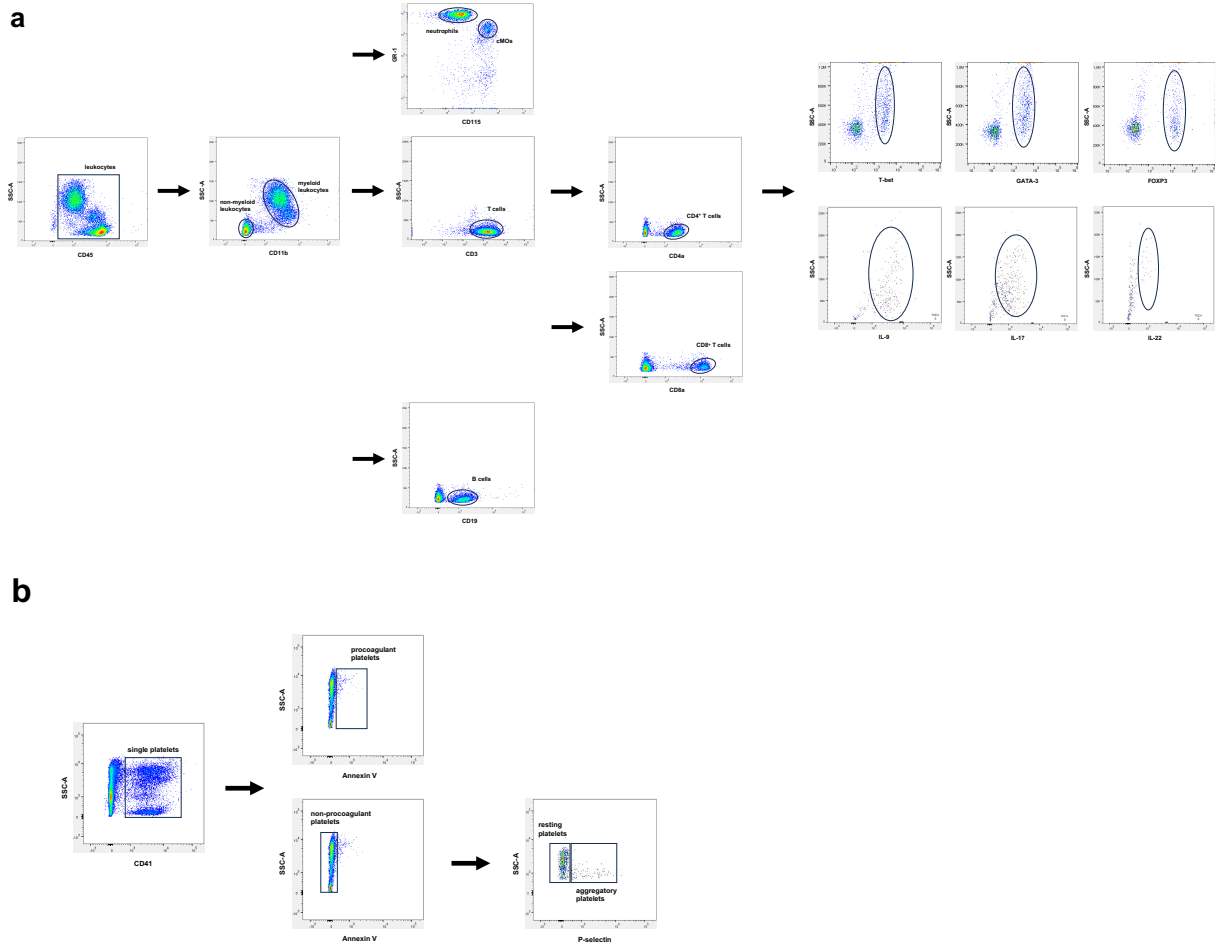


Figure S18. Effects of anti-platelet and immune checkpoint inhibitor therapy in experimental HNSCC. (a) Relative volume and weight of tumors as well as (b) relative infiltration by lymphocytes and myeloid leukocytes of orthotopically grown HNSCC tumors in mice receiving blocking anti-GPIIb/IIIa mAbs, anti-PD-1/-CTLA4 mAbs, or isotype control antibodies daily from day 7 – 14 after SCC VII tumor cell injection, quantitative data are shown (mean±SEM for n=5 mice per group; *p<0.05 vs. isotype control).



S19. Effects of platelets on early formation of tumor cell metastases in experimental TNBC. (a) Accumulation of different immune cells and (b) 4T1 tumor metastases in peripheral blood, bone marrow, liver, spleen, and lungs of orthotopically 4T1 tumor-bearing mice treated with platelet-depleting mAbs or isotype control antibodies, quantitative data are shown (mean±SEM for n=3-4 mice per group; *p<0.05 vs. isotype control).



S20. Gating strategies in flow cytometry analyses. Identification of (a) neutrophils ($CD45^+ CD11b^+ Gr-1^{high} CD115^{low}$), classical monocytes ($CD45^+ CD11b^+ Gr-1^{high} CD115^{low}$), B lymphocytes ($CD45^+ CD11b^- CD19^+$), $CD8^+$ T lymphocytes ($CD45^+ CD11b^- CD3^+ CD8a^+$), and $CD4^+$ T lymphocytes ($CD45^+ CD11b^- CD3^+ CD4a^+$), which are further differentiated by expression of T-bet (Th1), GATA-3 (Th2), FOXP3 (T_{reg}), IL-9 (Th9), IL-17 (Th17), and IL-22 (Th22). (b) Identification of procoagulant platelets ($CD41^+ Annexin V^{high}$) and non-procoagulant ($CD41^+ Annexin V^{low}$) platelets, which are further differentiated into P-selectin⁻ resting platelets and P-selectin⁺ aggregatory platelets, representative plots are shown.

Supplemental videos

Video S1. Interactions of platelets in the tumor microvasculature. Representative multi-channel *in vivo* microscopy video of platelets (GPIIb/IIIa; white) interacting with leukocytes (CD45; red) in the microvasculature (black) of a heterotopically (mouse auricle) grown 4T1 tumor (blue).

Video S2. Procoagulant platelet activation in the tumor microvasculature. Representative multi-channel *in vivo* microscopy video of procoagulant activated (Annexin V; red) platelets (GPIIb/IIIa; white) in the microvasculature (black) of a heterotopically (mouse auricle) grown 4T1 tumor (blue).



Supplemental References

1. Kaiser R, Escaig R, Kranich J, et al. Procoagulant platelet sentinels prevent inflammatory bleeding through GPIIBIIIA and GPVI. *Blood*. 2022;140(2):121-139.
2. Baez S. An open cremaster muscle preparation for the study of blood vessels by in vivo microscopy. *Microvasc Res*. 1973;5(3):384-394.
3. Zuchtriegel G, Uhl B, Pühr-Westerheide D, et al. Platelets Guide Leukocytes to Their Sites of Extravasation. *PLoS Biol*. 2016;14(5):e1002459.
4. Curtis C, Shah SP, Chin SF, et al. The genomic and transcriptomic architecture of 2,000 breast tumours reveals novel subgroups. *Nature*. 2012;486(7403):346-352.

4. Publication II



uPA-PAI-1 heteromerization promotes breast cancer progression by attracting tumorigenic neutrophils

Bernd Uhl^{1,2}, Laura A Mittmann^{1,2}, Julian Dominik^{1,2}, Roman Hennen³, Bojan Smiljanov^{1,2}, Florian Haring^{1,2}, Johanna B Schaubächer^{1,2}, Constanze Braun^{1,2}, Lena Padovan^{1,2}, Robert Pick², Martin Canis¹, Christian Schulz⁴, Matthias Mack⁵, Ewgenija Gutjahr⁶, Peter Sinn⁶, Jörg Heil⁷, Katja Steiger⁸, Sandip M Kanse⁹, Wilko Weichert^{8,10}, Markus Sperandio¹¹ , Kirsten Lauber³, Fritz Krombach² & Christoph A Reichel^{1,2,*} 

Abstract

High intratumoral levels of urokinase-type plasminogen activator (uPA)-plasminogen activator inhibitor-1 (PAI-1) heteromers predict impaired survival and treatment response in early breast cancer. The pathogenetic role of this protein complex remains obscure. Here, we demonstrate that heteromerization of uPA and PAI-1 multiplies the potential of the single proteins to attract pro-tumorigenic neutrophils. To this end, tumor-released uPA-PAI-1 utilizes very low-density lipoprotein receptor and mitogen-activated protein kinases to initiate a pro-inflammatory program in perivascular macrophages. This enforces neutrophil trafficking to cancerous lesions and skews these immune cells toward a pro-tumorigenic phenotype, thus supporting tumor growth and metastasis. Blockade of uPA-PAI-1 heteromerization by a novel small-molecule inhibitor interfered with these events and effectively prevented tumor progression. Our findings identify a therapeutically targetable, hitherto unknown interplay between hemostasis and innate immunity that drives breast cancer progression. As a personalized immunotherapeutic strategy, blockade of uPA-PAI-1 heteromerization might be particularly beneficial for patients with highly aggressive uPA-PAI-1^{high} tumors.

Keywords biomarker; breast cancer; fibrinolysis; innate immunity; neutrophils

Subject Categories Cancer; Immunology; Vascular Biology & Angiogenesis

DOI 10.15252/emmm.202013110 | Received 14 July 2020 | Revised 28 April 2021 | Accepted 25 March 2021 | Published online 16 May 2021

EMBO Mol Med (2021) 13: e13110

Introduction

Our immune system protects the organism from life-threatening infections and also from the development of malignant tumors. Importantly, however, distinct immune cell subsets are increasingly recognized to promote tumor initiation, progression, and metastasis formation in various cancer entities (Coffelt *et al*, 2016; Nicolas-Avila *et al*, 2017). In particular, the presence of neutrophilic granulocytes (neutrophils) in malignant lesions is associated with a very poor clinical outcome, despite representing a comparatively small leukocyte population in solid tumors (Gentles *et al*, 2015). In this regard, neutrophils are thought to support tumorigenesis *via* the production of cell injuring reactive oxygen species (ROS) and proteases, of pro-proliferative signals (*e.g.*, neutrophil elastase [NE]), of pro-angiogenic mediators (*e.g.*, matrix-metalloproteinase-9 [MMP-9], vascular endothelial growth factor [VEGF]), and of immunosuppressive factors (*e.g.*, arginase-1; Coffelt *et al*, 2016). In addition, neutrophils release net-like structures of DNA, histones, and other proteins (“neutrophil extracellular traps”; NETs) that facilitate tumor metastasis by sequestering circulating cancer cells (Demers *et al*, 2012; Cedervall *et al*, 2015). Interestingly, however,

1 Department of Otorhinolaryngology, University Hospital, Ludwig-Maximilians-Universität München, Munich, Germany

2 Walter Brendel Centre of Experimental Medicine, University Hospital, Ludwig-Maximilians-Universität München, Munich, Germany

3 Department of Radiation Oncology, University Hospital, Ludwig-Maximilians-Universität München, Munich, Germany

4 Department of Cardiology, University Hospital, Ludwig-Maximilians-Universität München, Munich, Germany

5 Department of Internal Medicine, University of Regensburg, Regensburg, Germany

6 Institute for Pathology, University of Heidelberg, Heidelberg, Germany

7 Department of Gynecology and Obstetrics, University of Heidelberg, Heidelberg, Germany

8 Department of Pathology, Technical University of Munich, Munich, Germany

9 Institute of Basic Medical Sciences, University of Oslo, Oslo, Norway

10 German Cancer Consortium (DKTK), partner site Munich, Ludwig-Maximilians-Universität München, Munich, Germany

11 Institute of Cardiovascular Physiology and Pathophysiology, Ludwig-Maximilians-Universität München, Munich, Germany

*Corresponding author. Tel: +49 89 4400 0; Fax: +49 89 2180 76538; E-mail: christoph.reichel@med.uni-muenchen.de

neutrophils have also been reported to exert anti-tumorigenic effects including antibody-dependent cell-mediated cytotoxicity (Coffelt *et al*, 2016). Accordingly, the existence of anti- (“N1”) and pro-tumorigenic (“N2”) phenotypes of neutrophils has been proposed (Fridlender *et al*, 2009). In contrast to these ambivalent functional properties of neutrophils in cancer, the mechanisms underlying the recruitment of these immune cells to malignant lesions remain largely unclear.

Fibrinolysis is a fundamental biological process that maintains tissue perfusion by preventing clot formation in blood vessels. Plasmin is the principal effector protease in the fibrinolytic system mediating the dissolution of fibrin polymers which is activated by proteolytic processing *via* the serine proteases uPA or tissue-plasminogen activator (tPA). The activity of these two plasminogen activators is tightly controlled by heteromerization with their inhibitor PAI-1. Besides their well-established role in fibrinolysis, it has been shown that the components of the fibrinolytic system are involved in additional biological processes including the regulation of cell adhesion, migration, and proliferation (Das *et al*, 2010; Smith & Marshall, 2010; Reichel *et al*, 2011b). In this context, plasmin, uPA, tPA, and PAI-1 have recently been demonstrated to promote neutrophil trafficking to sites of inflammation through their distinct proteolytic and non-proteolytic properties (Reichel *et al*, 2011a; Reichel *et al*, 2011b; Uhl *et al*, 2014; Praetner *et al*, 2018).

Breast cancer is the most frequently occurring oncological disorder in women worldwide (Carioli *et al*, 2017; Carioli *et al*, 2018). High intratumoral levels of uPA, PAI-1, and, especially, their heteromeric complexes have been identified as independent predictive factors for impaired survival (Andreasen *et al*, 1997; Schmitt *et al*, 1997; Knoop *et al*, 1998; Duffy *et al*, 1999; Foekens *et al*, 2000; Janicke *et al*, 2001; Sten-Linder *et al*, 2001; Look *et al*, 2002; Manders *et al*, 2004b) and treatment response (Harbeck *et al*, 2002a; Harbeck *et al*, 2002b; Manders *et al*, 2004a; Manders *et al*, 2004c) in early breast cancer, irrespective of the underlying histopathological subtype. Similarly, first clinical data suggest that high intratumoral expression of uPA-PAI-1 is related to poor survival rates in other malignancies such as pulmonary adenocarcinoma (Pappot *et al*, 2006). Although uPA-PAI-1 has been documented to exert a modest pro-proliferative and pro-migratory effect on cultured tumor cells (Webb *et al*, 1999; Webb *et al*, 2001), the precise function of this protein complex in the pathogenesis of (breast) cancer is still unknown.

Results

With respect to the emerging role of neutrophils in cancer (Coffelt *et al*, 2016; Nicolas-Avila *et al*, 2017), the recently uncovered effects of uPA and PAI-1 on neutrophil trafficking (Reichel *et al*, 2011b; Praetner *et al*, 2018), and the clinical observations of uPA-PAI-1 heteromers as an independent prognosticator of impaired survival (Andreasen *et al*, 1997; Schmitt *et al*, 1997; Knoop *et al*, 1998; Duffy *et al*, 1999; Foekens *et al*, 2000; Janicke *et al*, 2001; Sten-Linder *et al*, 2001; Look *et al*, 2002; Manders *et al*, 2004b) and treatment response (Harbeck *et al*, 2002a; Harbeck *et al*, 2002b; Manders *et al*, 2004a; Manders *et al*, 2004c) in early breast cancer, we hypothesize that this protein complex supports the progression of this oncologic

disorder by promoting the trafficking of pro-tumorigenic neutrophils to malignant lesions.

Effect of uPA-PAI-1 heteromerization on leukocyte trafficking

To prove this hypothesis, we first explored the effect of uPA-PAI-1 heteromerization on leukocyte trafficking. For this purpose, we examined the potential of the different components of the fibrinolytic system as well as of the heteromers of these proteins to attract circulating leukocytes by employing a mouse peritonitis assay and multi-channel flow cytometry. Intraperitoneal injection of recombinant mouse uPA, tPA, or PAI-1 induced a significant increase in numbers of neutrophils, classical monocytes, and non-classical monocytes, to the peritoneal cavity (Fig 1A). This increase was even more pronounced in animals receiving uPA-PAI-1 heteromers, whereas stimulation with tPA-PAI-1 heteromers did not initiate additional myeloid leukocyte responses as compared to the single proteins. Noteworthy, uPA-PAI-1 did not elicit the trafficking of B lymphocytes, CD4⁺ T lymphocytes, or CD8⁺ T lymphocytes to the peritoneal cavity. Moreover, uPA-PAI-1-dependent responses of classical monocytes were completely abolished in neutrophil-depleted animals (Fig 1B), collectively indicating that heteromerization of uPA and PAI-1 multiplies the potential of the single proteins to promote neutrophil trafficking.

To analyze the effect of uPA-PAI-1 heteromers on the trafficking of neutrophils (and classical monocytes) in more detail, we performed multi-channel *in vivo* microscopy in a cremaster muscle assay using CX₃CR-1^{+GFP} (monocyte reporter) mice. Although intrascrotal stimulation with uPA, PAI-1, or uPA-PAI-1 heteromers did not alter intravascular rolling of these innate immune cells, intravascular firm adherence and (subsequent) transmigration of Ly-6G⁺ CX₃CR-1⁻ neutrophils and Ly-6G⁻ CX₃CR-1^{low} classical monocytes (cMOs) to the perivascular tissue were significantly enhanced as compared to unstimulated controls (Fig 1C). In accordance with our previous findings, the potential of uPA-PAI-1 to induce these myeloid leukocyte responses was significantly higher as compared to the single proteins, but was similar as compared to the cytokine tumor necrosis factor (TNF; Appendix Fig S1A). Thus, uPA-PAI-1 heteromers potently mediate intravascular accumulation and subsequent extravasation of neutrophils to the perivascular space.

Cell-specific effects of uPA-PAI-1 heteromers

Leukocyte trafficking from the microvasculature to their target destination is dependent on a complex multicellular interplay of these immune cells with perivascular macrophages and endothelial cells (Ley *et al*, 2007; Kolaczowska & Kubes, 2013; Nourshargh & Alon, 2014). In a next step, we therefore sought to decipher cell-specific effects of uPA-PAI-1 heteromers. Employing immunostaining and confocal microscopy in cremasteric tissue whole mounts, uPA and PAI-1 were detected in the perivenular space of inflamed tissue as well as—to a lesser extent—on the microvascular endothelium of postcapillary venules (Fig 2A). To characterize the effect of extravascular uPA-PAI-1 heteromers on the activation of microvascular endothelial cells *in vivo*, these protein complexes were injected into the mouse scrotum. Here, uPA-PAI-1 induced a significant elevation in the expression of ICAM-1/CD54 and VCAM-1/CD106 on venular endothelial cells as compared to unstimulated controls

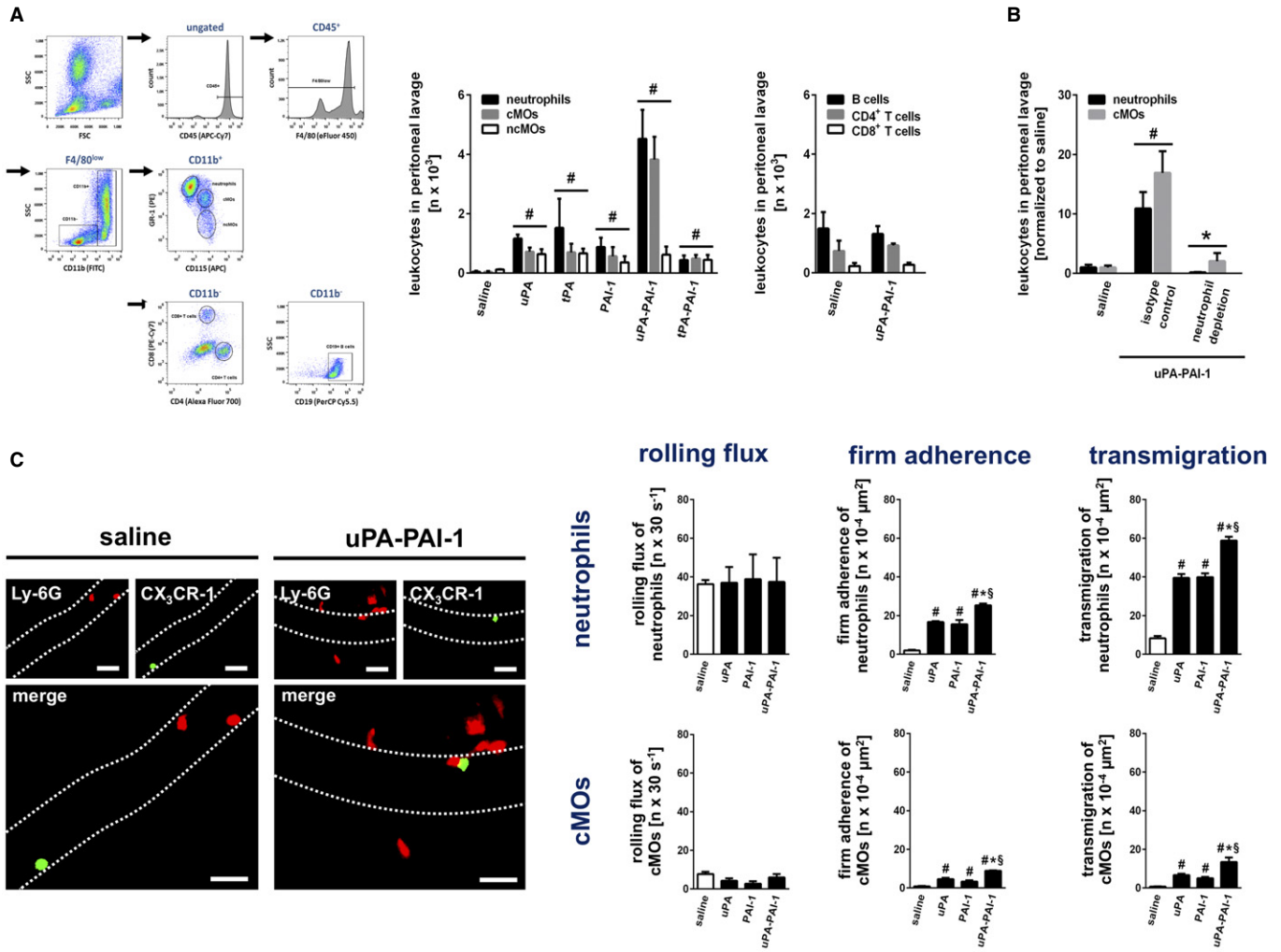


Figure 1. Effect of uPA-PAI-1 heteromerization on leukocyte trafficking.

A Trafficking of neutrophils (N), classical monocytes (cMOs), non-classical monocytes (ncMOs), B lymphocytes, CD4⁺ T lymphocytes, and CD8⁺ T lymphocytes to the peritoneal cavity as assessed 6 h after intraperitoneal stimulation with recombinant murine uPA, tPA, PAI-1, uPA-PAI-1, or tPA-PAI-1 in WT mice by multi-channel flow cytometry. The gating strategy and quantitative data are shown (mean ± SEM for n = 5 mice per group; [#]P < 0.05 vs. saline; one-way ANOVA).

B Neutrophil and cMO trafficking to the peritoneal cavity elicited by recombinant murine uPA-PAI-1 as assessed in WT mice receiving neutrophil-depleting anti-Ly-6G mAbs or isotype control ABs, quantitative data are shown (mean ± SEM for n = 4 mice per group; [#]P < 0.05 vs. saline; ^{*}P < 0.05 vs. isotype; one-way ANOVA).

C Intravascular endothelial cell interactions and transmigration of neutrophils (Ly-6G⁺ CX₃CR-1^{low}; red) and cMOs (Ly-6G⁺ CX₃CR-1^{low}; green) to the perivascular tissue as assessed 6 h after intrascrotal stimulation with recombinant murine uPA, PAI-1, or uPA-PAI-1 in postcapillary venules of the cremaster of CX₃CR-1^{GFP/+} mice by multi-channel *in vivo* microscopy. Representative still images (scale bar: 50 μm) and quantitative data are shown (mean ± SEM for n = 4 mice per group; [#]P < 0.05 vs. saline; ^{*}P < 0.05 vs. uPA; [§]P < 0.05 vs. PAI-1; one-way ANOVA).

(Fig 2B). This effect of uPA-PAI-1 was more pronounced as compared to the single proteins (Appendix Fig S1B). In multiplex ELISA (Fig EV1A and B) and multi-channel flow cytometry (Fig 2C) *in vitro* analyses, we further identified that uPA-PAI-1 heteromers potently stimulate cultured mouse macrophages to produce a variety of CC and CXC chemokines as well as of cytokines including TNF. This uPA-PAI-1-elicited release of TNF was confirmed in primary mouse macrophages (Appendix Fig S2A). In contrast to TNF, however, exposure to uPA-PAI-1 heteromers did not directly activate cultured mouse microvascular endothelial cells *in vitro* as indicated by unchanged surface expression of ICAM-1/CD54 and VCAM-1/CD106 (Fig 2D). Consequently, co-culture with uPA-PAI-1

(or TNF)-stimulated RAW macrophages induced the surface expression of ICAM-1/CD54 and VCAM-1/CD106 in bEND.3 endothelial cells (Appendix Fig S2B). Hence, uPA-PAI-1 heteromers stimulate cytokine release from perivascular macrophages that, in turn, activates microvascular endothelial cells.

Intraluminal adherence to the microvascular endothelium of intravascularly rolling leukocytes is facilitated by interactions between endothelial members of the immunoglobulin superfamily (e.g., ICAM-1/CD54, VCAM-1/CD106) and leukocyte β1 or β2 integrins in higher affinity conformation as elicited by endothelially presented chemokines (Ley *et al*, 2007; Kolaczowska & Kubes, 2013; Nourshargh & Alon, 2014). Similar to chemokines, uPA and

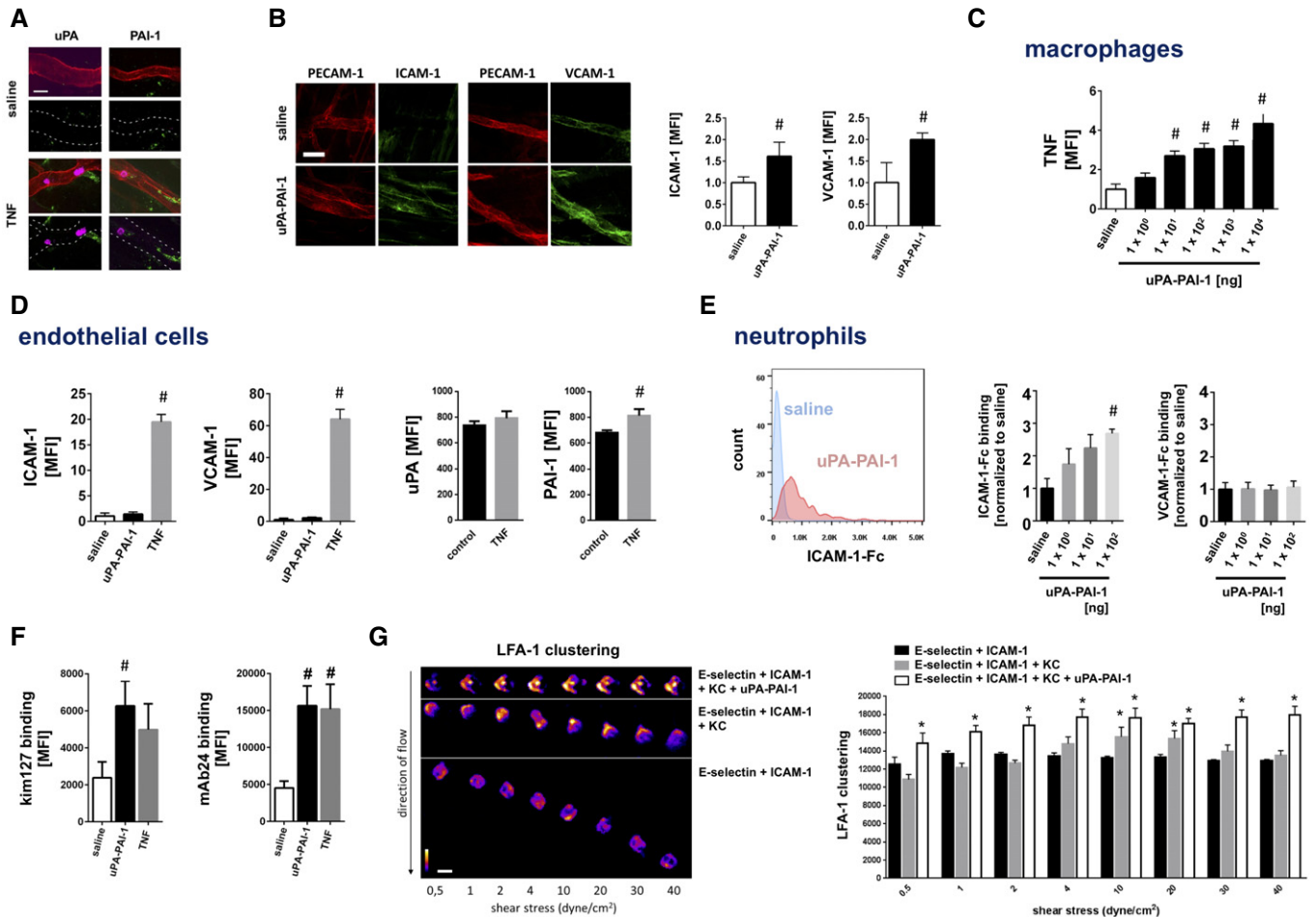


Figure 2. Mechanisms underlying uPA-PAI-1-dependent neutrophil trafficking.

- A** Deposition of uPA or PAI-1 (green) in the cremaster muscle of WT mice as assessed separately *ex vivo* by confocal laser scanning microscopy 6 h after intrascrotal injection of TNF or saline. PECAM-1/CD31⁺ postcapillary venules (red) and Ly-6G⁺ neutrophils (purple) are depicted. Representative images are shown (scale bar: 50 μ m).
- B** Expression of PECAM-1/CD31 (red) and ICAM-1/CD54 or VCAM-1/CD106 (green) in the cremaster muscle of WT mice as assessed *ex vivo* by confocal laser scanning microscopy 6 h after intrascrotal injection of recombinant murine uPA-PAI-1 or saline, representative images (scale bar: 50 μ m), and quantitative data are shown (mean \pm SEM for $n = 4$ mice per group; $^{\#}P < 0.05$ vs. saline; *t*-test).
- C, D** (C) Production of TNF was analyzed in mouse RAW 264.7 macrophages and (D) surface expression of ICAM-1/CD54, VCAM-1/CD106, uPA, and PAI-1 on mouse bEnd.3 microvascular endothelial cells as assessed *in vitro* by multi-channel flow cytometry upon exposure to recombinant murine uPA-PAI-1, TNF, or saline, quantitative data are shown (mean \pm SEM for $n = 4$ experiments per group; $^{\#}P < 0.05$ vs. saline; one-way ANOVA/*t*-test).
- E, F** (E) Binding of ICAM-1/CD54-Fc or VCAM-1/CD106-Fc to primary mouse neutrophils and (F) binding of conformation-specific mAbs to primary human neutrophils ("mAb 24" recognizing high-affinity conformation, "kim127" recognizing intermediate and high-affinity conformation of β_2 integrins) as assessed upon exposure to recombinant murine/human uPA-PAI-1, TNF, or saline by multi-channel flow cytometry, a representative histogram plot and quantitative data are shown (mean \pm SEM for $n = 4$ –7 mice/human blood samples per group; $^{\#}P < 0.05$ vs. saline; one-way ANOVA).
- G** Quantitative analysis of LFA-1/CD11a clustering on the surface of mouse neutrophils under increasing flow conditions *in vitro* in the presence of either E-selectin/CD62E + ICAM-1/CD54, E-selectin/CD62E + ICAM-1/CD54 + KC, or E-selectin/CD62E + ICAM-1/CD54 + KC + uPA-PAI-1 as assessed by spinning disk confocal microscopy, representative images and quantitative data are shown (scale bar: 10 μ m; mean \pm SD; $n = 3$ mice; $n = 10$ –13 flow chambers, $n = 122$ –222 cells); $^*P < 0.05$ vs. E-selectin/CD62E + ICAM-1/CD54; one-way ANOVA).

PAI-1 were also found on the endothelium of inflamed postcapillary venules (Fig 2A). Since activation of cultured microvascular endothelial cells did not substantially alter the surface expression of uPA or PAI-1 (Fig 2D), these circulating molecules are thought to be deposited on the surface of activated endothelial cells. In addition, uPA-PAI-1-elicited trafficking of neutrophils and classical monocytes to the peritoneal cavity were significantly reduced upon antibody blockade of the β_1 integrin VLA-4/CD49d, the β_2 integrins LFA-1/

CD11a or Mac-1/CD11b, or their counter receptors ICAM-1/CD54 or VCAM-1/CD106 (Fig EV2A). Consequently, endothelially deposited uPA-PAI-1 heteromers might also induce conformational changes in integrins on the surface of intravascularly rolling neutrophils, ultimately facilitating the adhesion of these innate immune cells to the inner vessel wall. In further experiments, uPA-PAI-1 heteromers (dose-dependently) increased the clustered binding of ICAM-1/CD54-Fc, but not of VCAM-1/CD106-Fc, to the surface of

neutrophils isolated from the peripheral blood of mice (Fig 2E; Appendix Fig S2C) which is indicative for the induction of higher affinity conformations in neutrophil $\beta 2$ integrins. To directly evaluate the effect of uPA-PAI-1 heteromers on conformational changes in neutrophil $\beta 2$ integrins, we also analyzed the binding of conformation-specific $\beta 2$ integrin antibodies (only available in the human system) to human blood neutrophils. Exposure to uPA-PAI-1 led to enhanced recognition of the conformation-specific antibodies kim127 (indicating the presence of intermediate and high-affinity conformations of $\beta 2$ integrins) and mAb24 (indicating the presence of the high-affinity conformation of $\beta 2$ integrins; Fig 2F). Employing spinning disk confocal microscopy in an *in vitro* detachment assay under flow conditions, we further observed that uPA-PAI-1 also supports the clustering of $\beta 2$ integrins such as lymphocyte function-associated integrin-1 (LFA-1/CD11a) on the surface of adhering murine neutrophils (Fig 2G). In summary, these data suggest that endothelially deposited uPA-PAI-1 heteromers promote neutrophil responses through effects on activation and surface clustering of $\beta 2$ integrins.

Mechanisms underlying uPA-PAI-1-dependent neutrophil responses

In fibrinolysis, the activity of uPA is controlled by heteromerization with its inhibitor PAI-1 which, in turn, allows for the endocytic clearance of these protein complexes from the circulation by endothelial receptors of the LDL receptor family such as very low-density lipoprotein receptor (VLDLr) or low-density lipoprotein receptor-related protein-1 (LRP-1) and subsequent activation of intracellular mitogen-activated protein kinases (MAPK) (Conese *et al*, 1995; Webb *et al*, 1999; Webb *et al*, 2001; Strickland *et al*, 2002). Consequently, uPA-PAI-1 heteromers might mediate neutrophil trafficking *via* such molecular events. Employing our peritonitis assay, antibody blockade of VLDLr, but not of LRP-1, as well as inhibition of downstream MAPK-dependent intracellular signaling pathways almost completely abolished uPA-PAI-1-elicited neutrophil recruitment to the peritoneal cavity (Fig EV2B). Moreover, these uPA-PAI-1-dependent neutrophil responses were not significantly altered when replacing native mouse uPA in the heteromers by human uPA (which does not bind to murine uPAR) or by DFP-uPA (in which the proteolytic activity of uPA is inhibited; Fig EV2C). In this context, multi-channel flow cytometry revealed that VLDLr is significantly stronger expressed on the surface of mouse neutrophils and macrophages as compared to LRP-1 (Fig EV3A). Accordingly, uPA-PAI-1-elicited TNF synthesis in macrophages (Fig EV3B) and ICAM-1/CD54-Fc binding (indicative for integrin affinity changes) in neutrophils (Fig EV3C) were significantly diminished upon antibody blockade of VLDLr or pharmacological inhibition of MAPK. Specifically, blocking antibodies directed against the N-terminal cysteine-rich domains 3–6 (clone 1H10), 1–2, and 5–6 (clone 1H5), but not against the cysteine-rich domains 7–8 (clone 5F3) of VLDLr (Yakovlev *et al*, 2016), as well as inhibitors of ERK and JNK MAPK, but not of p38 MAPK, significantly reduced these uPA-PAI-1-dependent processes in macrophages and neutrophils. These data suggest that uPA-PAI-1 heteromers mediate neutrophil trafficking through VLDLr and MAPK-dependent signaling pathways, but independently of the protease activity of uPA or the receptors LRP-1 and uPAR.

Interrelation of uPA / PAI-1 expression, neutrophil infiltration, and disease outcome in human breast cancer

To explore the role of uPA-PAI-1 heteromers for neutrophil trafficking in human breast cancer, we analyzed a retrospective cohort of human breast cancer cases for neutrophilic infiltration (Appendix Table S1). In the tissue samples, uPA and PAI-1 protein expression (as assessed for clinical decision making during the time of treatment by the uPA/PAI-1 Femtelle assay (Schmitt *et al*, 2008)) positively correlated with neutrophil infiltration of low grade, but not of intermediate or high-grade tumors (Figs 3A and EV4). To complement these data, we studied RNA microarray data from the METABRIC breast cancer cohort (Curtis *et al*, 2012). Here, we found that in early, but not in advanced stages of disease, high RNA expression of PLAU and SERPINE1 (the genes encoding uPA and PAI-1) in the tumor is related to impaired overall survival of breast cancer patients (Figs 3B and EV5A and B). Importantly, this was not confounded by statistically significant enrichment of a distinct molecular subtype in the PLAU or SERPINE1 high expressing cases (Fig EV5C). Additionally, we observed a significant positive correlation between the RNA expression levels of PLAU and formyl peptide receptor 1 (FPR1), an established marker gene of neutrophils (Fig 3B). Thus, our results suggest that neutrophils attracted by uPA-PAI-1 to malignant lesions in human breast cancer are pro-tumorigenic.

Phenotypic and functional properties of uPA-PAI-1-primed neutrophils

Neutrophils are supposed to adopt anti- and pro-tumorigenic properties according to their surface protein signatures (*e.g.*, NE, MMP-9, or VEGF) (Fridlender *et al*, 2009). Using multi-channel flow cytometry, we found that uPA-PAI-1-recruited neutrophils isolated from the peritoneal cavity of mice exhibit significantly higher levels of NE as compared to unstimulated neutrophils from the peripheral blood, whereas the surface expression of MMP-9 and VEGF remained unchanged (Fig 3C). To further characterize pro-tumorigenic properties of uPA-PAI-1-primed neutrophils, we employed different *in vitro* and *ex vivo* assays. Co-incubation of 4T1 breast cancer cells with uPA-PAI-1-primed neutrophils, but not direct exposure of uPA-PAI-1 protein to the tumor cells or blockade of uPA-PAI-1 heteromerization by a novel small-molecule inhibitor (WX-340), significantly increased the proliferation of 4T1 cells (Fig 3D; Appendix Fig S2D). This increase was significantly reduced upon application of a NE inhibitor. In contrast, neither co-incubation with uPA-PAI-1-primed neutrophils, exposure to uPA-PAI-1 protein, nor treatment with WX-340 altered the proliferation of cultured microvascular endothelial cells (Fig 3E). In addition, uPA-PAI-1 heteromers—unlike TNF—did not induce NET formation in neutrophils (Fig 3F), as evidenced by confocal microscopy on cremasteric tissue whole mounts. Hence, uPA-PAI-1-primed neutrophils exhibit distinct pro-tumorigenic properties that stimulate tumor cell proliferation *via* NE.

Effect of inhibition of uPA-PAI-1 heteromerization on neutrophil trafficking and subsequent disease progression in 4T1 breast cancer

With respect to our present findings, we hypothesize that pharmacological inhibition of uPA-PAI-1 heteromerization interferes with

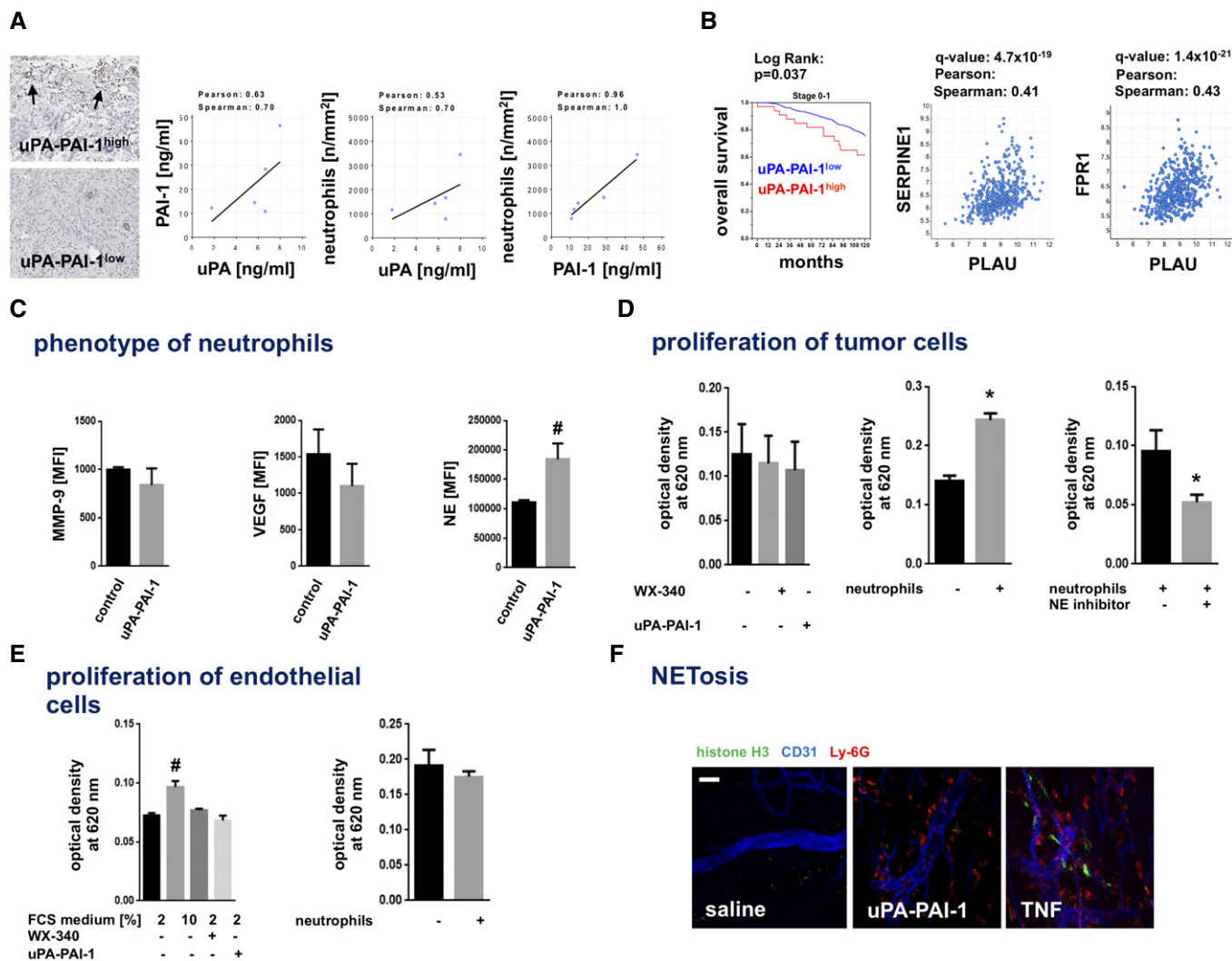


Figure 3. Phenotypic and functional properties of uPA-PAI-1-primed neutrophils.

- A** Correlation of uPA or PAI-1 protein expression and neutrophil infiltration in tumors as assessed by ELISA as well as immunohistochemistry and light microscopy in human breast cancer samples (histological grade: G1), representative images (scale bar: 100 μ m) and quantitative data are shown.
- B** Correlation analyses of RNA expression levels of uPA (PLAU gene), PAI-1 (SERPINE1 gene), and the neutrophil marker gene FPR1, and overall survival of breast cancer patients (stages 0 and 1) with high and low PLAU or SERPINE1 gene expression levels (cutoff $z \geq 2.0$) in the METABRIC breast cancer cohort.
- C** Surface expression of MMP-9, VEGF, and NE as assessed on circulating neutrophils isolated from the peripheral blood of WT mice (saline) or from the peritoneal cavity of WT mice 6 h after intraperitoneal stimulation with uPA-PAI-1 (uPA-PAI-1) by multi-channel flow cytometry, quantitative data are shown (mean \pm SEM for $n = 4-6$ mice per group; $^{\#}P < 0.05$ vs. saline; t-test).
- D, E** Proliferation of (D) 4T1 breast cancer cells or (E) bEnd.3 microvascular endothelial cells upon exposure to recombinant murine uPA-PAI-1, the uPA-PAI-1 inhibitor WX-340, or primary neutrophils isolated from the peritoneal cavity of WT mice undergoing 6 h of intraperitoneal stimulation with uPA-PAI-1 with or without addition of a NE inhibitor as assessed by a MTT assay, quantitative data are shown (mean \pm SEM for $n = 3$ experiments per group; $^{\#}P < 0.05$ vs. neutrophils; $^*P < 0.05$ vs. neutrophils + vehicle / $^{\#}P < 0.05$ vs. 2% FCS medium; one-way ANOVA/t-test).
- F** Formation of NETs (histone H3⁺; green) as assessed *ex vivo* by confocal microscopy in the cremaster muscle of WT mice 6 h after intrascrotal injection of uPA-PAI-1, TNF, or saline, PECAM-1/CD31⁺ postcapillary venules (blue) and Ly-6C⁺ neutrophils (red) are depicted. Representative images are shown (scale bar: 50 μ m).

pro-tumorigenic neutrophil responses in breast cancer and consequently attenuates tumor growth and metastasis. To prove this hypothesis, we first sought to characterize the effect of pharmacological inhibition of uPA and PAI-1 heteromerization on neutrophil trafficking. For this purpose, we used again the small-molecule inhibitor WX-340 that competitively and dose-dependently interferes with the binding of recombinant murine PAI-1 protein to uPA protein as evidenced in our ELISA analyses (Fig 4A). Using multi-

channel *in vivo* microscopy on the mouse cremaster muscle, intrascrotal stimulation with TNF induced a significant elevation in numbers of intravascularly adherent and (subsequently) transmigrated neutrophils and classical monocytes (Fig 4B). This elevation was significantly diminished in animals treated with WX-340, indicating that blockade of uPA-PAI-1 heteromerization potently interferes with neutrophil trafficking to the inflamed perivascular space.

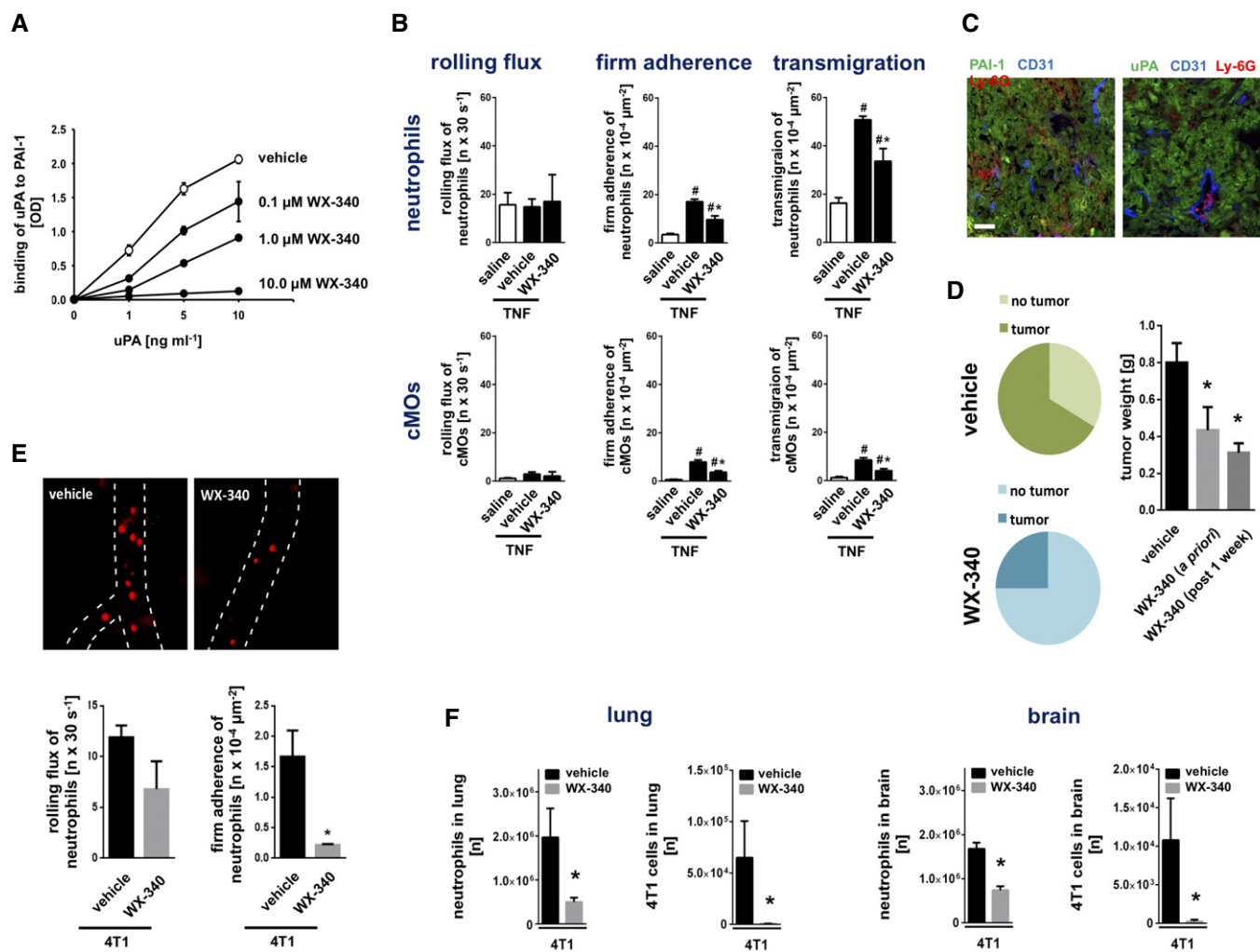


Figure 4. Effect of WX-340 on experimental breast cancer progression and metastasis formation.

A Effect of compound WX-340 on binding of recombinant murine uPA to PAI-1 protein as assessed by ELISA, quantitative data are shown (mean ± SEM for n = 3 experiments per group; #P < 0.05 vs. drug vehicle; one-way ANOVA).

B Intravascular rolling and firm adherence as well as transmigration of neutrophils and classical monocytes (cMOs) to the inflamed perivascular tissue as assessed 6 h after intrascrotal injection of TNF in postcapillary venules of the cremaster muscle of WT mice, quantitative data are shown (mean ± SEM for n = 6 mice per group; #P < 0.05 vs. saline; *P < 0.05 vs. drug vehicle; one-way ANOVA).

C Expression of uPA or PAI-1 (green) in tumors as assessed in an orthotopic model of 4T1 breast cancer in WT mice by confocal microscopy, PECAM-1/CD31⁺ postcapillary venules (blue) and Ly-6G⁺ neutrophils (red) are depicted (scale bar: 100 μm).

D Relative development rates and tumor weight in animals treated with WX-340 *a priori* or therapeutically after 1 week after tumor cell injection on a daily basis as assessed in an orthotopic model of 4T1 breast cancer in WT mice (mean ± SEM for n = 4–6 mice per group; *P < 0.05 vs. drug vehicle; one-way ANOVA).

E Intravascular rolling and firm adherence of neutrophils as assessed in the tumor microvasculature 14 days after intradermal injection of 4T1 cells in the right ear of WT mice treated with WX-340 or vehicle by multi-channel *in vivo* microscopy, quantitative data are shown (mean ± SEM for n = 4–6 mice per group; *P < 0.05 vs. drug vehicle; t-test).

F Numbers of neutrophils and 4T1 tumor cells in lungs and brain of WT mice receiving WX-340 or vehicle therapeutically after 1 week after tumor cell injection on a daily basis as assessed 14 days after intravenous injection of 4T1 tumor cells by multi-channel flow cytometry, quantitative data are shown (mean ± SEM for n = 4–6 mice per group; *P < 0.05 vs. drug vehicle; t-test).

To examine the effect of this compound on breast cancer progression, we established an orthotopic, syngeneic mouse model of 4T1 breast cancer which is well known for its strong intratumoral expression of uPA and PAI-1 (Fig 4C). In addition to tumor cells, infiltrated immune cells such as neutrophils also express these proteins (Reichel *et al*, 2011b; Praetner *et al*, 2018) (Appendix Fig S3A). Here, we demonstrate that both *a priori* and therapeutic

treatment with WX-340 significantly diminished the local growth of these malignant tumors at early, pre-metastatic stages (Fig 4D; Appendix Fig S3B). In a heterotopic model of this oncological disorder in the auricle, we additionally document by multi-channel *in vivo* microscopy that WX-340 significantly reduced neutrophil trafficking to the neoplasms already on the level of intravascular adherence in the tumor microvasculature (Fig 4E). Conversely, depletion

of neutrophils almost completely abolished tumor growth, whereas depletion of cMOs only partially inhibited tumor progression in the orthotopic breast cancer model, further indicating that particularly neutrophils contribute to uPA-PAI-1-dependent tumorigenesis (Appendix Fig S3C and Appendix Table S2). To evaluate the effect of this inhibitor of uPA-PAI-1 heteromerization on metastasis formation in 4T1 breast cancer, we performed a final series of experiments. Similarly to our results for local tumor growth, both *a priori* and therapeutic treatment with WX-340 effectively attenuated metastasis formation and neutrophil recruitment to the malignant lesions in lungs and brain of the diseased mice (Fig 4E; Appendix Fig S4). Collectively, our data indicate that counteracting uPA-PAI-1 heteromerization by a small-molecule inhibitor effectively interferes with the trafficking of pro-tumorigenic neutrophils in experimental breast cancer and subsequently attenuates disease progression.

Discussion

Clinical studies revealed that high intratumoral levels of uPA-PAI-1 heteromers predict impaired overall survival (Andreasen *et al*, 1997; Schmitt *et al*, 1997; Knoop *et al*, 1998; Duffy *et al*, 1999; Foekens *et al*, 2000; Janicke *et al*, 2001; Sten-Linder *et al*, 2001; Look *et al*, 2002; Manders *et al*, 2004b) and treatment response (Harbeck *et al*, 2002a; Harbeck *et al*, 2002b; Manders *et al*, 2004a; Manders *et al*, 2004c) in early breast cancer. The pathogenetic role of this protein complex, however, is still unclear. In line with previous reports (Reichel *et al*, 2011b; Uhl *et al*, 2014; Praetner *et al*, 2018), we here demonstrate that uPA, tPA, or PAI-1 induce the trafficking of neutrophils and—to a lesser extent—of classical monocytes. Most interestingly, heteromerization of uPA and PAI-1, but not of tPA and PAI-1, synergistically increased the potential of the single proteins to induce responses of these myeloid leukocytes. Notably, the migration of classical monocytes elicited by this protein complex was entirely dependent on the presence of neutrophils. In this context, we show that uPA-PAI-1 complexes mediate neutrophil extravasation very early on by triggering the intravascular adhesion of these innate immune cells, similar as the pro-inflammatory cytokine TNF. Importantly, uPA-PAI-1 heteromers did not induce detectable lymphocyte responses, collectively indicating that these protein complexes specifically promote the trafficking of neutrophils to their target destination.

Toward a more comprehensive understanding of these potent neutrophil-attracting properties of uPA-PAI-1 heteromers, we sought to identify the underlying mechanisms. Intravascular adherence and (subsequent) transmigration of neutrophils to the interstitial tissue requires interactions between endothelially expressed ICAM-1/CD54 or VCAM-1/CD106 and neutrophil $\beta 1$ or $\beta 2$ integrins in higher affinity conformations (Ley *et al*, 2007; Kolaczowska & Kubek, 2013; Nourshargh & Alon, 2014). In our experiments, uPA and PAI-1 were found to be primarily present in the perivascular space of inflamed tissue, where the protein heteromers more potently induced surface expression of ICAM-1/CD54 and VCAM-1/CD106 on microvascular endothelial cells than the single proteins. However, we cannot clearly state to what extent intracellular and extracellular uPA-PAI-1 heteromerization occurs. In this context, uPA-PAI-1 did not directly activate microvascular endothelial cells, but initiated the release of various pro-inflammatory mediators in perivascular macrophages

including CC and CXC motif chemokines and the cytokine TNF. These macrophage-derived signals, in turn, induced surface expression of ICAM-1/CD54 and VCAM-1/CD106 on microvascular endothelial cells. In addition, circulating uPA and PAI-1 were deposited on the luminal surface of microvascular endothelial cells in inflamed tissue (Reichel *et al*, 2011b; Praetner *et al*, 2018). Subsequent complex formation of these proteins allowed them to induce higher affinity conformations of $\beta 2$ integrins and supported the clustering of these adhesion molecules on the surface of adhering murine neutrophils. This process further strengthens the interactions of neutrophil $\beta 2$ integrins and their endothelial counter receptor ICAM-1/CD54 and stabilizes the adhesion of these immune cells under increasing shear stress (Herter & Zarbock, 2013; Iwamoto & Calderwood, 2015; Ortega-Gomez *et al*, 2016), which is a prerequisite for the subsequent extravasation of neutrophils to the perivascular space.

To prevent hyperfibrinolysis, the fibrinolytic activity of uPA is antagonized by rapid, covalent binding to its inhibitor PAI-1 (Ellis *et al*, 1990). This exposes a cryptic binding site of PAI-1 that allows for high-affinity binding of the complexed protein (Croucher *et al*, 2007) to endothelially expressed receptors of the LDL receptor family including VLDLr and low-density lipoprotein receptor-related protein-1 (Conese *et al*, 1995; Webb *et al*, 1999; Strickland *et al*, 2002). As a consequence of such interactions, uPA-PAI-1 is endocytosed and induces sustained activation of intracellular MAPK (Webb *et al*, 2001), ultimately clearing this protein complex from the circulation. Nevertheless, the resulting effect of these molecular events on neutrophil trafficking is so far unknown. Here, we show that VLDLr, but not LRP-1, as well as MAPK-dependent intracellular signaling pathways mediate neutrophil recruitment to the peritoneal cavity elicited by uPA-PAI-1. The dispensability of LRP-1 in this context might be explained by the very low expression levels of this receptor protein on macrophages and neutrophils as compared to VLDLr. Accordingly, uPA-PAI-1-elicited cytokine synthesis in macrophages and integrin affinity changes in neutrophils were found to be facilitated through VLDLr as well as (subsequent) activation of ERK and JNK MAPK. Analyses with different site-specific blocking antibodies further revealed that the N-terminal cysteine-rich domains 3–6 (clone 1H10), 1–2, and 5–6 (clone 1H5), but not the cysteine-rich domains 7–8 (clone 5F3) of VLDLr (Yakovlev *et al*, 2016), are critical for mediating these uPA-PAI-1-dependent effects. Noteworthy, neither the protease activity of uPA nor its receptor uPAR were required for uPA-PAI-1-dependent neutrophil trafficking. This is in line with previous findings documenting that uPA mediates neutrophil responses *in vivo* independently of uPAR or its protease activity (Reichel *et al*, 2011b). Hence, uPA-PAI-1 promotes neutrophil trafficking under contribution of VLDLr and MAPK-dependent signaling events.

To elucidate the pathogenetic role of uPA-PAI-1-dependent neutrophil trafficking in breast cancer, we evaluated a retrospective cohort of breast cancer patients for neutrophilic infiltration. In this cohort, uPA and PAI-1 protein expression positively correlated with neutrophil infiltration of low grade, but not of intermediate or high-grade neoplasms. The missing link in tumors of higher histological grade might be due to the fact that neutrophilic infiltrations in these neoplasms are frequently triggered by necrosis which clearly follows different biological mechanisms (Munoz *et al*, 2017). In addition, analysis of RNA microarray data from the METABRIC breast cancer

cohort (Curtis *et al*, 2012) revealed that in early, but not in advanced stages of disease, RNA expression levels of the genes encoding uPA and PAI-1 are related to poor survival of breast cancer patients without enrichment of distinct molecular subtypes. Additionally, we observed a significant positive correlation between the RNA expression levels of the gene encoding uPA and a prominent marker gene of neutrophils, collectively suggesting that neutrophils attracted by uPA-PAI-1 exhibit pro-tumorigenic properties. In line with this assumption, we found that mouse neutrophils recruited by uPA-PAI-1 show higher expression levels of NE as compared to circulating neutrophils from the peripheral blood of unstimulated mice, which has been supposed (Fridlender *et al*, 2009) to point to a pro-tumorigenic phenotype of these immune cells. Furthermore, co-incubation of 4T1 breast cancer cells with uPA-PAI-1-primed neutrophils, but not direct exposure of uPA-PAI-1 protein to the tumor cells, potently increased the proliferation of 4T1 cells *in vitro*. This effect of uPA-PAI-1-primed neutrophils on the proliferation of breast cancer cells was largely dependent on NE which is thought to degrade insulin receptor substrate 1, a key regulator of phosphoinositide 3-kinase, and upregulate MAPK activity, ultimately stimulating tumor cell proliferation (Chen *et al*, 2004; Houghton *et al*, 2010). In contrast to our findings, however, uPA-PAI-1 heteromers have previously been reported to exhibit direct (*e.g.*, pro-proliferative) effects on MCF-7 and MDA-MB-435 breast cancer as well as HT 1080 fibrosarcoma cells by utilizing VLDLr (Webb *et al*, 1999; Webb *et al*, 2001). A possible explanation for these divergent results is the high degree of molecular heterogeneity of malignant tumor cells which might also include the expression of functional VLDLr. Importantly, uPA-PAI-1-primed neutrophils did not exhibit elevated surface expression levels of pro-angiogenic factors such as MMP-9 or VEGF as compared to circulating neutrophils and did not alter the proliferation of microvascular endothelial cells. Moreover, uPA-PAI-1 did not directly induce neutrophil extracellular trap (NET) formation in neutrophils sequestering circulating tumor cells (Demers *et al*, 2012; Cedervall *et al*, 2015), thus indicating that uPA-PAI-1 primes neutrophils toward a pro-tumorigenic phenotype that particularly exerts pro-proliferative effects on breast cancer cells *via* the release of NE.

To directly evaluate the functional relevance of uPA-PAI-1 heteromerization for the trafficking of pro-tumorigenic neutrophils in breast cancer, we tested the compound WX-340, a novel small-molecule inhibitor that competitively interferes with the binding of uPA to PAI-1. In accordance with our previous findings, this inhibitor effectively suppresses neutrophil adhesion to activated microvascular endothelium *in vivo*. To analyze the effect of this compound on the progression of malignant disease, we employed orthotopic and heterotopic syngeneic models of 4T1 breast cancer in mice exhibiting a robust expression of uPA and PAI-1 in the tumors. *A priori* application of WX-340 severely compromised the progression of these malignant lesions *in vivo*, whereas this compound did not directly alter the proliferation of 4T1 tumor cells or microvascular endothelial cells *in vitro*. In these experiments, WX-340 affected the trafficking of circulating neutrophils to these highly aggressive neoplasms already on the level of intravascular adherence. Moreover, metastatic seeding of 4T1 tumors in lungs and brain as well as the associated neutrophil influx into the metastatic lesions were almost completely abrogated in inhibitor-treated animals. Most interestingly, even therapeutic application of WX-340 to animals with already established tumors and advanced stages of disease effectively interfered with local progression and

metastatic tumor spread. Our findings extend previous observations of the anti-tumor and anti-metastatic activity of this compound in rat BN-472 mammary carcinoma and mouse HT1080 fibrosarcoma models (Setyono-Han *et al*, 2007).

In conclusion, our experimental data uncover a previously unrecognized biological role of uPA-PAI-1 heteromerization in breast cancer that potently promotes the trafficking of pro-tumorigenic neutrophils to malignant lesions. Counteracting this molecular process by a novel small-molecule inhibitor effectively interfered with pro-tumorigenic neutrophil responses and prevented advanced stages of this common oncological disorder in animal model systems. As an innovative personalized immunotherapeutic strategy, targeting this interplay between hemostasis and innate immunity might be particularly beneficial for patients with highly aggressive uPA-PAI-1^{high} tumors in breast cancer.

Materials and Methods

Ethics

All animal experiments were approved by the local governmental authorities (“Regierung von Oberbayern”) and conducted according to the guidelines to ensure animal welfare. During all surgical and experimental procedures, animals were anesthetized using ketamine (100 mg/kg; zoetis, Parsippany, New Jersey, USA) and xylazine (10 mg/kg; Bayer, Leverkusen, Germany.).

Animals

Male C57BL/6 and female Balb/C mice were purchased from Charles River (Sulzfeld, Germany). Male CX₃CR-1^{+GFP} mice (“monocyte reporter mice”) were generated as described previously (Jung *et al*, 2000) and backcrossed to the C57BL/6 background for 10 generations. CX₃CR-1^{+GFP} mice exhibit GFP^{low} classical monocytes and GFP^{high} non-classical monocytes.

Animals were housed under standard conditions (22 ± 2°C, 30–60% humidity, 12 h light/dark cycle, lights on at 7 am) with access to food and water *ad libitum*. Experiments were performed with animals aging 6–8 weeks (body weight of 15–18 g).

Cell lines

The murine mammary carcinoma cell line 4T1 was obtained from ATCC (Manassas, Virginia, USA) and stably transfected with ptd-Tomato-N1 (Clontech, Saint-Germain-en-Laye, France). Cells were cultured in RPMI-1640 media (Thermo Fisher Scientific, Waltham, Massachusetts, USA) media, supplemented with 10 % FBS (Biochrom, Berlin, Germany) and 1 % HEPES (PromoCell, Heidelberg, Germany) at 37°C and 5% CO₂. The murine endothelial cell line bEnd.3 and macrophage cell line RAW 264.7 were purchased from ATCC and cultured in DMEM (ATCC) supplemented with 10% FBS. Cells were routinely tested for mycoplasma contamination.

Proteins

Recombinant murine high-molecular-weight uPA and PAI-1 as well as human uPA and PAI-1 (varying doses; Molecular Innovations,

Novi, MI) were used to induce leukocyte responses in different *in vitro* and *in vivo* assays (see below). In selected experiments, recombinant murine tumor necrosis factor (TNF; Abcam, Cambridge, UK) was used as positive control. For the generation of uPA-PAI-1 heteromers or DFP-uPA, murine uPA was titrated with murine PAI-1 or diisopropylfluorophosphate (DFP; Calbiochem, Darmstadt, Germany) so that no proteolytic activity remained.

Inhibitors

The MAPK inhibitors FR180204 (ERK1/2 MAPK; 30 mg/kg body weight *i.v.*), SB202580 (p38 MAPK; 30 mg/kg body weight *i.v.*), or SP600125 (JNK MAPK; 30 mg/kg body weight *i.v.*; Sigma Aldrich GmbH, Taufkirchen, Germany) were used to characterize the functional relevance of MAPK for uPA-PAI-1-elicited neutrophil trafficking. A NE inhibitor (sivelestat; 150 μ M; Sigma Aldrich) was used to evaluate the role of NE for 4T1 tumor cell proliferation. The competitive small-molecule WX-340 (10 mg/kg body weight *i.p.* for *in vivo* experiments; Heidelberg Pharma AG, Ladenburg, Germany) was used to inhibit heteromerization of uPA and PAI-1.

Experimental groups in animal experiments

In first experiments, leukocyte recruitment to the peritoneal cavity of C57BL/6 mice was analyzed by multi-channel flow cytometry 6 h after intraperitoneal injection of recombinant murine uPA, tPA, PAI-1, uPA-PAI-1, tPA-PAI-1 (1 μ g in 400 μ l PBS), or PBS only ($n = 5$ per group; Fig 1A). In selected experiments, mice received neutrophil-depleting anti-Ly-6G or isotype control antibodies ($n = 4$ per group; Fig 1B). Subsequently, leukocyte-endothelial cell interactions were studied in postcapillary venules of the cremaster muscle of CX₃CR-1^{+GFP} mice by multi-channel *in vivo* microscopy 6 h after intrascrotal injection of recombinant murine uPA, PAI-1, uPA-PAI-1, TNF (1 μ g in 400 μ l PBS), or PBS only ($n = 4$ per group; Fig 1C). In further experiments, the effect of compound WX-340 (10 mg/kg body weight *i.p.*) on leukocyte-endothelial cell interactions was assessed in postcapillary venules of the cremaster muscle of CX₃CR-1^{+GFP} mice by multi-channel *in vivo* microscopy 6 h after intrascrotal injection of recombinant murine TNF (1 μ g in 400 μ l PBS; $n = 6$ per group; Fig 4B). Furthermore, the effect of WX-340 on neutrophil infiltration and tumor growth was assessed in an orthotopic model of 4T1 breast cancer in female BALB/c mice receiving WX-340 (10 mg/kg body weight *i.p.*, daily) or drug vehicle *a priori* (starting on the same day as tumor cell injection) or therapeutically (starting on day 7 after tumor cell injection; $n = 4-6$ per group; Fig 4D). In separate experiments, animals received neutrophil- or cMO-depleting antibodies ($n = 7$ per group). In addition, the effect of WX-340 on neutrophil-endothelial cell interactions in tumors was analyzed in an heterotopic model of 4T1 breast cancer in female BALB/c mice receiving WX-340 (10 mg/kg body weight *i.p.*, daily, starting on the same day as tumor cell injection) or drug vehicle ($n = 4-6$ per group; Fig 4E). Moreover, the effect of WX-340 on neutrophil infiltration and tumor metastasis was assessed in a tumor metastasis model of 4T1 breast cancer in female BALB/c mice receiving WX-340 (10 mg/kg body weight *i.p.*, daily) or drug vehicle *a priori* (starting on the same day as tumor cell injection) or therapeutically (starting on day 7 after tumor cell injection; $n = 4-6$ per group; Fig 4F; Appendix Fig S4A).

Peritonitis assay

Leukocyte recruitment to the peritoneal cavity was studied 6 h after induction of peritoneal inflammation. Mice were sacrificed, and their peritoneal cavity was washed with 10 ml of ice-cold saline. The total number of leukocytes in the peritoneal lavage fluid was measured with the ProCyte Hematology analyzer (IDEXX, Westbrook, Maine, USA).

Samples were then immunostained using antibodies (0.25 μ g in 100 μ l PBS) directed against CD45 (APC/Cy7, BioLegend, San Diego, California, USA), CD11b (FITC, BioLegend, San Diego, California, USA), Gr-1 (PE, BioLegend, San Diego, California, USA), CD115 (APC, BioLegend, San Diego, California, USA), F4/80 (eFluor 450, eBioscience/Thermo Fisher, San Diego, California, USA), CD19 (PerCP/Cy5.5, BioLegend, San Diego, California, USA), CD4 (Alexa Fluor 700, BioLegend, San Diego, California, USA), or CD8a (PE/Cy7, BioLegend, San Diego, California, USA) for 30 min on ice. After lysing erythrocytes (1:10, BD FACS Lysing solution, BD Bioscience) and two washing steps with PBS, samples were resuspended in 200 μ l PBS.

Mouse cremaster assay

The surgical preparation of the mouse cremaster muscle was performed as previously described by Baez with minor modifications (Baez, 1973). Briefly, the left femoral artery of anesthetized mice was cannulated in a retrograde manner in order to allow administration of substances including antibodies or inhibitors. In a next step, the right cremaster muscle was exposed through a ventral incision of the scrotum. The muscle was then opened ventrally and spread over a pedestal of a custom-made microscopy stage. After the epididymis and testicle were carefully detached from the cremaster muscle, they were placed back into the abdominal cavity. Throughout the surgical preparation and *in vivo* microscopy, the muscle was superfused with warm buffered saline.

Orthotopic 4T1 tumor model

Tumor cells of the cell line 4T1 (at a concentration of 2×10^5 cells/20 μ l) were injected into the left mammary fat pad of Balb/C mice, followed by daily treatment with WX-340 (10 mg/kg body weight in 50 μ l saline; *i.p.*) or vehicle for 14 days. In separate experiments, WX-340 (10 mg/kg body weight in 50 μ l saline; *i.p.*) was administered daily from day 7 until day 14 after tumor cell inoculation. Tumor size was morphometrically quantified on a daily basis using a digital caliper. Two weeks after application of tumor cells, tumor tissue and blood were harvested. The tumors were weighed and then homogenized in 15 ml saline. Of each sample, 100 μ l were then immunostained with 0.25 μ g anti-mouse antibodies directed against CD45 (APC/Cy7, BioLegend, San Diego, California, USA), CD11b (PerCp/Cy5.5, BioLegend, San Diego, California, USA), Ly-6G (PE, BioLegend, San Diego, California, USA) and F4/80 (eFluor 450, eBioscience/Thermo Fisher, San Diego, California, USA) as well as in selected experiments CD19 (APC, BioLegend, San Diego, California, USA), CD8a (PE/Cy7, BioLegend, San Diego, California, USA), and anti-CD4 (Alexa Fluor 700, BioLegend, San Diego, California, USA) for 30 min on ice. Erythrocytes were lysed using a lysing solution (1:10, BD FACS

Lysing solution, BD Bioscience). After two washing steps with PBS, samples were resuspended in 200 μ l PBS and analyzed using multi-channel flow cytometry.

Heterotopic 4T1 tumor model

4T1 tumor cells were injected into the left auricle of Balb/c mice at a concentration of 2×10^5 cells/20 μ l, followed by daily treatment with WX-340 (10 mg/kg body weight in 50 μ l saline; i.p.) or vehicle for 7 days. On day 3 or day 7 after tumor cell injection, mice ears were placed on a custom-made microscopy stage. Upon intradermal application of anti-Ly-6G PE (BioLegend, San Diego, California, USA; *via* the tail vein) mAb, *in vivo* microscopy analyses of neutrophil interactions in the tumor microvasculature were performed.

4T1 tumor metastasis model

Mice were inoculated with 2×10^5 4T1 tumor cells *via* tail vein injection, followed by daily treatment with WX-340 (10 mg/kg body weight in 50 μ l saline; i.p.) or vehicle for 14 days. In separate experiments, WX-340 (10 mg/kg body weight in 50 μ l saline; i.p.) was administered daily from day 7 until day 14 after tumor cell inoculation. Mice were sacrificed on day 14 after tumor cell inoculation. Subsequently, blood and organs were harvested (and homogenized) for further multi-channel flow cytometry analysis (see below).

Flow cytometry

Employing multi-channel flow cytometry (Gallios, Beckman Coulter Inc, Brea, California USA), myeloid leukocytes were identified by the expression of CD45 and CD11b. After exclusion of macrophages *via* high expression of F4/80, these cells were further divided into neutrophils (Gr-1^{high} CD115⁻), classical monocytes (Gr-1^{high} CD115⁺), and non-classical monocytes (Gr-1^{low} CD115⁺). In separate experiments, CD4⁺ T lymphocytes (CD45⁺ CD11b⁻ CD4⁺), CD8⁺ T lymphocytes (CD45⁺ CD11b⁻ CD8a⁺), and B lymphocytes (CD45⁺ CD11b⁻ CD19⁺) were analyzed. In the tumor metastasis assay (see above), tumor cells were identified as Tomato⁺ cells. All results were further processed by using the FlowJo Software (Treestar, Ashland, Oregon, USA).

In vivo microscopy

In vivo microscopy was performed using an AxioTech-Vario 100 Microscope (Zeiss MicroImaging GmbH, Goettingen, Germany), equipped with a Colibri LED light source (Zeiss MicroImaging GmbH) for fluorescence epi-illumination microscopy. All microscopy videos were obtained with an AxioCam Hsm digital camera using a 40 \times water immersion lens (0.5 NA, Zeiss MicroImaging GmbH) and processed with the AxioVision 4.6 software (Zeiss MicroImaging GmbH). Video records were later analyzed by using the imaging software Fiji (Schindelin *et al.*, 2012).

In the cremaster muscle of male CX₃CR-1^{+/GFP} mice, neutrophils were identified as Ly-6G⁺ CX₃CR-1⁻ cells, classical monocytes as Ly-6G⁻ CX₃CR-1^{low} cells, and non-classical monocytes as Ly-6G⁻ CX₃CR-1^{high} cells upon intravenous injection of PE-labeled, non-

depleting monoclonal anti-Ly-6G antibodies. In the heterotopic tumor model, neutrophils were identified as Ly-6G⁺ cells (anti-Ly-6G mAb, clone 1A8; 5 μ g i.v.). Rolling leukocytes were defined as those moving slower than the associated blood flow and quantified for 30 s per venule. Firmly adherent cells were determined as those resting in the associated blood flow for > 30 s and related to the luminal surface per 100 μ m vessel length.

Immunostaining and confocal microscopy

Tumors were surgically removed from tumor-bearing mice and embedded in Tissue-Tek (Sakura, Alphen am Rhein, Netherlands). After storing the samples at -80°C , sections were cut at 20 μ m using a cryostat (Thermo Fisher Scientific) and mounted onto glass slides (Thermo Fisher Scientific). Subsequently, sections were fixed with 4% formaldehyde (Microcos, Garching, Germany) for 10 min at RT, followed by washing the slides in PBS for 10 min. Blocking and permeabilization was achieved by incubating the slides in 2% BSA (Sigma Aldrich, St. Louis, Missouri, USA) in PBS with 0.001% Triton X-100 (Sigma Aldrich) for 1.5 h at room temperature. Finally, sections were incubated with anti-CD31/PECAM-1 AF647 (BioLegend) and primary anti-uPA (Santa Cruz Biotechnology, Santa Cruz, CA/USA) or anti-PAI-1 antibody (Abcam, Cambridge, UK; for 4 h at room temperature; 1 μ g in 200 μ l PBS), before incubation with secondary Alexa Fluor 488-linked antibodies (Invitrogen, Carlsbad, CA; 1 μ g in 200 μ l PBS) in blocking solution at 4°C over night. After washing the slides twice in PBS for 5 min, samples were mounted using PermaFluor (Beckman Coulter, Brea, California, USA) and stored at 4°C .

In order to evaluate the expression of uPA or PAI-1 (6 h after intrascrotal injection of TNF) or ICAM-1/CD54 and VCAM-1/CD106 (6 h after intrascrotal injection of recombinant murine uPA, PAI-1, uPA-PAI-1 or saline) in cremasteric tissue, excised mouse cremaster muscles were fixed in 4% paraformaldehyde. Next, tissues were blocked and permeabilized using 2% BSA in PBS with 0.001% Triton X-100 for 1.5 h at room temperature. Sections were then incubated with anti-CD31/PECAM-1 (AF647; BioLegend) and primary anti-uPA (Santa Cruz Biotechnology, Santa Cruz, CA/USA) or anti-PAI-1 antibodies (Abcam, Cambridge, UK; for 4 h at room temperature; 1 μ g in 200 μ l PBS), before incubation with secondary Alexa Fluor 488-linked antibodies (Invitrogen, Carlsbad, CA; 1 μ g in 200 μ l PBS) in blocking solution at 4°C over night. In separate experiments, sections were incubated with anti-CD31/PECAM-1 (AF647; BioLegend) as well as with anti-ICAM-1/CD54 (Alexa Fluor 488, BioLegend) or anti-VCAM-1/CD106 antibodies (APC, BioLegend). Finally, immunostained sections were mounted in PermaFluor (Thermo Fisher Scientific) on glass slides. Confocal z-stacks (z-spacing 1 μ m) were acquired using a Leica SP8 confocal laser scanning microscope (Leica Microsystems, Wetzlar, Germany) with an oil-immersion lens (Leica; 40 \times ; NA 1.40). The fluorescence signal was quantified using the software Fiji. Background signal was subtracted.

Spinning disk confocal microscopy in autoperfused flow chamber assays

CD11a/LFA-1 clustering under flow was evaluated by time-lapse microscopy using an upright spinning disk confocal microscope

(Examiner; Zeiss) with a confocal scanner unit CSU-X1 (Yokogawa Electric Corporation, Japan), an EMCCD camera (Evolve; Photometrics), and a x20/1.0 NA water immersion objective (Plan Apochromat; Zeiss). For flow chamber experiments, IBIDI-Slide IV 0.1 flow chambers (Ibidi, Munich, Germany) were coated for 3 h with a combination of 20 µg/ml CD62E/E-Selectin and 15 µg/ml CD54/ICAM-1 (Fc chimera, R&D Systems), 15 µg/ml CXCL1 (Peptotech), and/or 15 µg/ml uPA-PAI-1 heteromers (Molecular Innovations). For analysis of CD11a/LFA-1 clustering, neutrophils from murine bone marrow were isolated with Percoll (Density 1.08/1.11, Sigma) and incubated overnight with WEHI supernatant and 1 µl SIR-actin (F-actin Labeling Probe, Spirochrome). Subsequently, neutrophils were incubated for 10 min with a non-blocking rat anti-mouse CD11a/LFA-1 Alexa Fluor 546 antibody (clone 2D7, BioLegend) and a neutrophil-specific rat anti-mouse Ly6G Alexa Fluor 488 antibody (Clone 1A8, BioLegend). Flow chambers were then filled with labeled neutrophils and allowed to attach for 5 min. Thereafter, chambers were flushed, and detachment assays performed over 10 min with increasing flow rates (0.5–40 dyne/cm²) using high-precision syringe pump (Model KDS-232, KD Scientific, USA) and recorded as time-lapse movie. Movies were then analyzed offline for CD11a/LFA-1 and actin colocalization (signal intensity) using Fiji software.

Depletion of neutrophils or classical monocytes

For the depletion of circulating neutrophils, mice received injections of anti-Ly-6G monoclonal antibodies (clone 1A8; 50 µg intravenously (i.v.); 24 h and 6 h prior to induction of inflammation in the peritonitis model or every other day for one week in the tumor model; BD Biosciences, San Jose, CA, USA) as described elsewhere (Zuchtriegel *et al* 2016). This specifically depletes neutrophils (Daley *et al* 2008/2008) by Fc-dependent opsonization and phagocytosis of the antibody-bound cells (Bruhn *et al* 2016). For depletion of classical monocytes in the tumor model, mice received injections of anti-CCR2 antibodies (clone MC-21; 25 µg i.v. every day for one week; provided by Matthias Mack, Department of Internal Medicine, University of Regensburg, Regensburg, Germany; Bruhl *et al*, 2007).

ELISA analysis of uPA-PAI-1 heteromerization

The effect of WX-340 on heteromerization of uPA and PAI-1 was analyzed using an enzyme-linked Immunosorbent Assay (ELISA). First, wells of a 96-well plate were coated with recombinant murine PAI-1 (Molecular Innovations, Novi, Michigan, USA) at 4°C overnight. After washing three times with PBS, the wells were incubated with recombinant uPA (0, 1, 5, 10 ng/ml, Molecular Innovations, Novi, Michigan, USA) each combined with different doses of the inhibitor WX-340 (0, 0.1, 1, 10 µM). After incubation for 60 min and subsequent washing of the wells three times with PBS, the amount of uPA bound to PAI-1 in the wells was quantified employing a Mouse uPA total antigen assay ELISA kit (Molecular Innovations, Novi, Michigan, USA).

Multiplex cytokine ELISA analyses

Cytokine production by RAW 264.7 macrophages stimulated with recombinant murine uPA-PAI-1 (1 µg/ml) was analyzed in

undiluted culture supernatants using the Bio-Plex Pro™ Mouse chemokine panel 33-Plex on a Bio-Plex 200 system according to the manufacturer's protocol (Bio-Rad laboratories, Munich, Germany). Group comparisons were performed by unpaired Student's *t*-test with subsequent Benjamini–Hochberg correction. FDR *q*-value < 0.1 was used as cutoff for statistical significance.

Activation of neutrophils

As a measure of neutrophil activation, surface expression of the integrins LFA-1/CD11a, Mac-1/CD11b, and VLA-4/CD49d was determined in anticoagulated blood samples incubated for 30 min with recombinant murine uPA-PAI-1 (100 ng/ml) or saline. Subsequently, samples were washed with PBS and cells were immunostained using antibodies (0.25 µg in 100 µl PBS) directed against CD45 (APC/Cy7, BioLegend, San Diego, California, USA), CD11b (PerCp/Cy5.5, BioLegend, San Diego, California, USA), Ly-6G (PE, BioLegend, San Diego, California, USA) and F4/80 (eFluor 450, eBioscience/Thermo Fisher, San Diego, California, USA), and CD11a (PE/Cy7, eBioscience), and CD49d (FITC, eBioscience). Lyses of erythrocytes with lysing solution followed. After washing the samples twice in PBS, samples were resuspended in 200 µl PBS and analyzed by multi-channel flow cytometry.

As a measure of conformational changes of integrins, binding of ICAM-1/CD54-Fc to neutrophils was analyzed. Briefly, blood was taken from WT mice, anticoagulated, and suspended in Hanks balanced salt solution containing 1 mM CaCl₂ and MgCl₂ (Life Technologies, Carlsbad, California, USA). Subsequently, cells were incubated with recombinant murine uPA-PAI-1 (1 µg/ml) or PBS as negative control for 30 min at 37°C, followed by adding ICAM-1/CD54-Fc (10 µg/ml, R&D Systems) and PE-conjugated anti-human IgG1 (10 µg/ml, Fc-specific, Southern Biotechnology, Birmingham, Alabama, USA) for 5 min at 37°C. Next, cells were labeled with antibodies (0.25 µg in 100 µl PBS) directed against CD45 (APC/Cy7, BioLegend, San Diego, California, USA), CD11b (FITC, BioLegend, San Diego, California, USA), Ly-6G (Alexa Fluor 700, BioLegend, San Diego, California, USA), and F4/80 (eFluor 450, eBioscience/Thermo Fisher, San Diego, California, USA). Binding of ICAM-1/CD54-Fc to neutrophils was measured by using multi-channel flow cytometry.

The conformation-specific antibodies (0.25 µg in 100 µl PBS) mAb24 (high-affinity conformation of β2 integrins; mouse anti-human, monoclonal; Abcam, Cambridge, United Kingdom) and kim127 (intermediate-affinity and high-affinity conformation of β2 integrins; mouse anti-human, monoclonal) were used to analyze the integrin conformation status in human neutrophils after incubation with uPA-PAI-1 recombinant murine uPA-PAI-1, TNF (100 ng/ml), or saline for 30 min by multi-channel flow cytometry.

Activation of endothelial cells

To measure activation of cultured mouse endothelial cells (bEnd.3), cells were seeded into 12-well plates and exposed to recombinant murine uPA-PAI-1, TNF (100 ng/ml), or saline for 6 h at 37°C. Cells were collected and resuspended in saline before they were then immunostained using antibodies (0.25 µg in 100 µl PBS) directed against ICAM-1/CD54 (Alexa Fluor 488, BioLegend), VCAM-1/CD106 (APC, BioLegend), primary anti-uPA (Santa Cruz Biotechnology, Santa Cruz, CA/USA), or primary anti-PAI-1 antibodies (Abcam,

Cambridge, UK) followed by incubation with secondary Alexa Fluor 488-linked antibodies (Invitrogen, Carlsbad, CA). In separate experiments, bEnd.3 endothelial cells were co-cultured for 6 h with RAW macrophages, which were, prior to this, exposed for 3 h to recombinant mouse TNF, uPA-PAI-1 (100 ng/ml), or saline. After washing the samples twice in PBS, samples were resuspended in 200 μ l PBS and analyzed by multi-channel flow cytometry.

TNF production in macrophages

To measure intracellular TNF production of cultured mouse macrophages (RAW 264.7) or peritoneal macrophages from C57BL/6J mice, cells were seeded into 12-well plates, treated with Brefeldin A and Monensin (Protein Transport Inhibitor Cocktail, eBioscience/Thermo Fisher, San Diego, California, USA) and then exposed to recombinant murine uPA-PAI-1 (1 μ g/ml) or saline for 6 h at 37°C. After detaching and resuspending the cells in saline, intracellular TNF was then detected by using antibodies directed against TNF (0.25 μ g in 100 μ l PBS; PE, BioLegend, San Diego, California, USA) after permeabilizing cells with an intracellular staining permeabilization wash buffer (BioLegend, San Diego, California, USA). After washing the samples twice in PBS, samples were resuspended in 200 μ l PBS and analyzed by multi-channel flow cytometry.

Cell proliferation assay

4T1 tumor cells or bEnd.3 endothelial cells were seeded on 96-well plate and exposed to WX-340 (10 μ M), recombinant murine uPA-PAI-1 (1 μ g/ml), or vehicle. After 48 h, serum-free media and the MTT reagent were added according to the manufacturer's protocol (Abcam, Cambridge, UK) for 3 h at 37°C. Next, the MTT solvent was added and the plate was placed on an orbital shaker for 15 min. Finally, absorbance was measured at 590 nm in a microplate reader (Tecan, Männedorf, Switzerland). Cell proliferation was determined as the percentage of change as compared to the negative control after background subtractions.

In separate experiments, neutrophils were isolated with the Easy-Sep™ Mouse Neutrophil Enrichment Kit (STEMCELL Technologies, Vancouver, Canada) from the peritoneal cavity of C57BL/6J mice 6 h after intraperitoneal injection of recombinant murine uPA-PAI-1 (1 μ g/ml), as described by the manufacturer. Isolated neutrophils were placed in the cell culture and incubated over night at 37°C. On the following day, supernatants from the isolated neutrophils were placed onto tumor cells or endothelial cells and exposed to the NE inhibitor and/or WX-340. After incubation for 24 h at 37°C, the MTT assay was performed.

Human breast cancer samples

Written informed consent was obtained from all subjects. The experiments conformed to the principles set out in the WMA Declaration of Helsinki and the Department of Health and Human Services Belmont report. The protocol was approved by the ethics committee of the Heidelberg University Clinical Centre, Heidelberg/Germany.

An overall of 44 breast cancer cases, which were surgically treated in the University Hospital Heidelberg, Germany, were included in the cohort. Cohort details are given in Appendix Table S1. In all these cases, the commercially available diagnostic grade ELISA-based

The paper explained

Problem

Breast cancer is the most common oncological disorder in women worldwide. High intratumoral levels of heteromers of the serine protease urokinase-type plasminogen activator (uPA) and its inhibitor plasminogen activator inhibitor-1 (PAI-1) predict impaired survival and treatment response already in early stages of breast cancer. Although these single proteins are well known to control tissue perfusion by regulating clot formation as key components of the fibrinolytic system, the pathogenetic role of this protein complex in breast cancer remains obscure.

Results

Utilizing patient data and different syngeneic mouse models of breast cancer, we demonstrate that heteromerization of uPA and PAI-1 multiplies the potential of the single proteins to attract pro-tumorigenic neutrophils. To this end, tumor-released uPA-PAI-1 utilizes the very low-density lipoprotein receptor and intracellular mitogen-activated protein kinases to initiate a pro-inflammatory program in perivascular macrophages in the proximity of malignant tumors. This enforces neutrophil trafficking to cancerous lesions and skews these immune cells toward a pro-tumorigenic phenotype, thus supporting tumor growth and metastasis. Blockade of uPA-PAI-1 heteromerization by a novel small-molecule inhibitor interfered with these events and effectively prevented tumor progression.

Impact

Our findings identify a therapeutically targetable, hitherto unknown interplay between hemostasis and innate immunity that drives breast cancer progression. As a personalized immunotherapeutic strategy, blockade of uPA-PAI-1 heteromerization might be particularly beneficial for patients with highly aggressive uPA-PAI-1^{high} tumors.

FEMTELLE® uPA/PAI-1 assay (<https://www.femtelle.de/de/>) was performed on the obtained surgical specimens in the context of routine diagnostic workup. PAI-1 as well as uPA protein concentrations were extracted from the respective reports.

For the exact quantification of neutrophils in the same tumor cohort, slides were cut from formalin-fixed paraffin-embedded tissue blocks comprising the central tumor area. Immunohistochemistry was performed on a BenchMark XT automated stainer (Ventana, Tucson, AZ) with an antibody directed against myeloperoxidase (Thermo Fisher Scientific, RB-373-A) using the ultraVIEW DAB Detection Kit (all reagents from Ventana, Tucson, AZ). Briefly, the tissue sections were deparaffinized with EZ Prep at 75°C and 76°C, heat pretreated in Cell Conditioning 1 (CC1) for antigen retrieval at 76°C–100°C, and then incubated with the primary antibody diluted in antibody diluent 1:100 for 28 min at 37°C after inactivation of the endogenous peroxidase using UV inhibitor for 4 min at 37°C. Antibody binding was detected using DAB as chromogen and counterstained with hematoxylin for 10 min with subsequent bluing in bluing reagent for 10 min. Slides were then dehydrated manually by alcohol washes of increasing concentrations (70%, 96%, 100%) and xylene and coverslipped using Pertex® mounting medium (Histolab, 00801).

Stained slides were scanned with a high-throughput slide scanner (AT2, Leica Microsystems), and tumor areas were annotated by a board-certified pathologist (WW) using a Wacom Cintiq22HD display (Wacom) on the eSlideManager database (Leica Biosystems). Neutrophils were quantified by counting stained cells in the core tumor region pre-marked by the pathologist in a blinded manner and normalized to mm².

Analyses of RNA microarray data from the METABRIC breast cancer cohort

For analyses of RNA microarray data of the METABRIC breast cancer cohort (Curtis *et al*, 2012), CBioportal was employed (Gao *et al*, 2013). The subcohort of patients with documented tumor stage and available RNA microarray data was used ($n = 1,466$), and follow-up was cut to 120 months. RNA co-expression analyses were done utilizing Spearman and Pearson algorithms. Survival analyses were performed in subgroups of different tumor stages with the Cox proportional hazard model, and target gene expression z-values of ≥ 2.0 were used as strata.

Statistics

Data analysis was performed using the statistical software package (SigmaStat for Windows; Jandel Scientific). Unpaired Student's *t*-tests (2 groups) or one-way ANOVA test followed by multiple *post hoc* tests with Tukey's correction (> 2 groups) was used for the estimation of stochastic probability in intergroup comparisons. Data are presented as mean \pm SEM. *P*-values < 0.05 were considered significant.

Data availability

This study includes no data deposited in external repositories.

Expanded View for this article is available online.

Acknowledgments

This study is part of the doctoral thesis of J.C.D. We thank the NCT Tissue Bank in Heidelberg, Germany, and the MTBIO biobank as well as the Comparative Experimental Pathology (CEP) Unit at the TU Munich, Munich, Germany, for technical support. This study was supported by Deutsche Forschungsgemeinschaft (DFG, SFB 914, projects B01 to M.S., B03 to C.A.R., B06 to K.L., Z03 to M.S.). In addition, certain aspects of the study were supported by a grant of the German Cancer Aid to W.W. as part of the INTEGRATE-TN consortium. Open Access funding enabled and organized by Projekt DEAL.

Author contributions

BU and CAR conceived the study and wrote the manuscript. BU, LM, JD, RH, BS, FH, JS, CB, LP, RP, and KS performed experiments and data analysis. WW, MS, KL, and CAR contributed to data analysis. MC, CS, MM, EG, PS, JH, SMK, WW, MS, KL, and FK contributed to the writing of the manuscript.

Conflict of interest

The authors declare that they have no conflict of interest.

For more information

<https://www.femtelle.de>

References

Andreassen PA, Kjoller L, Christensen L, Duffy MJ (1997) The urokinase-type plasminogen activator system in cancer metastasis: a review. *Int J Cancer* 72: 1–22

- Baez S (1973) An open cremaster muscle preparation for the study of blood vessels by *in vivo* microscopy. *Microvasc Res* 5: 384–394
- Brühl H, Cihak J, Plachý J, Kunz-Schughart L, Niedermeier M, Denzel A, Rodriguez Gomez M, Talke Y, Luckow B, Stangassinger M *et al* (2007) Targeting of Gr-1+, CCR2+ monocytes in collagen-induced arthritis. *Arthritis Rheum* 56: 2975–2985
- Bruhn KW, Dekitani K, Nielsen TB, Pantapalangkoor P, Spellberg B (2015) Ly6G-mediated depletion of neutrophils is dependent on macrophages. *Results Immunol* 6: 5–7
- Carioli G, Malvezzi M, Rodriguez T, Bertuccio P, Negri E, La Vecchia C (2017) Trends and predictions to 2020 in breast cancer mortality in Europe. *Breast* 36: 89–95
- Carioli G, Malvezzi M, Rodriguez T, Bertuccio P, Negri E, La Vecchia C (2018) Trends and predictions to 2020 in breast cancer mortality: Americas and Australasia. *Breast* 37: 163–169
- Cedervall J, Zhang Y, Huang H, Zhang L, Femel J, Dimberg A, Olsson AK (2015) Neutrophil extracellular traps accumulate in peripheral blood vessels and compromise organ function in tumor-bearing animals. *Can Res* 75: 2653–2662
- Chen HC, Lin HC, Liu CY, Wang CH, Hwang T, Huang TT, Lin CH, Kuo HP (2004) Neutrophil elastase induces IL-8 synthesis by lung epithelial cells via the mitogen-activated protein kinase pathway. *J Biomed Sci* 11: 49–58
- Coffelt SB, Wellenstein MD, de Visser KE (2016) Neutrophils in cancer: neutral no more. *Nat Rev Cancer* 16: 431–446
- Conese M, Nykjaer A, Petersen CM, Cremona O, Pardi R, Andreassen PA, Gliemann J, Christensen EI, Blasi F (1995) alpha-2 Macroglobulin receptor/Ldl receptor-related protein(Lrp)-dependent internalization of the urokinase receptor. *J Cell Biol* 131: 1609–1622
- Croucher DR, Saunders DN, Stillfried GE, Ranson M (2007) A structural basis for differential cell signalling by PAI-1 and PAI-2 in breast cancer cells. *Biochem J* 408: 203–210
- Curtis S, Shah SP, Chin S-F, Turashvili G, Rueda OM, Dunning MJ, Speed D, Lynch AG, Samarajiwa S, Yuan Y *et al* (2012) The genomic and transcriptomic architecture of 2,000 breast tumours reveals novel subgroups. *Nature* 486: 346–352
- Daley JM, Thomay AA, Connolly MD, Reichner JS, Albina JE (2008) Use of Ly6G-specific monoclonal antibody to deplete neutrophils in mice. *J Leukoc Biol* 83: 64–70
- Das R, Pluskota E, Plow EF (2010) Plasminogen and its receptors as regulators of cardiovascular inflammatory responses. *Trends Cardiovasc Med* 20: 120–124
- Demers M, Krause DS, Schatzberg D, Martinod K, Voorhees JR, Fuchs TA, Scadden DT, Wagner DD (2012) Cancers predispose neutrophils to release extracellular DNA traps that contribute to cancer-associated thrombosis. *Proc Natl Acad Sci USA* 109: 13076–13081
- Duffy MJ, Maguire TM, McDermott EW, O'Higgins N (1999) Urokinase plasminogen activator: a prognostic marker in multiple types of cancer. *J Surg Oncol* 71: 130–135
- Ellis V, Wun TC, Behrendt N, Ronne E, Dano K (1990) Inhibition of receptor-bound urokinase by plasminogen-activator inhibitors. *J Biol Chem* 265: 9904–9908
- Foekens JA, Peters HA, Look MP, Portengen H, Schmitt M, Kramer MD, Brunner N, Janicke F, Meijer-van Gelder ME, Henzen-Logmans SC *et al* (2000) The urokinase system of plasminogen activation and prognosis in 2780 breast cancer patients. *Can Res* 60: 636–643
- Fridlender ZG, Sun J, Kim S, Kapoor V, Cheng G, Ling L, Worthen GS, Albelda SM (2009) Polarization of tumor-associated neutrophil phenotype by TGF-beta: "N1" versus "N2" TAN. *Cancer Cell* 16: 183–194

- Gao J, Aksoy Ba, Dogrusoz U, Dresdner G, Gross B, Sumer So, Sun Y, Jacobsen A, Sinha R, Larsson E et al (2013) Integrative analysis of complex cancer genomics and clinical profiles using the cBioPortal. *Sci Signal* 6: pl1
- Gentles AJ, Newman AM, Liu CL, Bratman SV, Feng W, Kim D, Nair VS, Xu Y, Khuong A, Hoang CD et al (2015) The prognostic landscape of genes and infiltrating immune cells across human cancers. *Nat Med* 21: 938–945
- Harbeck N, Kates RE, Look MP, Meijer-Van Gelder ME, Klijn JG, Kruger A, Kiechle M, Janicke F, Schmitt M, Foekens JA (2002a) Enhanced benefit from adjuvant chemotherapy in breast cancer patients classified high-risk according to urokinase-type plasminogen activator (uPA) and plasminogen activator inhibitor type 1 ($n = 3,424$). *Can Res* 62: 4617–4622
- Harbeck N, Kates RE, Schmitt M (2002b) Clinical relevance of invasion factors urokinase-type plasminogen activator and plasminogen activator inhibitor type 1 for individualized therapy decisions in primary breast cancer is greatest when used in combination. *J Clin Oncol* 20: 1000–1007
- Herter J, Zarbock A (2013) Integrin Regulation during Leukocyte Recruitment. *J Immunol* 190: 4451–4457
- Houghton AM, Rzymkiewicz DM, Ji H, Gregory AD, Egea EE, Metz HE, Stolz DB, Land SR, Marconcini LA, Kliment CR et al (2010) Neutrophil elastase-mediated degradation of IRS-1 accelerates lung tumor growth. *Nat Med* 16: 219–223
- Iwamoto DV, Calderwood DA (2015) Regulation of integrin-mediated adhesions. *Curr Opin Cell Biol* 36: 41–47
- Janicke F, Prechtel A, Thomssen C, Harbeck N, Meisner C, Untch M, Sweep CG, Selbmann HK, Graeff H, Schmitt M et al (2001) Randomized adjuvant chemotherapy trial in high-risk, lymph node-negative breast cancer patients identified by urokinase-type plasminogen activator and plasminogen activator inhibitor type 1. *J Natl Cancer Inst* 93: 913–920
- Jung S, Aliberti J, Graemmel P, Sunshine MJ, Kreutzberg GW, Sher A, Littman DR (2000) Analysis of fractalkine receptor CX₃CR1 function by targeted deletion and green fluorescent protein reporter gene insertion. *Mol Cell Biol* 20: 4106–4114
- Knoop A, Andreassen PA, Andersen JA, Hansen S, Laenkholm AV, Simonsen AC, Andersen J, Overgaard J, Rose C (1998) Prognostic significance of urokinase-type plasminogen activator and plasminogen activator inhibitor-1 in primary breast cancer. *Br J Cancer* 77: 932–940
- Kolaczowska E, Kubes P (2013) Neutrophil recruitment and function in health and inflammation. *Nat Rev Immunol* 13: 159–175
- Ley K, Laudanna C, Cybulsky MI, Nourshargh S (2007) Getting to the site of inflammation: the leukocyte adhesion cascade updated. *Nat Rev Immunol* 7: 678–689
- Look MP, van Putten WJ, Duffy MJ, Harbeck N, Christensen IJ, Thomssen C, Kates R, Spyrtatos F, Ferno M, Eppenberger-Castori S et al (2002) Pooled analysis of prognostic impact of urokinase-type plasminogen activator and its inhibitor PAI-1 in 8377 breast cancer patients. *J Natl Cancer Inst* 94: 116–128
- Manders P, Tjan-Heijnen VC, Span PN, Grebenchtchikov N, Foekens JA, Beex LV, Sweep CG (2004a) Predictive impact of urokinase-type plasminogen activator: plasminogen activator inhibitor type-1 complex on the efficacy of adjuvant systemic therapy in primary breast cancer. *Can Res* 64: 659–664
- Manders P, Tjan-Heijnen VC, Span PN, Grebenchtchikov N, Geurts-Moespot A, van Tienoven DT, Beex LV, Sweep FC (2004b) Complex of urokinase-type plasminogen activator with its type 1 inhibitor predicts poor outcome in 576 patients with lymph node-negative breast carcinoma. *Cancer* 101: 486–494
- Manders P, Tjan-Heijnen VC, Span PN, Grebenchtchikov N, Geurts-Moespot AJ, van Tienoven DT, Beex LV, Sweep FC (2004c) The complex between urokinase-type plasminogen activator (uPA) and its type-1 inhibitor (PAI-1) independently predicts response to first-line endocrine therapy in advanced breast cancer. *Thromb Haemost* 91: 514–521
- Munoz LE, Leppkes M, Fuchs TA, Hoffmann M, Herrmann M (2017) Missing in action-The meaning of cell death in tissue damage and inflammation. *Immunol Rev* 280: 26–40
- Nicolas-Avila JA, Adrover JM, Hidalgo A (2017) Neutrophils in homeostasis, immunity, and cancer. *Immunity* 46: 15–28
- Nourshargh S, Alon R (2014) Leukocyte migration into inflamed tissues. *Immunity* 41: 694–707
- Ortega-Gomez A, Salvermoser M, Rossaint J, Pick R, Brauner J, Lemnitzer P, Tilgner J, de Jong RJ, Megens RTA, Jamasbi J et al (2016) Cathepsin G controls arterial but not Venular myeloid cell recruitment. *Circulation* 134: 1176–1188
- Pappot H, Pedersen AN, Brunner N, Christensen IJ (2006) The complex between urokinase (uPA) and its type-1 inhibitor (PAI-1) in pulmonary adenocarcinoma: relation to prognosis. *Lung Cancer* 51: 193–200
- Praetner M, Zuchtriegel G, Holzer M, Uhl B, Schaubächer J, Mittmann L, Fabritius M, Fürst R, Zahler S, Funken D et al (2018) Plasminogen Activator Inhibitor-1 Promotes Neutrophil Infiltration and Tissue Injury on Ischemia-Reperfusion. *Arterioscler Thromb Vasc Biol* 38: 829–842
- Reichel CA, Lerchenberger M, Uhl B, Rehberg M, Berberich N, Zahler S, Wymann MP, Krombach F (2011a) Plasmin inhibitors prevent leukocyte accumulation and remodeling events in the postischemic microvasculature. *PLoS One* 6: e17229
- Reichel CA, Uhl B, Lerchenberger M, Pühr-Westerheide D, Rehberg M, Liebl J, Khandoga A, Schmalix W, Zahler S, Deindl E et al (2011b) Urokinase-type plasminogen activator promotes paracellular transmigration of neutrophils via Mac-1, but independently of urokinase-type plasminogen activator receptor. *Circulation* 124: 1848–1859
- Schindelin J, Arganda-Carreras I, Frise E, Kaynig V, Longair M, Pietzsch T, Preibisch S, Rueden C, Saalfeld S, Schmid B et al (2012) Fiji: an open-source platform for biological-image analysis. *Nat Methods* 9: 676–682
- Schmitt M, Harbeck N, Thomssen C, Wilhelm O, Magdolen V, Reuning U, Ulm K, Hofer H, Janicke F, Graeff H (1997) Clinical impact of the plasminogen activation system in tumor invasion and metastasis: prognostic relevance and target for therapy. *Thromb Haemost* 78: 285–296
- Schmitt M, Mengele K, Gkazepis A, Napieralski R, Magdolen V, Reuning U, Harbeck N (2008) Assessment of urokinase-type plasminogen activator and its inhibitor PAI-1 in breast cancer tissue: historical aspects and future prospects. *Breast care* 3: 3–10
- Setyono-Han B, Schneider A, Timmermanns M, Sieuwerts A, Blasi F, Schmalix W, Foekens J (2007) Anti-tumor and anti-metastatic activity of WX-340 a highly specific uPA-inhibitor in the rat BN-472 mammary carcinoma model. *Can Res* 67: 5615
- Smith HW, Marshall CJ (2010) Regulation of cell signalling by uPAR. *Nat Rev Mol Cell Biol* 11: 23–36
- Sten-Linder M, Seddighzadeh M, Engel G, Rutqvist LE, Linder S, Skoog L, Wima B (2001) Prognostic importance of the uPa/PAI-1 complex in breast cancer. *Anticancer Res* 21: 2861–2865
- Strickland DK, Gonias SL, Argraves WS (2002) Diverse roles for the LDL receptor family. *Trends Endocrinol Metab* 13: 66–74
- Uhl B, Zuchtriegel G, Pühr-Westerheide D, Praetner M, Rehberg M, Fabritius M, Hessenauer M, Holzer M, Khandoga A, Fürst R et al (2014) Tissue-Type Plasminogen Activator Promotes Postischemic Neutrophil Recruitment via Its Proteolytic and Nonproteolytic Properties. *Arterioscler Thromb Vasc Biol* 34: 1495–1504

Webb DJ, Nguyen DH, Sankovic M, Gonias SL (1999) The very low density lipoprotein receptor regulates urokinase receptor catabolism and breast cancer cell motility *in vitro*. *J Biol Chem* 274: 7412–7420

Webb DJ, Thomas KS, Gonias SL (2001) Plasminogen activator inhibitor 1 functions as a urokinase response modifier at the level of cell signaling and thereby promotes MCF-7 cell growth. *J Cell Biol* 152: 741–752

Yakovlev S, Belkin AM, Chen L, Cao C, Zhang L, Strickland DK, Medved L (2016) Anti-VLDL receptor monoclonal antibodies inhibit fibrin-VLDL receptor interaction and reduce fibrin-dependent

leukocyte transmigration. *Thromb Haemost* 116: 1122–1130

Zuchtriegel G, Uhl B, Puhr-Westerheide D, Pörnbacher M, Lauber K, Krombach F, Reichel CA (2016) Platelets guide leukocytes to their sites of extravasation. *PLoS Biol*. 14: e1002459



License: This is an open access article under the terms of the Creative Commons Attribution License, which permits use, distribution and reproduction in any medium, provided the original work is properly cited.

APPENDIX

Appendix tables S1, S2, and S3

Appendix figures S1, S2, S3, and S4

Appendix tables

specimen number	histology	grade	PAI-1 protein [ng/ml]	uPA protein [ng/ml]	extravascular neutrophils [n / mm ²]	intravascular neutrophils [n / mm ²]
1	mixed invasive lobular/ductal carcinoma	G1	10.83	6.64	782.68	545.50
2	invasive ductal carcinoma	G1	14.49	5.67	1,423.29	1,501.63
3	invasive ductal carcinoma	G1	28.43	6.66	1,657.56	4,490.48
4	mixed invasive lobular/ductal carcinoma	G1	12.23	1.76	1,164.05	2,993.28
5	mixed invasive lobular/ductal carcinoma	G1	46.55	7.97	3,450.43	4,540.04
6	mixed invasive lobular/ductal carcinoma	G2	9.40	0.92	2,875.82	3,229.48
7	invasive ductal carcinoma	G2	15.64	3.32	1,028.08	639.07
8	invasive ductal carcinoma	G2	9.40	1.48	2,684.73	1,534.13
9	invasive lobular carcinoma	G2	27.75	3.68	625.64	2,027.54
10	invasive lobular carcinoma	G2	6,13	0,54	2,174.57	1,199.76
11	invasive lobular carcinoma	G2	16.98	1.73	4,114.31	16,228.70
12	invasive ductal carcinoma	G2	37.61	2.89	3,440.92	4,697.66
13	invasive ductal carcinoma	G2	25.68	1.55	274.74	595.28
14	invasive lobular carcinoma	G2	32.17	5.63	1,723.48	3,770.12
15	invasive ductal carcinoma	G2	35.01	5.36	3,133.51	3,240.09
16	invasive ductal carcinoma	G2	16.05	1.65	708.60	2,000.75
17	invasive ductal carcinoma	G2	12.00	2.68	4,279.50	4,054.26
18	mixed invasive lobular/ductal carcinoma	G2	20.54	1.86	1,094.44	2,736.09
19	invasive lobular carcinoma	G2	14.22	1.78	1,528.97	1,868.74
20	invasive micropapillary carcinoma	G2	10.81	3.32	989.33	2,398.78
21	mixed invasive lobular/ductal carcinoma	G2	23.68	3.76	412.04	1,381.53
22	invasive ductal carcinoma	G2	29.91	4.57	1,689.91	3,869.00
23	invasive lobular carcinoma	G2	20.35	2.30	355.83	1,392.37
24	invasive lobular carcinoma	G2	40.55	0.52	6,283.55	11,753.17
25	invasive ductal carcinoma	G2	18.52	2.99	978.07	2,941.62
26	invasive ductal carcinoma	G2	10.11	1.62	2,366.36	5,733.88
27	invasive ductal carcinoma	G2	13.95	6.85	668.17	2,111.41
28	invasive ductal carcinoma	G2	20.77	5.23	1,038.76	2,095.13
29	invasive lobular carcinoma	G2	29.59	2.92	2,400.83	3,906.34
30	invasive ductal carcinoma	G2	21.42	6.68	2,548.16	3,136.71
31	invasive ductal carcinoma	G2	21.03	5.28	1,165.98	4,387.78
32	invasive ductal carcinoma	G2	23.92	7.24	2,695.33	5,003.99
33	invasive ductal carcinoma	G2	48.69	7.56	583.23	1,621.37

34	invasive lobular carcinoma	G2	13.44	2.82	3,428.36	3,795.68
35	invasive ductal carcinoma	G3	16.76	9.91	890.42	1,307.80
36	invasive lobular carcinoma	G3	23.88	6.03	92.15	506.81
37	invasive ductal carcinoma	G3	15.01	6.17	7,298.70	15,977.51
38	invasive ductal carcinoma	G3	13.10	2.23	476.44	1,577.61
39	invasive ductal carcinoma	G3	10.01	1.29	1,022.30	3,553.12
40	invasive lobular carcinoma	G3	4.90	1.65	741.76	1,335.16
41	invasive ductal carcinoma	G3	19.97	3.59	3,779.61	7,447.35
42	invasive lobular carcinoma	G3	41.61	6.68	30,610.96	93,101.13
43	invasive ductal carcinoma	G3	194.82	9.35	5,311.23	6,030.04
44	invasive ductal carcinoma	G3	10.01	1.29	570.91	1,534.33

Appendix table S1. Characteristics of human breast cancer samples. Histopathological characteristics including histological subtype and grade as well as uPA/PAI-1 protein content and neutrophil accumulation in the analyzed breast cancer samples are shown.

antibody	systemic neutrophil count [$\times 10^3 \mu\text{l}^{-1}$]
isotype control	4.09 \pm 0.2
anti-Ly-6G mAb (clone 1A8)	0.04 \pm 0.1 [#]

antibody	systemic cMO count [$\times 10^3 \mu\text{l}^{-1}$]
isotype control	0.41 \pm 0.04
anti-CCR2 mAb (MC-21)	0.03 \pm 0.01 [#]

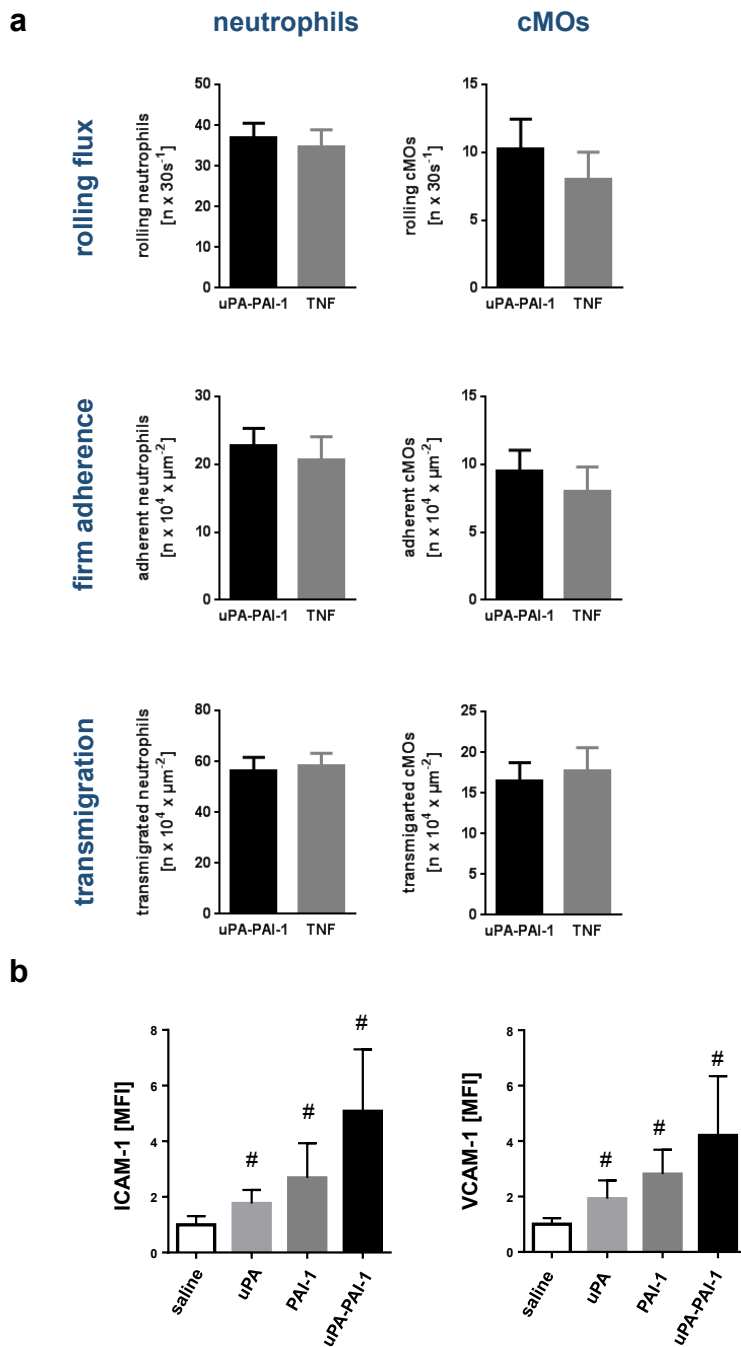
Appendix table S2. Depletion of neutrophils and cMOs. Systemic counts of neutrophils and cMOs in the peripheral blood of 4T1 tumor-bearing WT mice receiving neutrophil-depleting (anti-Ly-6G), cMO-depleting (anti-CCR2), or isotype control antibodies. Quantitative data are shown (mean \pm SEM for n=7; #p<0.05 vs. isotype control).

figure	n	p value	statistical test
1a (left, neutrophils)	5	< 0.0001	One-way ANOVA
1a (left, cMOs)	5	< 0.0001	One-way ANOVA
1a (left, ncMOs)	5	0.0217	One-way ANOVA
1a (right, B cells)	5	0.7697	t test
1a (right, CD4+ cells)	5	0.6088	t test
1a (right, CD8+ cells)	5	0.7311	t test
1b (neutrophils)	4	0.002	One-way ANOVA
1b (cMOs)	4	0.0012	One-way ANOVA
1c (neutrophil rolling)	4	0.9983	One-way ANOVA
1c (neutrophil adherence)	4	< 0.0001	One-way ANOVA
1c (neutrophil transmigration)	4	< 0.0001	One-way ANOVA
1c (cMO rolling)	4	0.1212	One-way ANOVA
1c (cMO adherence)	4	< 0.0001	One-way ANOVA
1c (cMO transmigration)	4	< 0.0001	One-way ANOVA
2b (ICAM-1)	4	0.0436	t test
2b (VCAM-1)	4	0.0428	t test
2c	4	< 0.0001	One-way ANOVA
2d (ICAM-1)	4	< 0.0001	One-way ANOVA
2d (VCAM-1)	4	< 0.0001	One-way ANOVA
2d (uPA)	4	0.6479	t test
2d (PAI-1)	4	0.0108	t test
2e (ICAM-1)	4	0.0219	One-way ANOVA
2e (VCAM-1)	4	0.9798	One-way ANOVA
2f (kim127)	6	0.0499	One-way ANOVA
2f (mAB24)	6	0.0096	One-way ANOVA
2g	30	< 0.0001	One-way ANOVA
3c (MMP-9)	4-6	0.8857	t test
3c (VEGF)	4-6	0.4688	t test
3c (NE)	6	0.0174	t test
3d (left)	6	0.6109	One-way ANOVA
3d (mid)	3	0.0125	t test
3d (right)	3	0.0088	t test
4a (0)	3	< 0.0001	One-way ANOVA
4a (0.1)	3	0.0005	One-way ANOVA
4a (1)	3	< 0.0001	One-way ANOVA
4a (10)	3	< 0.0001	One-way ANOVA
4b (neutrophil rolling)	6	0.9345	One-way ANOVA
4b (neutrophil adherence)	6	< 0.0001	One-way ANOVA
4b (neutrophil transmigration)	6	< 0.0001	One-way ANOVA
4b (cMO rolling)	6	0.213	One-way ANOVA
4b (cMO adherence)	6	< 0.0001	One-way ANOVA
4b (cMO transmigration)	6	< 0.0001	One-way ANOVA
4d	6	0.0091	One-way ANOVA
4e (rolling)	4-6	0.1948	t test
4e (adherence)	4-6	0.0105	t test
4f (lung neutrophils)	4	0.0413	t test
4f (lung tumor cells)	4	0.0489	t test
4f (brain neutrophils)	4	0.0012	t test
4f (brain tumor cells)	4	0.0456	t test
EV 1b (IL-6)	5	0.0029	t test
EV 1b (TNF)	5	< 0.0001	t test
EV 1b (CXCL2)	5	0.0059	t test
EV1b (CCL4)	5	< 0.0001	t test

EV2a (left, neutrophils)	4	0.0274	One-way ANOVA
EV2a (left, cMOs)	4	0.0015	One-way ANOVA
EV2a (right, neutrophils)	4	0.0002	One-way ANOVA
EV2a (right, cMOs)	4	< 0.0001	One-way ANOVA
EV2b (left, neutrophils)	4	0.0256	One-way ANOVA
EV2b (left, cMOs)	4	0.0006	One-way ANOVA
EV2b (right, neutrophils)	4	0.066	One-way ANOVA
EV2b (right, cMOs)	4	0.0003	One-way ANOVA
EV2c (neutrophils)	4	0.012	One-way ANOVA
EV2c (cMOs)	4	0.0081	One-way ANOVA
EV3a (macrophages)	4	0.0215	t test
EV3a (neutrophils)	4	0.0011	t test
EV3b	4	0.0440	One-way ANOVA
EV3c (left)	4	< 0.0001	One-way ANOVA
EV3c (right)	4	0.002	One-way ANOVA
Appendix Tab 2 (Ly-6G)	7	< 0.0001	t test
Appendix Tab 2 (CCR2)	7	< 0.0001	t test
Appendix Fig S1a (neutrophil rolling)	4	0.6966	t test
Appendix Fig S1a (neutrophil adherence)	4	0.6536	t test
Appendix Fig S1a (neutrophil transmigration)	4	0.7970	t test
Appendix Fig S1a (cMO rolling)	4	0.4831	t test
Appendix Fig S1a (cMO adherence)	4	0.5546	t test
Appendix Fig S1a (cMO transmigration)	4	0.7420	t test
Appendix Fig S1b (ICAM-1)	6	0.0014	One-way ANOVA
Appendix Fig S1b (VCAM-1)	6	0.0002	One-way ANOVA
Appendix Fig S2a	4	0.0002	t test
Appendix Fig S2b (left, ICAM-1)	6	0.0002	t test
Appendix Fig S2b (left, VCAM-1)	6	< 0.0001	t test
Appendix Fig S2b (right, ICAM-1)	6	< 0.0001	t test
Appendix Fig S2b (right, VCAM-1)	6	< 0.0001	t test
Appendix Fig S2d (left)	4	0.8803	t test
Appendix Fig S2d (right)	4	0.7205	t test
Appendix Fig S3b	6	0.3419 - 0.0062	One-way ANOVA
Appendix Fig S3c	7	0.0004	One-way ANOVA
Appendix Fig S4c (brain, neutrophils)	4-6	0.0035	One-way ANOVA
Appendix Fig S4c (brain, tumor cells)	4-6	0.0004	One-way ANOVA
Appendix Fig S4c (lungs, neutrophils)	4-6	< 0.0001	One-way ANOVA
Appendix Fig S4c (lungs, tumor cells)	4-6	< 0.0001	One-way ANOVA

Appendix table S3. Statistical data. For each dataset presented in the figures, exact n and p values as well as statistical tests employed are shown.

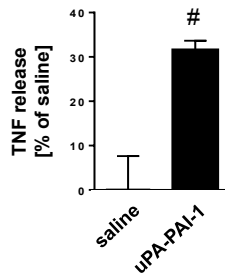
Appendix figures



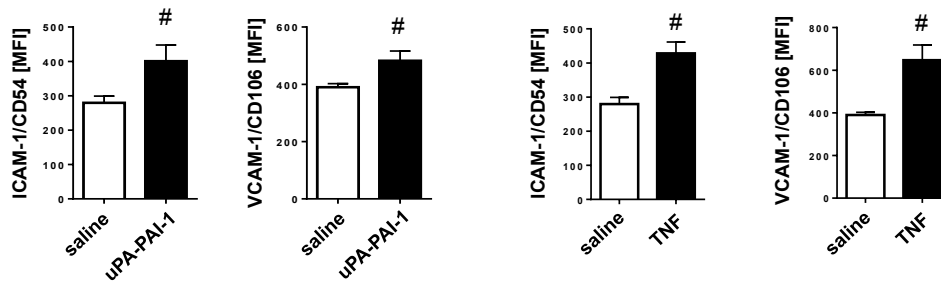
Appendix figure S1. Relative effect of uPA-PAI-1 on the trafficking of neutrophils and cMOs and on endothelial cell activation. (a) Intravascular endothelial cell interactions and transmigration of neutrophils (Ly-6G⁺ CX₃CR-1⁻) and cMOs (Ly-6G⁻ CX₃CR-1^{low}) to the perivascular tissue as assessed 6 h after intrascrotal stimulation with recombinant murine uPA-PAI-1 or TNF in postcapillary venules of the cremaster of CX₃CR-1^{GFP/+} mice by multi-channel *in vivo* microscopy. Quantitative data are shown (mean±SEM for n=4 mice/experiments per group). (b) Expression of ICAM-1/CD54 or VCAM-1/CD106 in the cremaster muscle of WT mice as assessed *ex vivo* by confocal laser scanning microscopy 6 h after intrascrotal injection of recombinant murine uPA, PAI-1, uPA-PAI-1, or saline. Quantitative data are shown (mean±SEM for n=4 mice per group; #p<0.05 vs. saline).

a

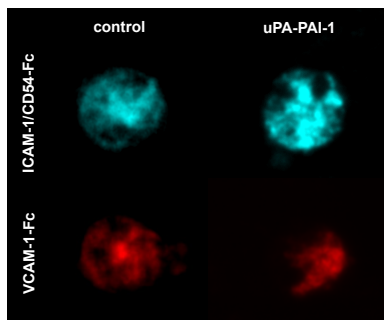
primary macrophages

**b**

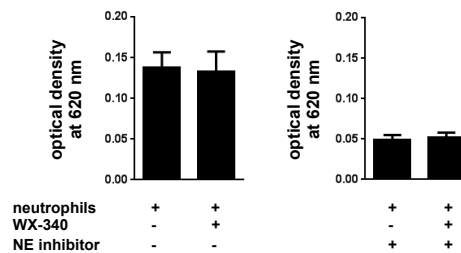
endothelial cells co-cultured with macrophages exposed to saline, TNF or, uPA-PAI-1

**c**

primary neutrophils

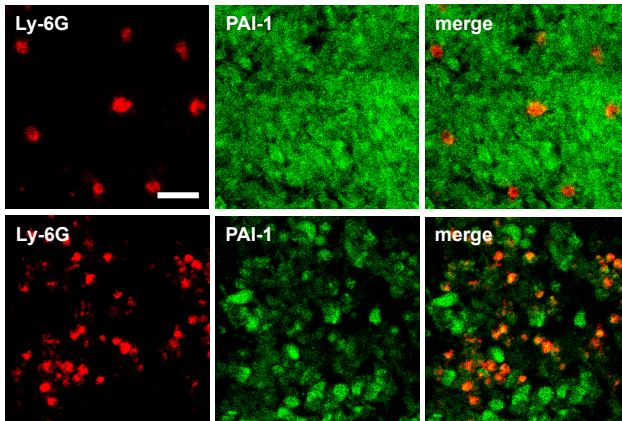
**d**

tumor cells

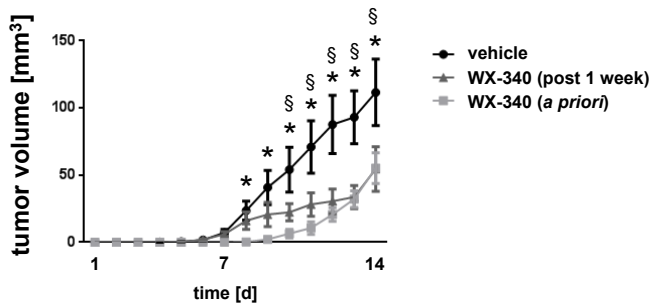


Appendix figure S2. Mechanisms underlying uPA-PAI-1-dependent cell activation. (a) Production of TNF was analyzed in peritoneal macrophages harvested from WT mice. (b) Surface expression of ICAM-1/CD54 or VCAM-1/CD106 on mouse bEnd.3 microvascular endothelial cells co-cultured with mouse RAW 264.7 macrophages prior to this exposed to saline, recombinant murine uPA-PAI-1, or TNF as assessed *in vitro* by multi-channel flow cytometry. Quantitative data are shown (mean±SEM for n=4-6 experiments per group; #p<0.05 vs. saline). (c) Binding of ICAM-1/CD54-Fc or VCAM-1/CD106-Fc to primary mouse neutrophils upon exposure to saline or recombinant murine uPA-PAI-1 as assessed by confocal microscopy, representative images are shown. (d) Proliferation of 4T1 breast cancer cells upon exposure to primary neutrophils isolated from the peritoneal cavity of WT mice undergoing 6 h of intra-peritoneal stimulation with uPA-PAI-1 with or without addition of compound WX-340 and a NE inhibitor as assessed by a MTT assay, quantitative data are shown (mean±SEM for n=4 experiments per group).

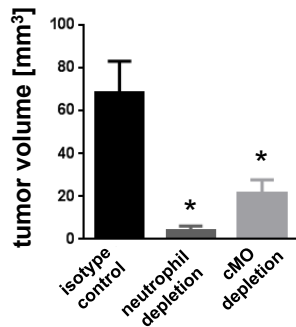
a



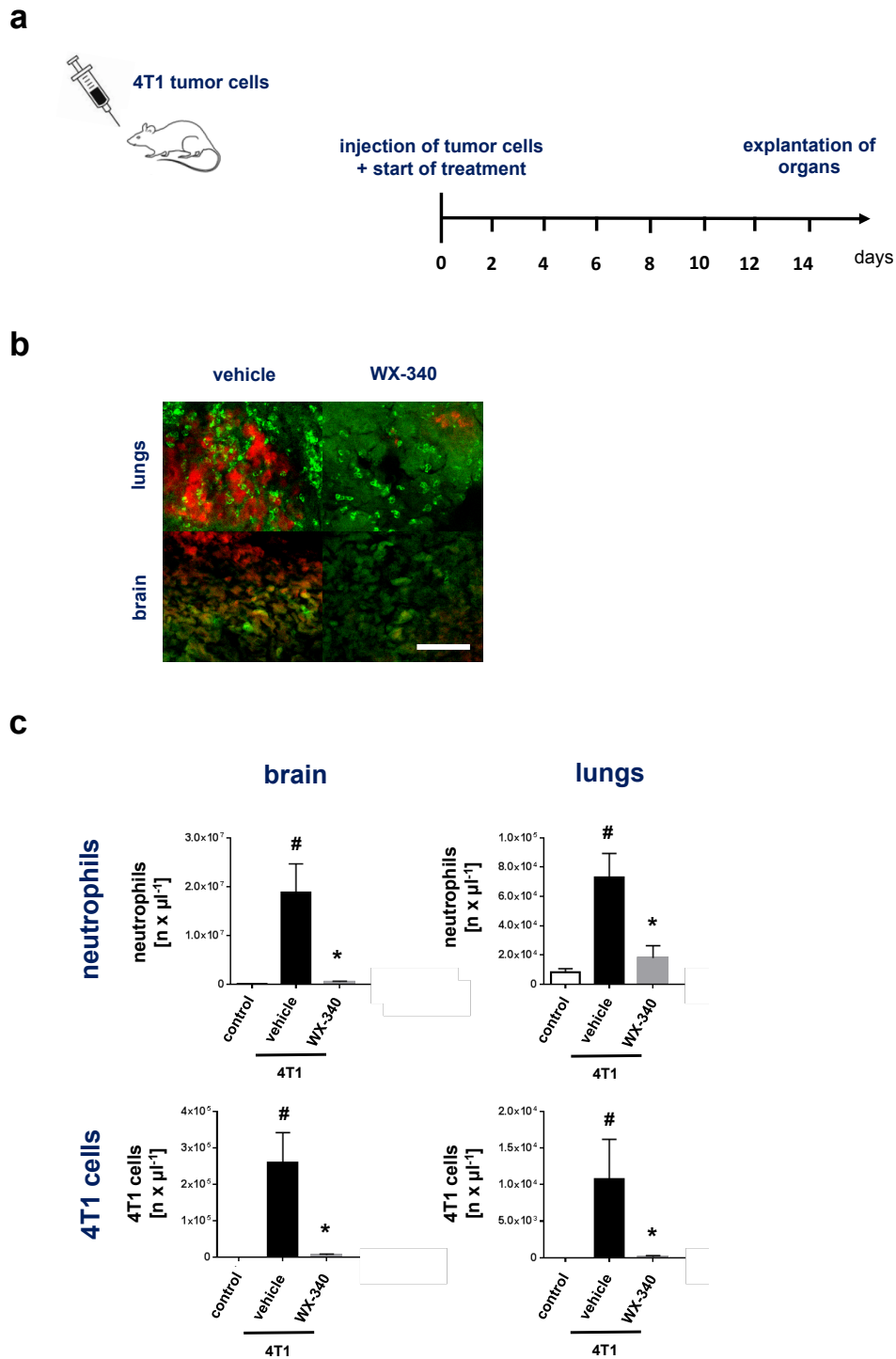
b



c



Appendix figure S3. Effect of WX-340 as well as of depletion of neutrophils and cMOs for local tumor growth. (a) Representative confocal microscopy images of uPA or PAI-1 expression (green) in mouse 4T1 tumors infiltrated by Ly-6G⁺ neutrophils (red; scale bar: 25 μ m). (b) Tumor volume in animals treated with WX-340 *a priori* or therapeutically after 1 week after tumor cell injection on a daily basis as assessed in an orthotopic model of 4T1 breast cancer in WT mice (mean \pm SEM for n=6 mice per group; *p<0.05 vs. drug vehicle). (c) Tumor volume in animals treated with neutrophil- or cMO-depleting monoclonal antibodies as assessed on day 14 after tumor-cell injection in an orthotopic model of 4T1 breast cancer in WT mice (mean \pm SEM for n=7 mice per group; *p<0.05 vs. isotype control).



Appendix figure S4. Effect of WX-340 on neutrophil infiltration and metastatic seeding in 4T1 breast cancer metastasis. Accumulation of neutrophils and 4T1 breast cancer cells in lungs and brains of WT mice treated *a priori* intra-peritoneally with WX-340 or drug vehicle (daily) as assessed 14 days after intravenous injection of 4T1 breast cancer cells by multi-channel flow cytometry in the tissue homogenates. **(a)** The experimental protocol, **(b)** representative confocal microscopy images of tumor metastases (red) and neutrophils (green; scale bar: 100 μm) in lungs and brain, and **(c)** quantitative data (mean±SEM for n=4-6 mice per group; #p<0.05 vs. control; *p<0.05 vs. vehicle) are shown.

Expanded View Figures

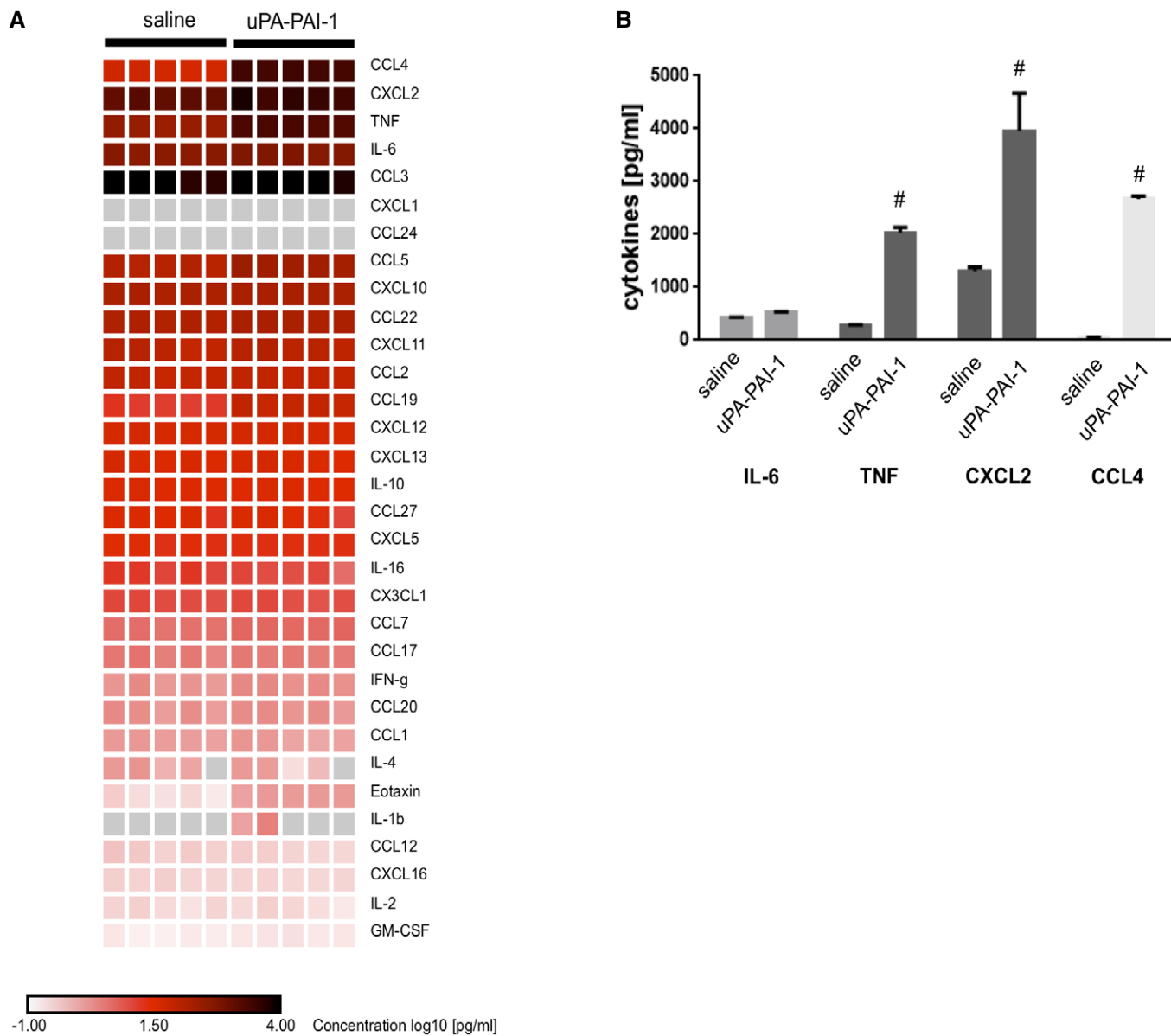


Figure EV1. Effect of uPA-PAI-1 heteromers on cytokine production in macrophages.

A Production of different cytokines by mouse RAW macrophages upon exposure to recombinant murine uPA-PAI-1 heteromers or saline as assessed by multiplex ELISA, results are shown as heatmap.

B In addition, quantitative data are provided for the most abundantly produced cytokines (mean ± SEM for *n* = 5 experiments per group; #*P* < 0.05 vs. saline; *t*-test).

Figure EV2. Molecular mechanisms underlying uPA-PAI-1-dependent neutrophil and cMO trafficking.

- A, B uPA-PAI-1-elicited recruitment of neutrophils (N) and classical monocytes (cMOs) to the peritoneal cavity of WT mice treated with anti-LFA-1/CD11a, anti-Mac-1/CD11b, anti-VLA-4/CD49d, anti-ICAM-1/CD54, anti-VCAM-1/CD106 mABs (A), anti-VLDLr mABs, anti-LRP-1 Abs, the MAPK inhibitors FR180204 (ERK1/2), SB202580 (p38), SP600125 (JNK) (B), or isotype control antibodies/drug vehicle as assessed by multi-channel flow cytometry, quantitative data are shown (mean \pm SEM for $n = 4-6$ mice per group; $^{\#}P < 0.05$ vs. saline; $*P < 0.05$ vs. isotype/vehicle; one-way ANOVA).
- C Recruitment of neutrophils (N) and classical monocytes (cMOs) to the peritoneal cavity of WT mice treated with recombinant murine uPA-PAI-1, recombinant human uPA-recombinant murine PAI-1 heteromers, recombinant murine DFP-uPA-PAI-1, or vehicle (mean \pm SEM for $n = 4-6$ mice per group; $^{\#}P < 0.05$ vs. saline; one-way ANOVA).

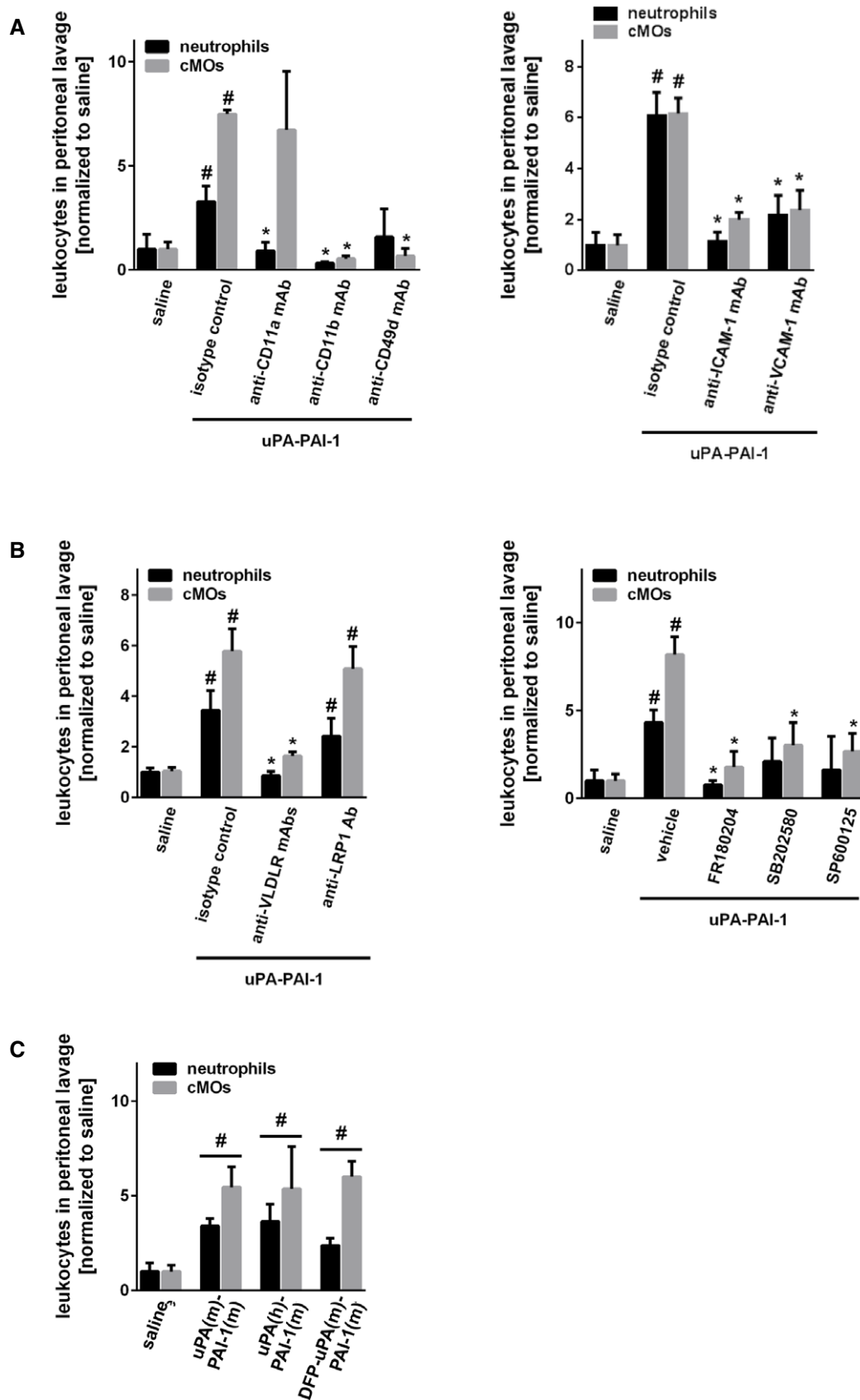


Figure EV2.

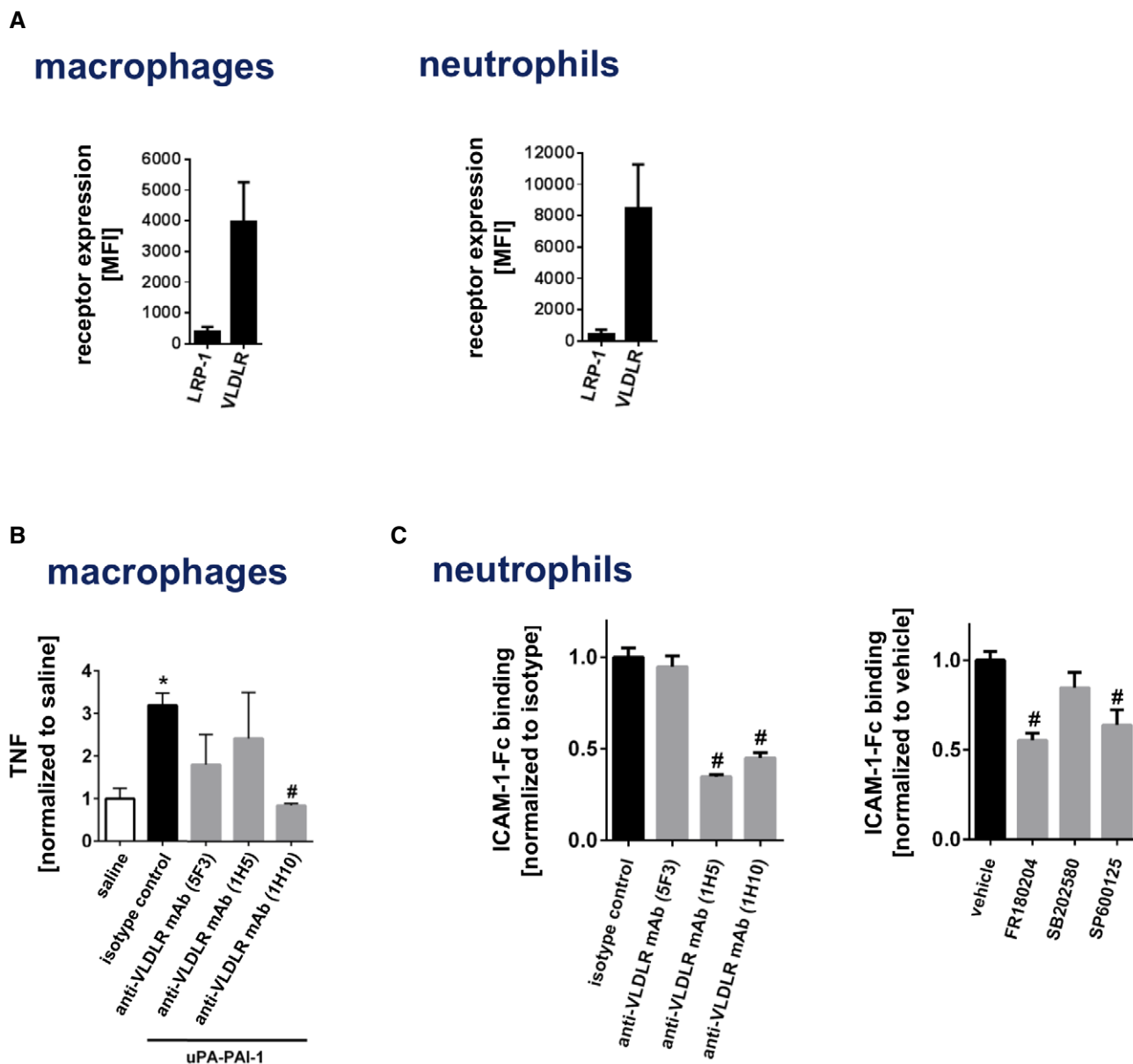


Figure EV3. Molecular mechanisms underlying uPA-PAI-1-dependent responses of macrophages and neutrophils.

- A Surface expression of LRP-1 or VLDLR on mouse RAW macrophages or bEnd.3 endothelial cells (mean \pm SEM for $n = 3$ experiments per group).
- B Production of TNF by mouse RAW macrophages upon exposure to blocking antibodies directed against different epitopes of VLDLR as assessed by multi-channel flow cytometry (mean \pm SEM for $n = 4-6$ experiments per group; * $P < 0.05$ vs. saline; # $P < 0.05$ vs. isotype control; one-way ANOVA).
- C Binding of recombinant murine ICAM-1/CD54-Fc to blood neutrophils from WT mice upon exposure to blocking antibodies directed against different epitopes of VLDLR or the MAPK inhibitors FR180204 (ERK), SB202580 (p38), or SP600125 (JNK) as assessed by flow cytometry (mean \pm SEM for $n = 4-6$ mice per group; # $P < 0.05$ vs. isotype control/vehicle; one-way ANOVA).

Figure EV4. Correlation of neutrophil infiltration and uPA/PAI-1 expression in human breast cancer samples.

- A, B Correlation of uPA or PAI-1 protein expression (ELISA) and neutrophil infiltration (histochemistry and light microscopy) in human breast cancer samples, representative images (A; histological grades: G1-3; scale bar: 100 μ m) and quantitative data (B; histological grades: G2 or G3; $n = 10-29$ samples per group).

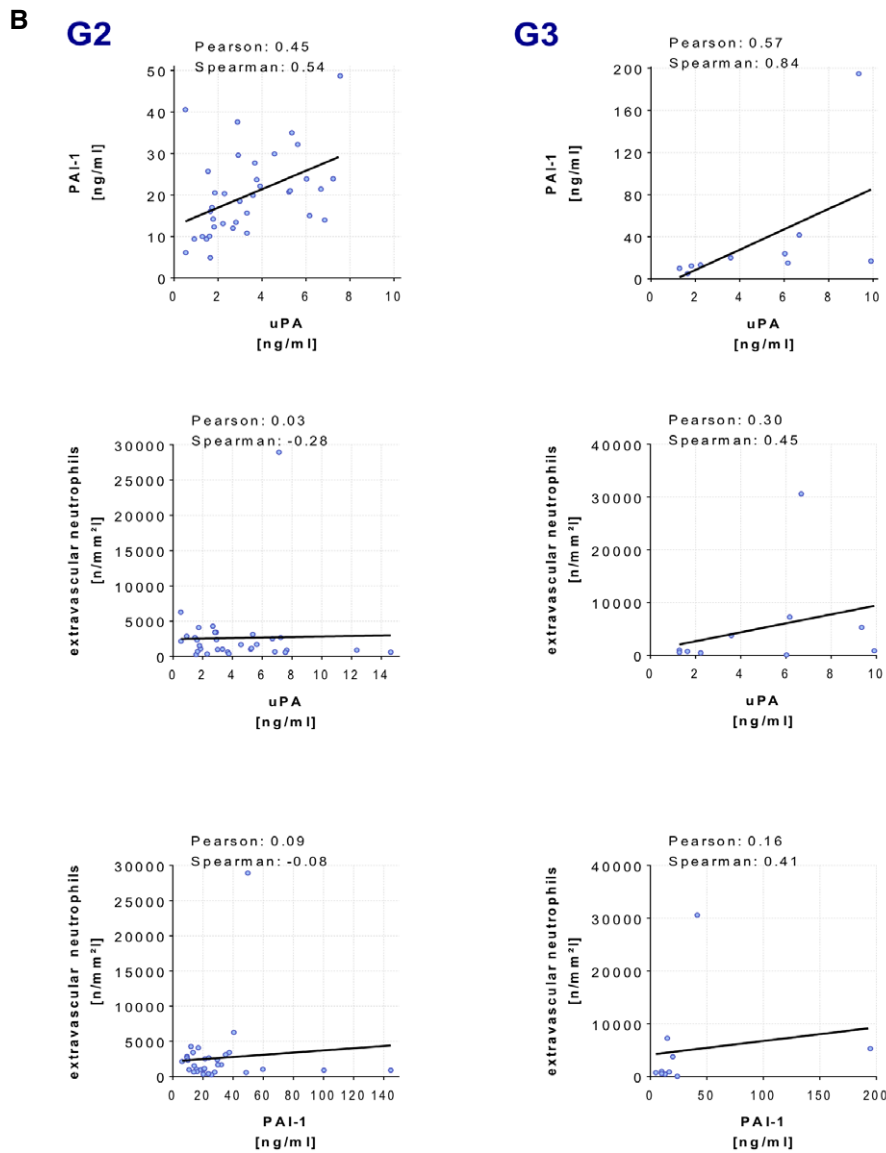
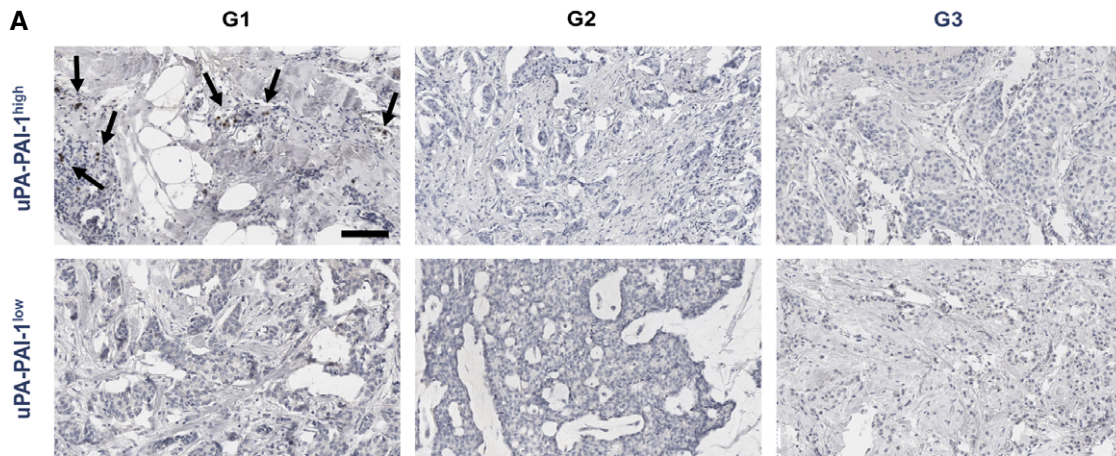


Figure EV4.

Figure EV5. Overall survival of breast cancer patients of the METABRIC cohort with respect to disease stage.

- A Composition of analyzed patients of the METABRIC cohort with respect to the disease stage.
- B Overall survival of PLAU-SERPINE1^{low} and PLAU-SERPINE1^{high} breast cancer patients in all disease stages (0–4) and advanced stages (2–4).
- C Mosaic plot depicting cross-tabulation and chi-squared analysis between high RNA expression of PLAU or SERPINE1 in the tumor and the molecular breast cancer subtype as defined by the 3-gene-classifier.

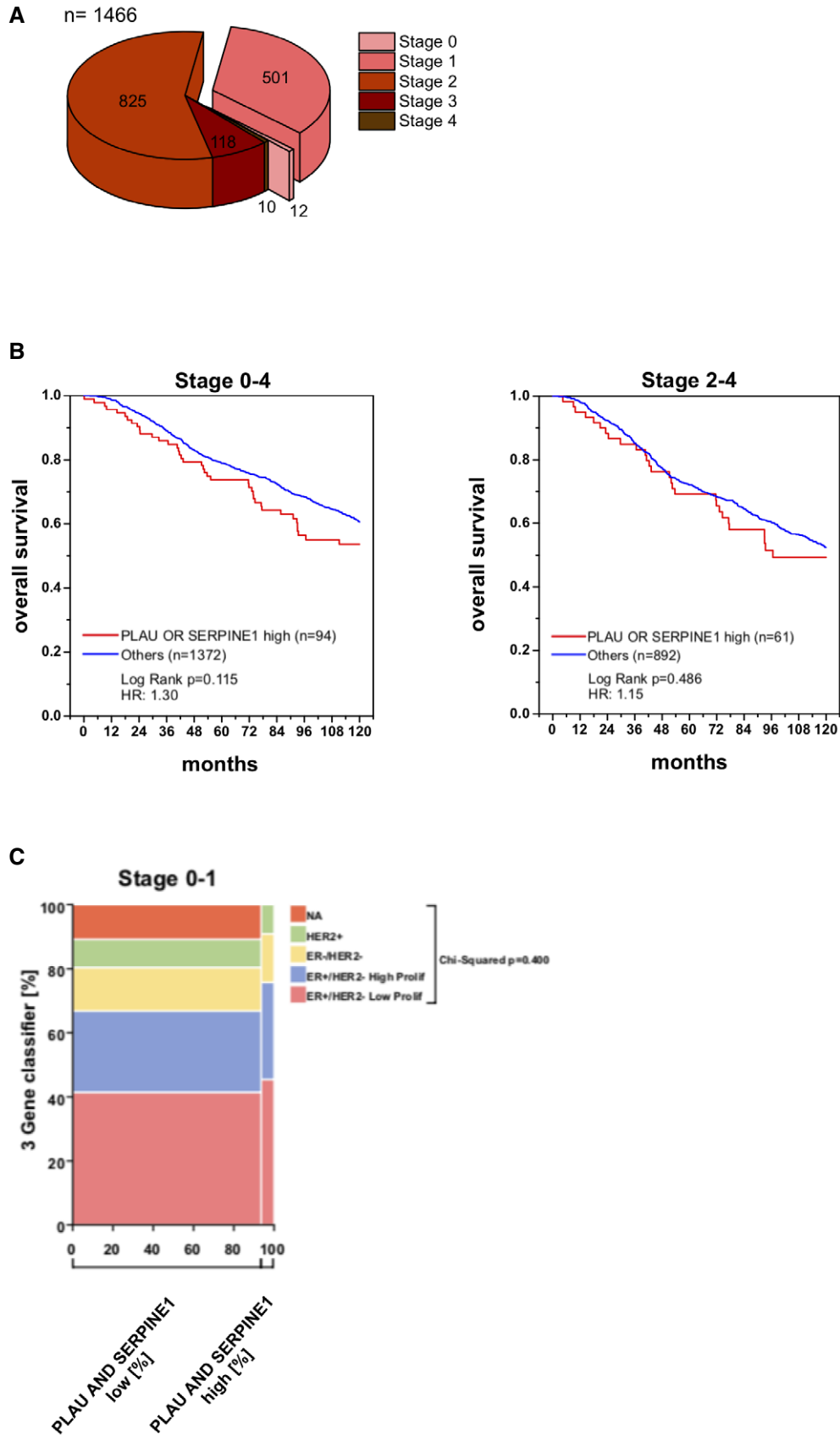


Figure EV5.

References

1. Brown, J.S., et al., *Updating the Definition of Cancer*. Mol Cancer Res, 2023. **21**(11): p. 1142-1147.
2. Schwartz, S.M., *Epidemiology of Cancer*. Clin Chem, 2024. **70**(1): p. 140-149.
3. Qazi, A.S., *Introduction and Overview of Cancer Therapeutics*. Cancer Treat Res, 2023. **185**: p. 1-13.
4. Chakraborty, S. and T. Rahman, *The difficulties in cancer treatment*. Ecancermedalscience, 2012. **6**: p. ed16.
5. Christodoulou, I., et al., *Mesenchymal stem cells in preclinical cancer cytotherapy: a systematic review*. Stem Cell Res Ther, 2018. **9**(1): p. 336.
6. Debela, D.T., et al., *New approaches and procedures for cancer treatment: Current perspectives*. SAGE Open Med, 2021. **9**: p. 20503121211034366.
7. Farkona, S., E.P. Diamandis, and I.M. Blasutig, *Cancer immunotherapy: the beginning of the end of cancer?* BMC Med, 2016. **14**: p. 73.
8. Liu, J., et al., *Cancer vaccines as promising immuno-therapeutics: platforms and current progress*. J Hematol Oncol, 2022. **15**(1): p. 28.
9. Lin, D., Y. Shen, and T. Liang, *Oncolytic virotherapy: basic principles, recent advances and future directions*. Signal Transduction and Targeted Therapy, 2023. **8**(1): p. 156.
10. Tin Tin, S., G.K. Reeves, and T.J. Key, *Endogenous hormones and risk of invasive breast cancer in pre- and post-menopausal women: findings from the UK Biobank*. Br J Cancer, 2021. **125**(1): p. 126-134.
11. Foulkes, W.D., I.E. Smith, and J.S. Reis-Filho, *Triple-negative breast cancer*. N Engl J Med, 2010. **363**(20): p. 1938-48.
12. Asleh, K., N. Riaz, and T.O. Nielsen, *Heterogeneity of triple negative breast cancer: Current advances in subtyping and treatment implications*. Journal of Experimental & Clinical Cancer Research, 2022. **41**(1): p. 265.
13. Marra, A., et al., *Practical classification of triple-negative breast cancer: intratumoral heterogeneity, mechanisms of drug resistance, and novel therapies*. NPJ Breast Cancer, 2020. **6**: p. 54.
14. Couzin-Frankel, J., *Breakthrough of the year 2013. Cancer immunotherapy*. Science, 2013. **342**(6165): p. 1432-3.
15. Han, Y., D. Liu, and L. Li, *PD-1/PD-L1 pathway: current researches in cancer*. Am J Cancer Res, 2020. **10**(3): p. 727-742.
16. Yang, Y., *Cancer immunotherapy: harnessing the immune system to battle cancer*. J Clin Invest, 2015. **125**(9): p. 3335-7.

17. Contardi, E., et al., *CTLA-4 is constitutively expressed on tumor cells and can trigger apoptosis upon ligand interaction*. *Int J Cancer*, 2005. **117**(4): p. 538-50.
18. Nowicki, T.S., et al., *Infiltration of CD8 T Cells and Expression of PD-1 and PD-L1 in Synovial Sarcoma*. *Cancer Immunol Res*, 2017. **5**(2): p. 118-126.
19. Ho-Yen, C.M., et al., *C-Met in invasive breast cancer: is there a relationship with the basal-like subtype?* *Cancer*, 2014. **120**(2): p. 163-71.
20. Ho-Yen, C.M., J.L. Jones, and S. Kermorgant, *The clinical and functional significance of c-Met in breast cancer: a review*. *Breast Cancer Res*, 2015. **17**(1): p. 52.
21. Mittendorf, E.A., et al., *Primary analysis of a prospective, randomized, single-blinded phase II trial evaluating the HER2 peptide AE37 vaccine in breast cancer patients to prevent recurrence*. *Ann Oncol*, 2016. **27**(7): p. 1241-8.
22. Kolaczkowska, E. and P. Kubes, *Neutrophil recruitment and function in health and inflammation*. *Nat Rev Immunol*, 2013. **13**(3): p. 159-75.
23. Hedrick, C.C. and I. Malanchi, *Neutrophils in cancer: heterogeneous and multifaceted*. *Nat Rev Immunol*, 2022. **22**(3): p. 173-187.
24. Summers, C., et al., *Neutrophil kinetics in health and disease*. *Trends Immunol*, 2010. **31**(8): p. 318-24.
25. Kennedy, A.D. and F.R. DeLeo, *Neutrophil apoptosis and the resolution of infection*. *Immunol Res*, 2009. **43**(1-3): p. 25-61.
26. Nauseef, W.M. and N. Borregaard, *Neutrophils at work*. *Nat Immunol*, 2014. **15**(7): p. 602-11.
27. Peiseler, M. and P. Kubes, *More friend than foe: the emerging role of neutrophils in tissue repair*. *J Clin Invest*, 2019. **129**(7): p. 2629-2639.
28. Greenlee-Wacker, M.C., *Clearance of apoptotic neutrophils and resolution of inflammation*. *Immunol Rev*, 2016. **273**(1): p. 357-70.
29. Tecchio, C. and M.A. Cassatella, *Neutrophil-derived chemokines on the road to immunity*. *Semin Immunol*, 2016. **28**(2): p. 119-28.
30. Rosales, C., et al., *Neutrophils: Their Role in Innate and Adaptive Immunity 2017*. *J Immunol Res*, 2017. **2017**: p. 9748345.
31. Tsioumpkou, M., et al., *The Role of Cytokines in Neutrophil Development, Tissue Homing, Function and Plasticity in Health and Disease*. *Cells*, 2023. **12**(15).
32. Wang, X., et al., *Understanding the Multifaceted Role of Neutrophils in Cancer and Autoimmune Diseases*. *Front Immunol*, 2018. **9**: p. 2456.
33. Antuamwine, B.B., et al., *N1 versus N2 and PMN-MDSC: A critical appraisal of current concepts on tumor-associated neutrophils and new directions for human oncology*. *Immunol Rev*, 2023. **314**(1): p. 250-279.
34. Poto, R., et al., *Neutrophil Extracellular Traps, Angiogenesis and Cancer*. *Biomedicines*, 2022. **10**(2).

35. Yin, H., et al., *Tumor-associated N1 and N2 neutrophils predict prognosis in patients with resected pancreatic ductal adenocarcinoma: A preliminary study*. *MedComm* (2020), 2022. **3**(4): p. e183.
36. Dutta, A., et al., *Neutrophils in Cancer and Potential Therapeutic Strategies Using Neutrophil-Derived Exosomes*. *Vaccines* (Basel), 2023. **11**(6).
37. Rawat, S., S. Vрати, and A. Banerjee, *Neutrophils at the crossroads of acute viral infections and severity*. *Mol Aspects Med*, 2021. **81**: p. 100996.
38. Agbani, E.O. and A.W. Poole, *Procoagulant platelets: generation, function, and therapeutic targeting in thrombosis*. *Blood*, 2017. **130**(20): p. 2171-2179.
39. Heemskerk, J.W.M., N.J.A. Matheij, and J.M.E.M. Cosemans, *Platelet-based coagulation: different populations, different functions*. *Journal of Thrombosis and Haemostasis*, 2013. **11**(1): p. 2-16.
40. Holinstat, M., *Normal platelet function*. *Cancer Metastasis Rev*, 2017. **36**(2): p. 195-198.
41. Jurk, K. and B.E. Kehrel, *Platelets: physiology and biochemistry*. *Semin Thromb Hemost*, 2005. **31**(4): p. 381-92.
42. Goubran, H., et al., *Platelet microparticles and cancer: An intimate cross-talk*. *Transfus Apher Sci*, 2015. **53**(2): p. 168-72.
43. Michael, J.V., et al., *Platelet microparticles infiltrating solid tumors transfer miRNAs that suppress tumor growth*. *Blood*, 2017. **130**(5): p. 567-580.
44. Varon, D. and E. Shai, *Role of platelet-derived microparticles in angiogenesis and tumor progression*. *Discov Med*, 2009. **8**(43): p. 237-41.
45. Li, S., et al., *The dynamic role of platelets in cancer progression and their therapeutic implications*. *Nature Reviews Cancer*, 2024. **24**(1): p. 72-87.
46. Labelle, M., S. Begum, and R.O. Hynes, *Direct signaling between platelets and cancer cells induces an epithelial-mesenchymal-like transition and promotes metastasis*. *Cancer Cell*, 2011. **20**(5): p. 576-90.
47. Boucharaba, A., et al., *Platelet-derived lysophosphatidic acid supports the progression of osteolytic bone metastases in breast cancer*. *J Clin Invest*, 2004. **114**(12): p. 1714-25.
48. Haemmerle, M., et al., *Platelets reduce anoikis and promote metastasis by activating YAP1 signaling*. *Nat Commun*, 2017. **8**(1): p. 310.
49. Gaertner, F. and S. Massberg, *Patrolling the vascular borders: platelets in immunity to infection and cancer*. *Nat Rev Immunol*, 2019. **19**(12): p. 747-760.
50. Zuchtriegel, G., et al., *Platelets Guide Leukocytes to Their Sites of Extravasation*. *PLoS Biol*, 2016. **14**(5): p. e1002459.

51. Lawrence, S.M., R. Corriden, and V. Nizet, *The Ontogeny of a Neutrophil: Mechanisms of Granulopoiesis and Homeostasis*. *Microbiol Mol Biol Rev*, 2018. **82**(1).
52. Dzierzak, E. and N.A. Speck, *Of lineage and legacy: the development of mammalian hematopoietic stem cells*. *Nat Immunol*, 2008. **9**(2): p. 129-36.
53. Rieger, M.A. and T. Schroeder, *Hematopoiesis*. *Cold Spring Harb Perspect Biol*, 2012. **4**(12).
54. Bao, Y., et al., *Extramedullary hematopoiesis secondary to malignant solid tumors: a case report and literature review*. *Cancer Manag Res*, 2018. **10**: p. 1461-1470.
55. Noh, J.Y., *Megakaryopoiesis and Platelet Biology: Roles of Transcription Factors and Emerging Clinical Implications*. *Int J Mol Sci*, 2021. **22**(17).
56. Patel, S.R., J.H. Hartwig, and J.E. Italiano, Jr., *The biogenesis of platelets from megakaryocyte proplatelets*. *J Clin Invest*, 2005. **115**(12): p. 3348-54.
57. Gaertner, F., et al., *Plasmacytoid dendritic cells control homeostasis of megakaryopoiesis*. *Nature*, 2024. **631**(8021): p. 645-653.
58. Cunin, P., et al., *Megakaryocyte emperipolesis mediates membrane transfer from intracytoplasmic neutrophils to platelets*. *Elife*, 2019. **8**.
59. Petzold, T., et al., *Neutrophil plucking on megakaryocytes drives platelet production and boosts cardiovascular disease*. *Immunity*, 2022. **55**(12): p. 2285-2299.e7.
60. Collen, D. and H.R. Lijnen, *The fibrinolytic system in man*. *Crit Rev Oncol Hematol*, 1986. **4**(3): p. 249-301.
61. Binder, B.R., et al., *Plasminogen activator inhibitor 1: physiological and pathophysiological roles*. *News Physiol Sci*, 2002. **17**: p. 56-61.
62. Ny, T., et al., *Regulation of tissue-type plasminogen activator activity and messenger RNA levels by gonadotropin-releasing hormone in cultured rat granulosa cells and cumulus-oocyte complexes*. *J Biol Chem*, 1987. **262**(24): p. 11790-3.
63. Kietsiroje, N., R.A.S. Ariëns, and R.A. Ajjan, *Fibrinolysis in Acute and Chronic Cardiovascular Disease*. *Semin Thromb Hemost*, 2021. **47**(5): p. 490-505.
64. Henderson, S.J., J.I. Weitz, and P.Y. Kim, *Fibrinolysis: strategies to enhance the treatment of acute ischemic stroke*. *J Thromb Haemost*, 2018. **16**(10): p. 1932-1940.
65. Bennur, S., et al., *Stress-induced spine loss in the medial amygdala is mediated by tissue-plasminogen activator*. *Neuroscience*, 2007. **144**(1): p. 8-16.
66. Duffy, M.J., et al., *Urokinase plasminogen activator as a predictor of aggressive disease in breast cancer*. *Enzyme Protein*, 1996. **49**(1-3): p. 85-93.

67. Look, M., et al., *Pooled analysis of prognostic impact of uPA and PAI-1 in breast cancer patients*. *Thromb Haemost*, 2003. **90**(3): p. 538-48.
68. Mahmood, N. and S.A. Rabbani, *Fibrinolytic System and Cancer: Diagnostic and Therapeutic Applications*. *Int J Mol Sci*, 2021. **22**(9).
69. Kwaan, H.C. and P.F. Lindholm, *Fibrin and Fibrinolysis in Cancer*. *Semin Thromb Hemost*, 2019. **45**(4): p. 413-422.
70. Kwaan, H.C., *The Role of Fibrinolytic System in Health and Disease*. *Int J Mol Sci*, 2022. **23**(9).
71. Südhoff, T. and W. Schneider, *Fibrinolytic mechanisms in tumor growth and spreading*. *Clin Investig*, 1992. **70**(8): p. 631-6.
72. Reichel, C.A., et al., *Plasmin inhibitors prevent leukocyte accumulation and remodeling events in the postischemic microvasculature*. *PLoS One*, 2011. **6**(2): p. e17229.
73. Praetner, M., et al., *Plasminogen Activator Inhibitor-1 Promotes Neutrophil Infiltration and Tissue Injury on Ischemia-Reperfusion*. *Arterioscler Thromb Vasc Biol*, 2018. **38**(4): p. 829-842.
74. Reichel, C.A., S.M. Kanse, and F. Krombach, *At the interface of fibrinolysis and inflammation: the role of urokinase-type plasminogen activator in the leukocyte extravasation cascade*. *Trends Cardiovasc Med*, 2012. **22**(7): p. 192-6.

Acknowledgements

This PhD journey would not have been as amazing as it was without all your support along the way. None of this would have been possible without you.

Christoph: I want to thank you for giving me the opportunity to do my PhD in your Laboratory, for believing in me and continuously supporting me over the past five years. Thank you for the great supervision and making me feel valued every step of the way. It was a pleasure working with you.

Claudia: Thank you for always being here for me and your support in every moment of this journey.

Verena: Thank you for providing me with great advice and keeping everything so well organized.

Constanze, Florian and Julian: Thanks guys for quidding, teaching and supporting me at the early beginning of my PhD time. I really appreciate it.

Joshua, Vera, Wu and Jonas P: Thank you for the beautiful time we spent together in the Lab.

Jonas H and Anais: As my favorite children and friends, I want to thank you for the amazing moments we shared together, having you on my side in every situation and for making the lab life so easy. Papa is so proud watching you successfully going your own way.

Julia, Valery, Jules, Theresa, Maren, Dom and Eli: I am grateful that I can call you friends. Thanks, guys, for every single second in and outside from the lab. I will take all beautiful memories from our well spent weekends in the mountains to our productive lunch conversations.

I also want to thank all the members from AG Massberg, AG Merkus, AG Kreth and AG Xeno. Thanks to all of you for helping me with your expertise whenever I need it and the beautiful moments we spent together.

Mama, Tate, Anche and Kate: You are the most important people in my life. Thank you for believing in me that I can reach this milestone and always reminding me that I am good enough for this. I love you!

Yours,
Bojan